An investigation of underground corrosion through the use of hyperspectral remote sensing

by

Benjamin Robert Lewis Arril
B.Sc., University of Victoria, 2007

A Thesis Submitted in Partial Fulfillment
of the Requirements for the Degree of

MASTER OF SCIENCE

in the Department of Geography

Supervisory Committee

An investigation of underground corrosion through the use of hyperspectral remote sensing

by

Benjamin Robert Lewis Arril
B.Sc., University of Victoria, 2007

Supervisory Committee

Dr. K. Olaf Niemann, (Department of Geography)
Supervisor

Dr. Douglas G. Maynard, (Department of Geography)
Departmental Member

Dr. Mark S. Flaherty, (Department of Geography)
Departmental Member

Abstract

Supervisory Committee

Dr. K. Olaf Niemann, (Department of Geography)
Supervisor

Dr. Douglas G. Maynard, (Department of Geography)
Departmental Member

Dr. Mark S. Flaherty, (Department of Geography)
Departmental Member

This thesis investigates the potential advantage of using remote sensing techniques to assess underground transmission tower corrosion. The data used in this study was collected from three electrical transmission towers in the Lower Fraser Valley, British Columbia, Canada. A comprehensive assessment of the corrosive environments have included the following factors: climate, soil pH, soil moisture content, soil resistivity, overlying plant spectral reflectance, and heavy metal content in soil and vegetation.

The principal method of protection against steel tower corrosion is zinc galvanization. As zinc serves as a sacrificial coating, once corroded, it leaches into the soil, and is then absorbed by surrounding vegetation. High concentrations of heavy metals may negatively influence plant growth. Plant Root Simulator (PRS™) probes were used to assess heavy metal supply rates by continuously adsorbing charged ionic species while in soil. Heavy metal content analysis was also conducted on sampled tower vegetation using an Inductively Coupled Plasma Atomic Emission Spectrometer (ICP-AES).

Remote sensing techniques, such as field spectroscopy, have great potential for monitoring spectral reflectance variations of various vegetation types and biophysical characteristics. The energy-matter interactions in the UV, VIS, NIR and IR wavelength

regions can be used for chemical analysis of compounds and mixtures. The combination of remote sensing analysis techniques, such as NDVI, leaf structural index R_{110}/R_{810}, water content index R_{900}/R_{970}, first order derivative analysis, and continuum removal can provide non-intrusive and continuous monitoring methods for the impact and content of certain heavy metals in plants growing in contaminated soils.

However, in this study, the high zinc concentrations recorded from the PRS™-probes and ICP-AES could not be correlated to the reflectance spectra measured by the field spectrometer. Although using zinc as a spectral corrosion identifier was not successful in this thesis, the presence of a chemical process in which by-products were produced and leached into the soil was evident. The integration of remote sensing techniques and underground corrosion explored in this thesis presents unique opportunities for further research in this area of study.

Table of Contents

List of Tables

Chapter 2

Chapter 3

Appendix A

Appendix B

Appendix C

Appendix D

Appendix E

Appendix G

List of Figures

Equations

Chapter 2

Chapter 3

Figures

Chapter 2

Chapter 3

Chapter 4

Chapter 5

Appendix F

Appendix G

Acknowledgments

First and foremost, I would like to thank Dr. Olaf Niemann, my supervisor, for working with me in pursuit of my master's degree. He gave me the freedom to pursue my interests in my research, and was always available for assistance when I needed it. I would like to thank the members of my graduate committee: Dr. Doug Maynard who sparked my interest in Pedology during my undergrad and for his involvement in the ICP-AES analysis, and Dr. Mark Flaherty who has served as my statistics guide over my university career. I would also like to thank Dr. Terri Lacourse for providing me with helpful feedback, advice, and guidance.

A special thanks to Fabio Visintini, Diana Parton, Rafael Loos, Christos Koulas, and everyone in the Hyperspectral and LiDAR research group for helping me with various aspects of my research in the lab and in the field. The support and encouragement they provided are appreciated a million times over.

This research would not have been possible without the help and support of Dr. Janos Toth and the British Columbia Transmission Corporation, BC Hydro, Western Ag Innovations Inc., and the University of Victoria Department of Geography.

Finally, I extend my thanks to my friends and family: in particular, to my parents, Robert and Leslie, for allowing me to find my own way through life and pursue my adventures; a special thanks to my wife, Jennifer, for her love, support, and patience; and to our dog, Wallace, whose comments were few and far between but who kept me company during those long days of writing.

Chapter 1 Introduction

1.1 RESEARCH CONTEXT

The British Columbia transmission system consists of approximately 20,500 steel transmission towers and 75,000 wood poles supporting over 18,000 kilometres of high-voltage electrical transmission lines (BCTC, 2007). Buried metallic structures, such as transmission towers, will eventually corrode as a result of the electrochemical activity of the soil and the atmosphere (Jones et al., 1987; Escalante, 1989; Zumdahl & Zumdahl, 2003). Metallic corrosion is a naturally occurring process whereby the surface of a metallic structure is oxidized into a corrosion by-product such as rust. A metallic surface is attacked by the passage of ions away from the surface, resulting in a loss of material over time (Perko, 2004; Zumdahl & Zumdahl, 2003). Since this material loss leads to a reduction in the compositional integrity and attractiveness of a metallic structure, this process can have a great economic impact (Zumdahl & Zumdahl, 2003).

Soil corrosion is the deterioration of metals or other materials brought about by the chemical, mechanical, and biological action of the underground environment (Escalante, 1989). The interactions of the organic and inorganic materials in soils give rise to many variations in soil characteristics that affect the corrosion process. Based on previous research conducted by Bushman and Mehalick (1989), Camitz and Vinka (1989), Corbett and Jenkins (1989), Escalante (1989), Fitzgerald (1989), Palmer (1989), Romanoff (1962), and Uhlig & Revie (1985), several factors can influence the corrosivity of soil including: soil texture, internal drainage, resistivity, temperature, pH, moisture content, soil aeration, and redox potential. The most commonly agreed upon criteria to rank the

degree of corrosivity among soils are resistivity and total acidity, although many other variables must be considered to correlate soil characteristics with actual corrosion (Corbett & Jenkins, 1989; Palmer, 1989). In general, soil resistivity is a measure of how easily a soil will allow an electric current to flow through it. The lower the resistivity of a soil, the better it will behave as an electrolyte, and the more likely it is to promote corrosion (Escalante, 1989; Palmer, 1989). Camitz and Vinka (1989) conclude that corrosion rates are generally higher in soils having a low pH (less than 4). However, soils rarely exceed a pH lower than 4 unless there is severe industrial contamination, or the presence of sulphate reducing organisms (Brady & Weil, 2002). The corrosivity of a particular soil is based upon the interaction of many soil parameters, and therefore no one parameter can necessarily indicate the corrosivity of a given soil.

The primary method of protection against corrosion is the application of a zinc (Zn) coating such as Zn paint or metal plating, to protect the metal from oxygen and moisture. This process is called galvanization. Zn is a more active metal than iron, thereby increasing the tendency for oxidation to occur. Thus, Zn acts as a sacrificial coating on steel and corrodes before the iron (Zumdahl & Zumdahl, 2003).

The identification of potential soil contaminants that affect surrounding vegetation is extremely important as they may act as indicators of the aboveground and underground corrosion process. This assessment requires that careful biological, chemical, and physical measurements be obtained from surrounding tower vegetation and within the soil horizon from field reconnaissance.

Jones et al. (1987) have shown that by-products of corroding steel transmission towers can leach into the surrounding soil, and be absorbed into the above vegetation. In their

study, corn plants growing in the area immediately beneath and around the towers absorbed Zn from soil contaminated by runoff from the lattice towers, and from falling water droplets resulting in higher than normal levels of Zn. Trace amounts of heavy metals are often required for proper development and growth of plants. However, high concentrations of heavy metals may influence plant growth in a negative way, and if they end up in agricultural crops, they pose a serious health threat (Brady & Weil, 2002; Jones et al., 1987). For instance, Zn is an essential element for normal plant growth, and acts as a plant nutrient, but at higher concentrations, it is toxic (Rout & Das, 2003; Schuerger et al., 2003).

Other by-products of corroding steel transmission towers may leach into the surrounding soil as well. For example, iron oxide is the chemical composition of rust which is formed by the open air oxidation of iron. Trace amounts of iron oxide may be absorbed into the neighbouring vegetation from the corroding tower legs.

Through the use of field spectroscopy, the effects of minute concentrations of trace heavy metal elements in vegetation are detectable through their emission spectrum (Kooistra et al., 2003; Schuerger et al., 2003). Spectrometers enable chemical analyses based on the extinction of light of a certain wavelength reflecting, absorbing, or transmitting through a sample (Milton et al., 2007). The energy-matter interactions utilized by spectroscopy in the ultraviolet (UV), visible (VIS), near-infrared (NIR), and infrared (IR) wavelength regions can be used for qualitative and quantitative analysis of chemical compounds and mixtures (Liang, 2004; Milton et al., 2007). However, only organic molecules, water, and most gases, exist in energy states that are able to absorb UV, VIS, NIR, and IR wavelengths. Metals and most inorganics, on the other hand, are

nearly incapable of absorbing electromagnetic radiation at these wavelengths (Clark, 1999). Therefore, most studies in the area of heavy metal remote sensing have focused on the detection of vegetation stress caused by increased heavy metal concentrations in soil (Clevers et al., 2004; Goetz et al., 1983; Horler et al., 1980; Kooistra et al., 2003; Kooistra et al., 2004; Schuerger et al., 2003; Schwaller et al., 1983; Sridhar et al., 2007). Accordingly, the research in this thesis will focus on the detection of vegetation stress caused by increased heavy metal concentrations from by-products of the corrosion process. This will be achieved through field data collection from three electrical transmission towers in the Lower Fraser Valley, British Columbia, Canada.

In order to maintain and repair corroded transmission towers, various methods are used to assess the extent of disintegration. Current techniques for assessing the extent of underground transmission tower corrosion involve direct excavation and inspection of the affected legs. However, these methods of investigation are often costly, time-consuming, and labour intensive. Results from this project will potentially provide tools to enable better initial estimates of the risk of site corrosion, and facilitate cost-benefit analysis of tower maintenance and placement.

Remote sensing techniques offer a non-intrusive method of continuous data collection that can cover large areas of land at a relatively low cost (Liang, 2004). Remote sensing instruments such as field spectrometers may be used to assess the extent of underground corrosion of steel transmission towers without the need for direct excavation.

1.2 PRIMARY RESEARCH OBJECTIVES

This thesis investigates the potential advantages of using remote sensing techniques to assess underground transmission tower corrosion. This will be achieved through the following research objectives:

1. To discuss the chemical process of the corrosion of steel transmission towers and to determine which soil properties affect the corrosion mechanism;
2. To establish the effect of the corrosion mechanism on soils around transmission towers;
3. To determine the effect the corrosion mechanism has on vegetation;
4. To explore the effect of corrosion on surface vegetation, and how this may be identified through the use of remote sensing techniques with a focus on field spectroscopy; and
5. To examine the relationship, if any, between underground steel tower corrosion, soil corrosion characteristics, and reflectance spectra of overlying vegetation.

1.3 THESIS ORGANIZATION

This thesis is organized into six chapters. The research context, objectives, and organization are presented in Chapter 1. Chapter 2 reviews research from applicable scientific literature on soil corrosion characteristics, heavy metals in soils and vegetation, and principals of spectroscopy. The study locations, field data acquisition, and

processing procedures are discussed in Chapter 3. In Chapter 4, results from each study location are presented. Chapter 5 discusses and interprets results, statistical analyses, and key findings. Finally, Chapter 6 details research conclusions and provides future research recommendations.

Chapter 2 Literature Review

2.1 INTRODUCTION

Through a review of current research literature, this section discusses the potential application of hyperspectral remote sensing techniques in the detection of heavy metal content in vegetation. This overview includes the basic principles involved in the corrosion of iron, the fundamentals of heavy metal contamination in soils and how it relates to plant health, and relevant vegetation characteristics that can be identified through the use of field spectroscopy.

2.2 CORROSION

Corrosion is both a natural reduction and a destructive attack of a refined metal by chemical or electrochemical reactions with the surrounding environment. Although other materials may deteriorate by chemical means, the term corrosion is primarily restricted to the chemical attack of metals (Uhlig & Revie, 1985). Corrosion involves the transformation of a metal or alloy to a non-reactive covalent compound which is often similar or even identical to the mineral from which the metals were extracted (Perko, 2004; Uhlig & Revie, 1985). To understand why this process occurs, it is important to understand how a metal, such as steel, is formed.

Steel is an alloy manufactured by refining low energy iron ore. During this process, a large amount of energy is added to the metal. Once the steel is placed in a corrosive environment, the stored energy, as in a thermodynamic system, flows from a higher to a lower state in order to reach a natural equilibrium. Over time, the stored energy in the

steel naturally returns to its original low energy state, releasing the energy gained during refinement (Uhlig & Revie, 1985).

During metallic corrosion, the surface of a structure is oxidized into a corrosion by-product such as rust. "Rusting" applies specifically to the corrosion of iron and iron-based alloys largely consisting of hydrous ferric oxides. Although nonferrous metals corrode, they do not rust (Perko, 2004; Uhlig & Revie, 1985). Oxidation involves the loss of electrons from metals reacting with water and oxygen. A metallic surface is attacked through the passage of ions away from the surface, resulting in a loss of material over time (Perko, 2004; Uhlig & Revie, 1985; Zumdahl & Zumdahl, 2003). Since this material loss leads to a reduction in the compositional integrity and attractiveness of a metallic structure, this process can have a great economic impact on industrial infrastructure where iron and its alloy, steel, are heavily relied upon (Ailor, 1971; Doyle et al., 2003; Romanoff, 1962; Zumdahl & Zumdahl, 2003). Accordingly, in explaining the corrosion mechanism, the focus here will be on iron and steel.

2.2.1 Corrosion of Steel

The corrosion of iron and steel is not actually a direct oxidation process, but an electrochemical reaction (Brady & Weil, 2002; Escalante, 1989; Uhlig & Revie, 1985). To be effective, the corroding system must have: 1. an anode/cathode system; 2. an electrically conducting path between the anode and the cathode; and 3. an electrolyte in contact with the anode cathode system (Escalante, 1989).

Steel generally has a non-uniform surface. This is due to two factors: first, the chemical composition of steel is not completely homogeneous; and second, physical

strains often leave stress points in the metal. These non-uniformities create areas in the iron that are more easily oxidized than others. The areas that are more easily oxidized are called anodic regions as opposed to the cathodic regions. In the anodic regions, iron dissolves forming a pit. The dissolution at the anode is where the oxidation reaction occurs, as each iron atom gives up two electrons to form the Fe^{2+} ion (Zumdahl & Zumdahl, 2003):

$$\mathbf{Fe \rightarrow Fe^{2+} + 2e^-}$$

The released electrons flow through the steel to a cathodic region, where they react with oxygen (Zumdahl & Zumdahl, 2003):

$$\mathbf{O_2 + 2H_2O + 4e^- \rightarrow 4OH^-}$$

Oxygen gas (O_2) is a strong oxidizing agent, because it rapidly accepts electrons from many other elements (Brady & Weil, 2002).

An electrolyte is a chemical medium, usually an aqueous solution that allows ions to travel between a cathode and anode (Escalante, 1989). The Fe^{2+} ions travel from the anodic to the cathodic regions through the available moisture, which acts as the electrolyte on the surface of the steel. There the Fe^{2+} ions react with the oxygen to form rust (hydrated iron(III) oxide):

$$\mathbf{4Fe^{2+}}\ (\textit{Aqueous Solution}) + \mathbf{O_2}\ (\textit{Gas}) + \mathbf{(4 + 2n)H_2O}\ (\textit{Liquid}) \rightarrow \underset{\textit{Rust}}{\mathbf{2Fe_2O_3 \cdot \mathit{n}H_2O}\ (\textit{Solid})} + \mathbf{8H^+}\ (\textit{Aqueous Solution})$$

This process is often observed when rust forms at sites that are at a distance from where the iron originally dissolved and formed pits in the steel (Figure 1) (Zumdahl & Zumdahl, 2003).

Because the corrosion of steel has an electrochemical mechanism, ion exchange must be possible between the cathodic and anodic areas on the surface of the steel in order for

rusting to occur. Moisture is a key element in the corrosion process as it acts as a mock salt bridge between the anodic and cathodic regions (Escalante, 1989; Palmer, 1989; Zumdahl & Zumdahl, 2003).

Salt should also be taken into consideration as it accelerates the formation of rust. Dissolved salt on a steel surface increases the conductivity of the aqueous solution formed there, thereby accelerating the electrochemical corrosion process (Zumdahl & Zumdahl, 2003). The rusting of cars in colder parts of Canada where salt is used on roads is a direct result of this process.

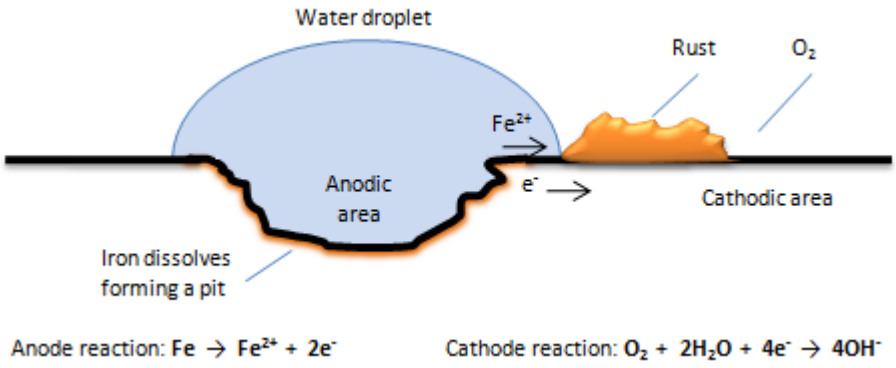

Figure 1 - The electrochemical corrosion of iron (adapted from Zumdahl & Zumdahl, 2003)

2.2.2 Types of Corrosion

Different types of corrosion occur in a variety of unique circumstances. However, most types of corrosion occur through an electrochemical mechanism (Uhlig & Revie, 1985). Depending on the factors that affect the electrochemical reaction, several types of corrosion with respect to surface appearance or altered physical properties are classified in Table 1.

Table 1 – Types of corrosion damage

Type	Characteristics
Uniform	Corrosion takes place at all areas of a metal at the same or similar rate. This includes rusting of iron, tarnishing of silver, fogging of nickel, and high-temperature oxidation of metals. Generally, the initial corrosion rate is greater than subsequent rates (Uhlig & Revie, 1985).
Localized	Due to heterogeneities in the metal or environment, some areas of a metal corrode at different rates than others. Localized attack can approach pitting (Uhlig & Revie, 1985).
Pitting	Highly localized corrosion at specific areas. This type of attack results in small pits that may penetrate to perforation. The rate of corrosion is greater at some areas than at others. Buried iron often corrodes with the formation of shallow pits, as opposed to stainless steel immersed in seawater which corrodes with the formation of deep pits (Uhlig & Revie, 1985).
Cracking	Cracking occurs when a metal is subjected to repeated or alternate tensile stresses in a corrosive environment (Uhlig & Revie, 1985).

2.2.3 Corrosion Prevention

Metals such as copper, gold, silver, and platinum, are relatively difficult to oxidize. This is due to their high positive reduction potential. These types of metals are known as noble metals. Cheaper metals, such as iron and steel, used mainly as structural materials for bridges, buildings, and vehicles, generally oxidize quite easily and have a lower reduction potential, making them extremely susceptible to corrosion (Zumdahl & Zumdahl, 2003).

To combat corrosion, most metals naturally develop a thin oxide coating, which tends to protect their internal atoms against further oxidation. Aluminum, for instance, forms a thin, adherent layer of aluminum oxide which greatly inhibits further corrosion. This extra layer increases the reduction potential of the metal, and causes it to behave much

like a noble metal (Zumdahl & Zumdahl, 2003). However, when some metals such as iron and steel are exposed to oxygen in moist air, the oxide that forms tends to scale off and expose new metal surfaces to corrosion, thereby causing localized corrosion on steel surfaces (Escalante, 1989). In many cases, the natural oxide coating is not enough to combat corrosion altogether. As a result, more direct protection methods are often required.

The primary method of direct protection against corrosion is the application of a coating such as paint or metal plating to protect the metal from oxygen and moisture. For instance, Zn is commonly used to coat steel in a process called galvanization. Galvanized Zn coatings protect steel in two ways: first, the Zn coating provides a protective layer between the steel and the environment; second, if the coating is scratched and the steel surface is exposed to the elements, the Zn coating, not the steel, will corrode (Escalante, 1989; Zumdahl & Zumdahl, 2003). Zn is a more active metal than iron, thereby increasing the tendency for oxidation to occur. Thus, Zn acts as a sacrificial coating on steel, and corrodes before the iron (Zumdahl & Zumdahl, 2003). In this case, Zn is a dissimilar metal in electrical contact with the steel. Therefore, the difference in potential between the two metals and their relative chemical performance (anode or cathode) can be assessed by examining the galvanic series shown in Table 2. The more active material at the top of the list will act as an anode and corrode while the more noble material at the bottom will be the cathode and therefore protected (Escalante, 1989).

Table 2 – Galvanic series in seawater (Escalante, 1989)

ACTIVE	Magnesium
	Zinc
	Beryllium
	Aluminum Alloys
	Cadmium
	Mild Steel, Cast Iron
	300 Series Stainless Steel (Active)
	Aluminum Bronze
	Naval Brass
	Tin
	Copper
	Lead-Tin Solder (50/50)
	90-10 Copper-Nickel
	Lead
	Silver
	300 Series Stainless Steel (Passive)
	Titanium
	Platinum
NOBLE	Graphite

In very aggressive soil corrosion environments, cathodic protection is the recommended method used to protect steel in buried conditions. For example, an active metal, such as magnesium, is connected by a wire to a buried steel object to be protected (Figure 2). Because magnesium is a better reducing agent than iron, electrons are supplied by the active metal rather than by the iron, keeping the iron from being oxidized (Uhlig & Revie, 1985; Zumdahl & Zumdahl, 2003). Again, the more active material will act as an anode and corrode, while the more noble metal will act as the cathode (Escalante, 1989). Eventually, the magnesium anode will dissolve entirely, and will therefore need to be replaced.

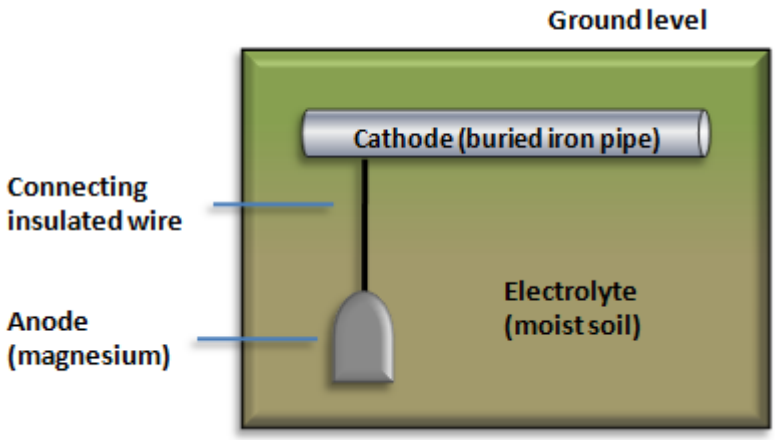

Figure 2 – Cathodic protection of an underground pipe
(adapted from Zumdahl & Zumdahl, 2003)

2.2.4 Corrosion in Soils

Soil corrosion is the deterioration of metals or other materials brought about by the chemical, mechanical, and biological action of the underground environment (Escalante, 1989). The basic concept of how corrosion affects an underground structure is much the same as described above. However, the interactions of the organic and inorganic materials in soils give rise to many variations in soil characteristics that affect the corrosion process. Based on previous work conducted by Bushman and Mehalick (1989), Camitz and Vinka (1989), Corbett and Jenkins (1989), Escalante (1989), Fitzgerald (1989), Palmer (1989), Romanoff (1962), and Uhlig & Revie (1985), several factors can influence the corrosivity of soil including: soil texture, internal drainage, resistivity, temperature, pH, moisture, soil aeration, and redox potential. The most commonly agreed upon criteria to rank the degree of corrosivity among soils are resistivity and total acidity, although many other variables must be considered to correlate soil characteristics with actual corrosion failures (Corbett & Jenkins, 1989; Palmer, 1989). The corrosivity of a particular soil is based upon the interaction of differing soil parameters, and no single

parameter can necessarily be taken as indicative of the corrosivity of a given soil (Fitzgerald, 1989). The characteristics of corrosion prone soils are reviewed:

1. Soil Texture;
2. Internal Drainage;
3. Resistivity;
4. Temperature;
5. pH;
6. Soil Moisture;
7. Soil Aeration; and
8. Redox Potential.

1. Soil Texture

Soil texture is determined by the relative proportions of sand, silt, and clay that make up a soil. Clay has the finest particle sizes and minimum pore volume between particles. Generally speaking, the lower the porosity, the lower the movement of air and water which causes poor aeration. Sand has the largest particle size, and promotes moisture movement and the entry of air into the soil. Soil textures behave differently under certain pH conditions and have an important influence on the transmission of soluble salts and gases (Brady & Weil, 2002). The major soil textural classes are described by the textural triangle in Figure 3.

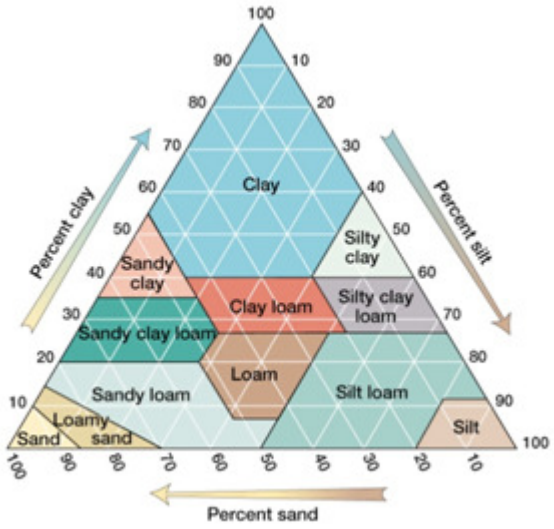

Figure 3 – Textural triangle
(adapted from Brady & Weil, 2002)

2. Internal Drainage

Internal drainage is related to soil texture and moisture content as it describes the water retention properties of a soil (Brady & Weil, 2002). However, internal drainage is also greatly affected by the height of the water table. If the water table is high enough, a soil that would normally have good moisture permeation would now have poor drainage and be completely saturated (Escalante, 1989).

3. Resistivity

Soil resistivity (conductivity^{-1}) is a measure of how easily a soil allows an electric current to flow through it. High resistivity designates poor conductors. The lower the resistivity and the higher the conductivity of a soil, the better it will behave as an electrolyte, and the more likely it is to promote corrosion (Escalante, 1989; Palmer, 1989). The resistivity of metallic conductors usually increases with a rise in temperature (Iverson, 1971). Resistivity generally decreases with increasing water content, and the

concentration of ionic species (Escalante, 1989). Electrical conductivity is a soil characteristic commonly associated with the salinity of a soil. As salt is dissolved in pure water, electrical conductivity increases and resistivity decreases. Therefore, the electrical conductivity in a soil can give an indirect measurement of the salt content (Brady & Weil, 2002; Hesse, 1971). As the soil salinity increases, the resistivity decreases and the conductivity increases, thereby accelerating the electrochemical corrosion process (Zumdahl & Zumdahl, 2003). Research conducted by Palmer (1989) suggests that soil resistivity is the major controlling factor in corrosion; however, it is by no means the only parameter affecting the risk of corrosion damage. A high soil resistivity does not necessarily guarantee absence of serious corrosion. Resistivity is measured in ohm-metres or ohm-centimetres, and can range from 30 ohm-cm in seawater to more than 100,000 ohm-cm in dry sand or gravel. Waters' (1952) work considers less than 900 ohm-cm to cause very severe corrosion. Table 3 shows the relationship between soil resistivity and soil corrosion.

Table 3 – Relationship between soil resistivity and soil corrosivity (Waters, 1952)

Soil Resistivity (ohm-cm)	Classification of Soil Corrosiveness
0 to 900	Very severe corrosion
900 to 2,300	Severely corrosive
2,300 to 5,000	Moderately corrosive
5,000 to 10,000	Mildly corrosive
10,000 to > 10,000	Very mildly corrosive

4. Temperature

An increase in soil temperature accelerates the rate of the chemical reaction of corrosion. Resistivity generally increases with a rise in temperature as well (Iverson, 1971). However, an increase in temperature also reduces the solubility of oxygen which

in turn reduces the rate of reaction at the cathode. The result is that moderate temperature changes actually have a negligible effect on the corrosion process (Escalante, 1989). In very low temperature environments, the corrosion mechanism may cease to function as chemical reaction rates may slow and available moisture may be reduced. As with any steel at low temperatures, the material may become brittle with extended use which can cause other structure issues (Escalante, 1989; Palmer, 1989).

5. pH

Soil pH is the degree of acidity or alkalinity of a soil expressed as the negative logarithm of the hydrogen ion concentration. Soil acidity is produced by mineral leaching, decomposition of acidic plants, industrial wastes, acid rain, and certain forms of microbiological activity (Brady & Weil, 2002). Most soils in North America tend to be somewhat acidic due to the leaching effect of rainfall and the presence of acid rain (Brady & Weil, 2002). Camitz and Vinka (1989) conclude that corrosion rates are generally higher in soils having a low pH (less than 4). However, soils rarely exceed a pH lower than 4 unless there is severe industrial contamination or the presence of sulphate reducing organisms (Brady & Weil, 2002). Pure water has a neutral pH value of 7. In the pH range of 4 to 8.5, iron can be immune (not corroding), passive (corroding very slowly), or actively corroding depending on its potential (Escalante, 1989). However, in this range, pH is not considered to be the dominant variable affecting corrosion rates. pH values are given much more consideration when they are lower than 4 or higher than 8.5 as they tend to adversely affect soils, and increase the rate of corrosion when more acidic (Palmer, 1989).

6. Moisture

In most circumstances, soil moisture content is directly related to corrosion rates (Bushman & Mehalick, 1989). Moisture provides the essential electrolyte required for electrochemical corrosion reactions, and acts as a mock salt bridge between anodic and cathodic regions (Escalante, 1989; Palmer, 1989; Zumdahl & Zumdahl, 2003). The amount of moisture held in the soil is a function of the soil texture. The finer the soil texture, the greater the soil's ability to maintain a high moisture content in the presence of precipitation (Brady & Weil, 2002; Jensen, 2000).

7. Soil Aeration

Aeration involves the circulation of oxygen (O_2) and carbon dioxide (CO_2) gases ventilating through the soil (Brady & Weil, 2002). The change in oxygen concentration has an important effect on corrosion rates due to its participation in the cathode reaction (Palmer, 1989). Oxygen gas is a strong oxidizing agent as it rapidly accepts electrons from many other elements (Brady & Weil, 2002). The degree of aeration is directly affected by soil texture and whether the soil is cultivated (disturbed) or uncultivated (undisturbed). For example, driving a steel pile into the ground causes minimal change to the soil and is considered to be undisturbed, whereas, tillage and agricultural practises causes disruption and increases available oxygen in the soil (Escalante, 1989).

8. Redox Potential

The redox potential gives a measure of the tendency of a substance to give up or acquire electrons. The redox potential of a soil is dependent on both the pH of the soil,

and the presence of electron acceptors (oxygen or other oxidizing agents). If a substance will accept electrons easily, it is known as an oxidizing agent; if a substance supplies electrons easily, it is a reducing agent. A low redox potential, indicates a strong reducing environment (Brady & Weil, 2002).

A measure of redox potential is also useful when distinguishing between aerobic soils and anaerobic soils that could support sulphate-reducing bacterial activity. These bacteria reduce sulphates to sulphides which may activate cathodic areas by consuming hydrogen, or produce corrosive products (Palmer, 1989). They shift the pH in the acidic direction, causing accelerated corrosion (Bushman & Mehalick, 1989). Sulphides can affect both metals and non-metallic materials, in both the presence and lack of oxygen (Escalante, 1989). With the lack of oxygen, sulphate-reducing bacteria produce hydrogen sulphide, causing sulphide stress cracking. In the presence of oxygen, some bacteria directly oxidize iron to iron oxides and hydroxides. This results in soil pH values below 3.5 and in severe cases as low as 2.0 (Brady & Weil, 2002). However, it is often found that high sulphate levels are generally more harmful toward the corrosion of concrete than metallic materials (Palmer, 1989).

Measured in volts or millivolts, testing for redox potentials is rather difficult, and must be conducted immediately after soil exposure (Palmer, 1989). Table 4 indicates a relationship between redox potential and soil corrosivity (Starkey & Wight, 1945).

Table 4 – Relationship between redox potential and soil corrosivity (Starkey & Wight, 1945)

Range of Soil Redox Potential (mV)	Classification of Corrosiveness
Below 100 mV	Severe
100 to 200 mV	Moderate
200 to 400 mV	Slight
Above 400 mV	Non-corrosive

2.3 HEAVY METALS IN SOILS AND PLANT HEALTH

The term "heavy metals" is inconsistently used in scientific literature. However, it is typically used as a group name for metals and metalloids on the periodic table that generally have densities of 5.0 Mg/m or greater, and have been associated with contamination and potential toxicity or eco-toxicity (Brady & Weil, 2002; Duffus, 2002). For the relevance of this thesis, the association with contamination and potential toxicity will be considered the consistent definition.

Heavy metal contamination of soils associated with industrial areas and manufactured products have become a major environmental concern. Activities such as mining, smelting, electroplating, ore refining, and corroding steel contaminate soils with heavy metal species such as arsenic (As), cadmium (Cd), copper (Cu), cobalt (Co), nickel (Ni), lead (Pb), zinc (Zn), and iron (Fe) (Jones et al. 1987; Levesque & King, 1999; Schuerger et al., 2003). High concentrations of heavy metals may influence plant growth in a negative way, and if they end up in agricultural crops, they pose a serious health threat (Brady & Weil, 2002; Jones et al., 1987). In extreme cases, these metals degrade or remove natural vegetation, causing them to grow less dense and vigorous because the underlying soils have become less productive, and more susceptible to degradation (Brady & Weil, 2002).

Jones et al. (1987) have shown that heavy metal by-products of corroding steel transmission towers can leach into the surrounding soil, and be absorbed into the above vegetation. In their study, corn plants growing in the area immediately beneath and around the towers absorbed higher than normal levels of Zn from soil contaminated by runoff from the lattice towers, and from falling water droplets. Trace amounts of heavy

metals are often required for proper development and growth of plants. For instance, Zn is an essential element for normal plant growth, and acts as a plant nutrient, but at higher concentrations, it is toxic (Rout & Das, 2003; Schuerger et al., 2003). Over time, plants respond to nutrient and element deficiencies, excesses, or imbalances through modifications of growth (Ustin et al., 1999). Zn deficiency in plants can impair the functionality of several physiological factors, but at toxic concentrations, it has been shown to impair electron transport and photophosphorylation, inhibit photosynthesis, and induce oxidative stress (Foy et al., 1978; Schuerger et al., 2003).

The potential for heavy metal uptake in vegetation depends on the strength of soil adsorption as well as root exudation (Rout & Das, 2003). Elements may also be transported through reworking by soil organisms (Ustin et al., 1999). Heavy metal toxicity in plants is mainly concerned with metal movement from soil to root, and metal absorption and translocation (Rout & Das, 2003). General symptoms of heavy metal contamination include reductions in plant canopies and leaf chlorophyll concentrations, plant stunting, leaf chlorosis, poorly developed root systems, and general growth inhibition (Foy et al., 1978; Rout & Das, 2003; Schuerger et al., 2003; Ustin et al., 1999).

2.4 PRINCIPALS OF SPECTROSCOPY

Spectroscopy is referred to as the study of light and other radiation as a function of wavelength that has been emitted, reflected, or scattered from a solid, liquid, or gas (Clark, 1999; Liang, 2004). It is based on the interaction of electromagnetic radiation with matter, and provides a precise analytical method for finding the constituents in material having an unknown chemical composition (Clark, 1999). Spectroscopy utilizes

ultraviolet (UV), visible (VIS), near-infrared (NIR), and infrared (IR) light for chemical analysis based on the extinction of light of a certain wavelength reflecting, absorbing, or transmitting through a sample (Liang, 2004; Milton et al., 2007). The energy-matter interactions in the UV, VIS, NIR and IR wavelength regions can be used for qualitative and quantitative analysis of chemical compounds and mixtures (Clark, 1999; Liang, 2004). For instance, through the use of field and lab spectroscopy, the effects of minute concentrations of trace heavy metal elements in vegetation can be detected through their emission spectrum (Kooistra et al., 2003; Schuerger et al., 2003).

The electromagnetic spectrum is divided into various regions according to the properties of the electromagnetic radiation. The subdivision of the electromagnetic spectrum is illustrated in Figure 4. Most spectrometers cover the UV, VIS, NIR, and IR wavelength regions, and have a spectral resolution of two to ten nanometres in the 350 to 2500 nm wavelength region (Milton et al., 2007). Field and laboratory spectrometers have been used for quantitative analysis in process monitoring and qualitative analysis of organic molecules for several decades and have become exceedingly useful in the detection of contaminated vegetation and soils (Milton et al., 2007; Schuerger et al., 2003).

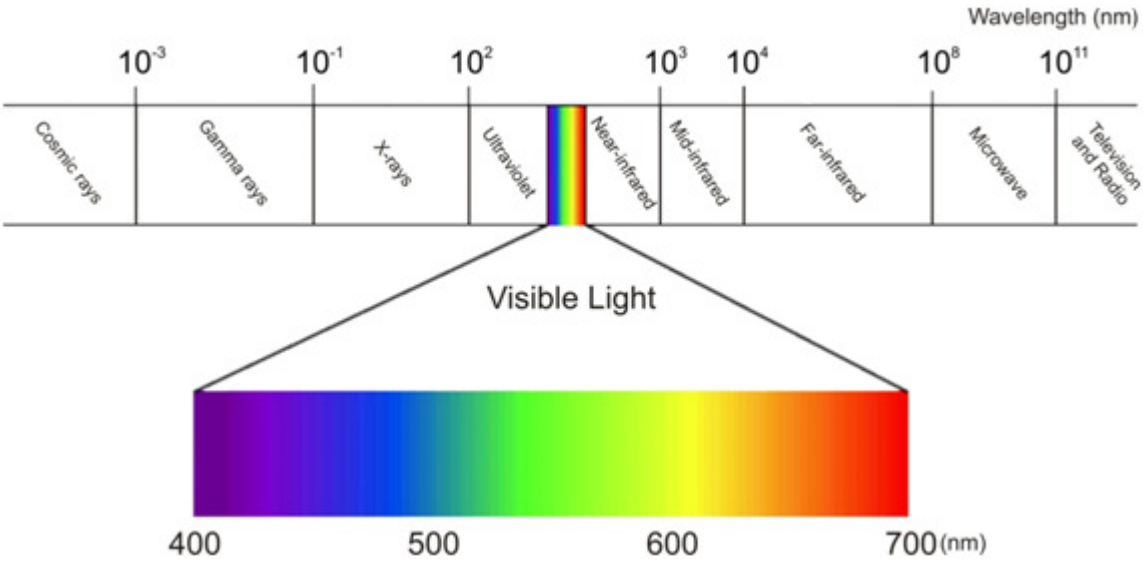

Figure 4 – The electromagnetic spectrum (adapted from Jensen, 2000)

Field and laboratory spectroscopy predates the development of airborne spectrometry as the sensing instrument can remain fixed over the area of interest which was technically less challenging. In contrast, airborne imaging spectrometers (or hyperspectral imagers) have to measure a considerably larger area which in itself is significantly more complicated (Jensen, 2000; Lagacherie et al., 2007; Milton et al., 2007).

A large range of surface cover materials have diagnostic adsorption features in the 350 to 2500 nm spectrum that are 20 to 40 nm wide (Hunt, 1980). Depending on the adsorption and reflection properties of the surface material, and the wavelength of the incident radiation, the reflected radiation typically shows characteristic absorption features (Green et al., 1998). This enables hyperspectral systems the ability to produce high resolution data for the identification of those materials (Goetz et al., 1983).

When taking laboratory spectroscopy measurements, the environmental conditions are usually controlled and optimized to the most favourable conditions for measurement. In contrast, airborne and field spectroscopy are most widely used to measure the reflectance of composite surfaces *in situ* and are carried out in uncontrolled environments. Target materials, atmospheric disturbances, and varying water vapour content are all characteristic factors in an uncontrolled environment and present data acquisition, processing, and interpretation challenges (Jensen, 2000; Milton et al., 2007).

The transfer of relationships established at the laboratory level up to higher scales such as field and airborne imaging spectroscopy also poses a number of problems associated with sensor characteristics such as spectral and spatial resolution, radiometric calibration, and atmospheric effects. These factors must be accounted for when calibrating hyperspectral data and field spectrometers (Lagacherie et al., 2007).

To describe the capabilities of spectrometers, five general system parameters are outlined in Table 5, including spectral operating range, band number, spectral resolution, signal-to-noise ratio, and radiometric resolution.

Table 5 – Key spectrometer parameters

System Parameter	Description
Spectral range	The spectral range of a spectrometer is characterized by the range of wavelengths it covers. Depending on the instrument, most spectrometers have a wavelength region from 350 to 2500 nm (Milton et al., 2007). Few imaging spectrometers acquire data in the spectral bands around the 1.4 (±0.05) µm and 1.9 (±0.05) µm as these are atmospheric water vapour adsorption bands (Jensen, 2000).
Spectral resolution	The spectral resolution or spectral bandwidth is defined by the dimension of specific wavelength intervals in the electromagnetic spectrum to which an instrument is sensitive (Clark, 1999; Jensen, 2000). The narrower the spectral bandwidth, the narrower the adsorption feature the spectrometer will measure accurately, provided that there are enough adjacent spectral samples (Clark, 1999). To discern minute adsorption features in surface materials, it is necessary to sample the spectrum over very short intervals. Many spectrometer systems sample at 2 - 10 nm wide (Milton et al., 2007). Bandwidths greater than 25 nm often lose the ability to detect important adsorption features (Clark, 1999).
Band number	Most systems have between 100 – 300 spectral bands (Milton et al., 2007). However, the bandwidth or spectral resolution is a function of the band number as many systems sample in selected wavelength regions that have only 20 – 50 spectral bands (Jensen, 2000).
Signal-to-noise ratio	The signal-to-noise (SNR) ratio is considered the ratio of the radiance to the noise created by the detector and the instrument (Liang, 2004). The SNR is dependent on the detector sensitivity, spectral resolution, and intensity of the light reflected or emitted from the surface under study (Clark, 1999). Due to overall decreasing radiance intensity towards longer wavelengths and atmospheric interferences, the SNR for spectrometers is always wavelength dependent (Liang, 2004).
Radiometric resolution	Radiometric resolution is defined as the sensitivity of an instrument to differences in signal strength as it records the energy reflected or emitted from the surface (Jensen, 2000). Radiometric resolution is usually expressed in bits.

2.5 VEGETATION SPECTROSCOPY

2.5.1 Spectral Behaviour of Vegetation

Plant reflectance in the visible region of the spectrum is governed by the distribution and concentration of foliar pigments. Internal cell structure is the dominant factor in the near-infrared regions, and water content is the main factor affecting short-wave infrared reflectance (Figure 5) (Clevers et al., 2004; Silva et al., 2007). In addition to these factors, at the canopy level, the leaf area index (LAI), the amount of green biomass, and the leaf angle distribution, shape the spectral signature (Silva et al., 2007; Sridhar et al., 2007).

Increased leaf reflectance in the visible (380 – 760 nm) or infrared (760 – 2500 nm) spectra are generally leaf responses to environmental conditions that inhibit growth. Changes in plant health due to stress are usually accompanied by a decrease in leaf chlorophyll content. When a plant is stressed, differences in reflectance generally occur in the green and red spectra (535 – 640 nm and 685 – 700 nm wavelength ranges), and major sensitivity maxima occur in the orange and red spectra (near 620 nm and 700 nm) where the absorptivity of chlorophyll-*a* is relatively low (Carter, 1993).

In cases of low absorptivity, even the smallest decreases in chlorophyll content can result in significantly decreased absorption and increased reflectance (Gao & Goetz, 1994). Therefore, difference and sensitivity maxima can be explained by stress-induced decreases in chlorophyll-*a* content, which occur consistently in the blue spectrum and near 670 nm. Increased reflectance in the visible spectrum is the most consistent leaf reflectance response to plant stress. Consistent responses in infrared only occur when

stress has developed sufficiently enough to cause severe leaf dehydration or internal leaf damage (Carter, 1993).

The red-edge region is an important indicator of plant stress, and has been documented by several researchers including: Blackburn, 1999; Carter, 1993; Dawson & Curran, 1998; Demetriades-Shah et al., 1990; Horler et al., 1983; Kochubey & Kazantsev, 2006; Murphy et al., 2005; Smith et al., 2004; Tsai & Philpot, 1998; Ustin et al., 1999; and Woolley, 1971. The red-edge is the area where there is a sharp change in reflectance between wavelengths 690 and 750 nm. This reflectance region characterises the boundary between strong absorption of red light by chlorophyll, and high scattering of radiation in leaf mesophyll (Smith et al., 2004). A shift of the red-edge toward shorter wavelengths is usually a leaf reflectance response to plant stress (Lamb et al., 2002; Murphy et al., 2005).

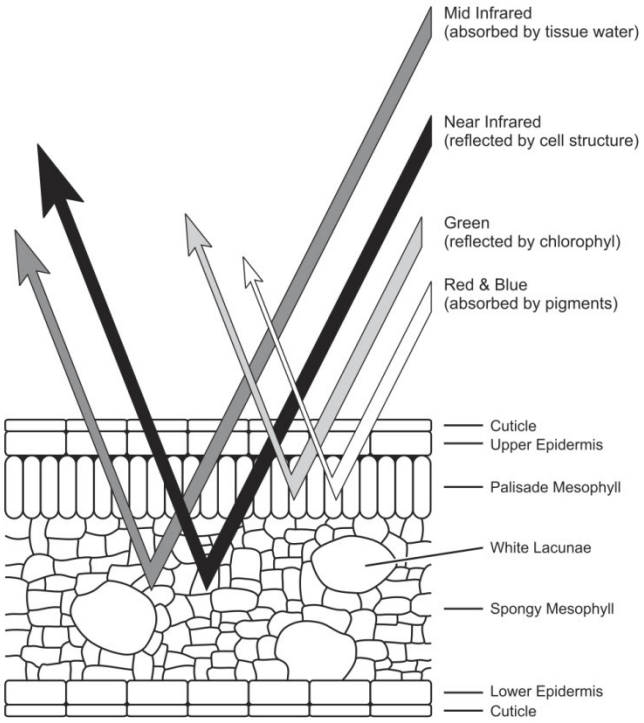

Figure 5 – Radiation interactions on a healthy green leaf. Arrow thickness is proportional to the magnitude of radiation fluctuation (Silva et al., 2007).

Liquid water is a major component of fresh, green leaves, accounting for 40 to 90% of its weight. This has a significant effect on the spectral behaviour of a plant. Two dominant water absorption bands appear at 1450 nm and 1950 nm, and two minor absorption bands attributed to water are observed at 975 nm and 1175 nm (Clark, 1999; Sridhar et al., 2007). However, other compounds, such as cellulose and lignin, have completely different reflective behaviours. For instance, the primary chlorophyll absorption bands in healthy green vegetation occur at 430 – 460 nm and 650 – 660 nm in the visible region (Clark, 1999; Gao & Goetz, 1994; Noomen et al., 2006). Because all plants are made of the same basic components, their spectra often appear similar. However, significant differences can be easily distinguished when analysing variations in

leaf water content. For instance, the spectral curves of healthy green vegetation, dry vegetation, and soil are illustrated in Figure 6.

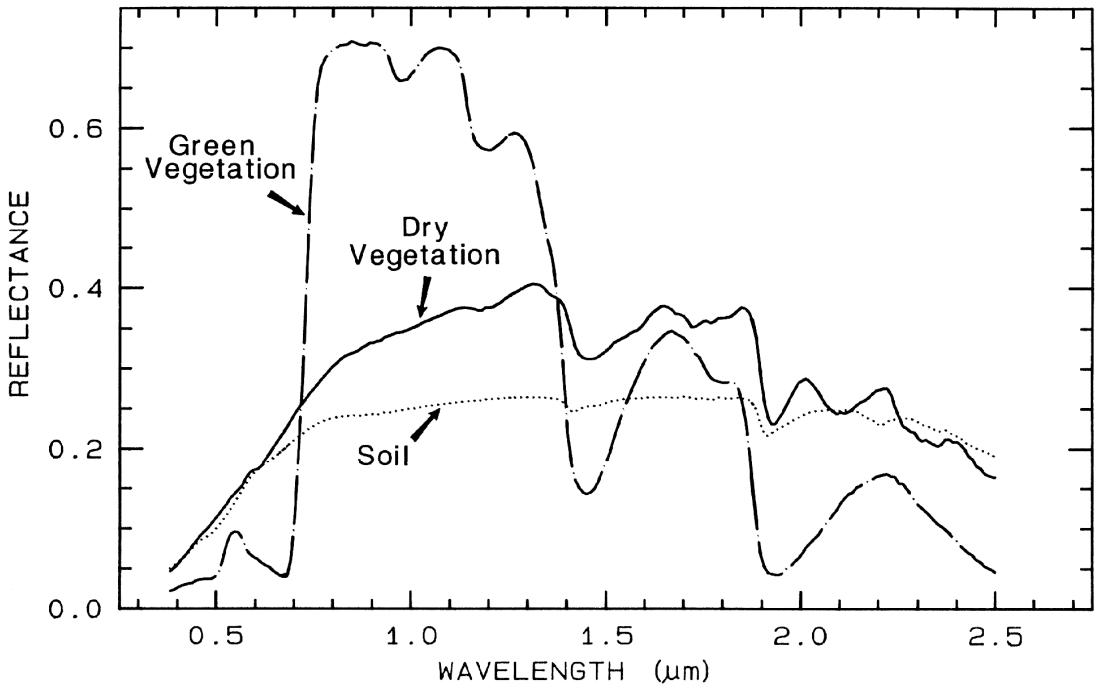

Figure 6 – Reflectance spectra of green photosynthetic vegetation, dry non-photosynthetic vegetation, and a soil (Clark, 1999). The primary chlorophyll absorption bands in healthy green vegetation occur at 0.43 – 0.46 μm and 0.65 – 0.66 μm in the visible region. Reflectance spectra at 0.975, 1.175, 1.450, and 1.95, μm are dominated by liquid water absorptions. Leaf reflectance is most likely to indicate plant stress in the sensitive 0.535 – 0.640 μm and 0.685 – 0.700 μm wavelength ranges.

2.5.2 Spectral Behaviour of Heavy Metal Contaminated Vegetation

As previously mentioned, the energy-matter interactions in the UV, VIS, NIR, and IR wavelength regions can be used for quantitative and qualitative analysis of chemical compounds and mixtures. However, when absorbed by vegetation, metals and most inorganics are almost incapable of absorbing electromagnetic radiation at these wavelengths. Therefore, metals and most inorganics absorbed by vegetation exhibit few characteristic absorption features, and are extremely difficult to identify in these

wavelength regions (Clark, 1999). Most studies have, therefore, focused on the detection of vegetation stress caused by increased heavy metal concentrations in soil (Clevers et al., 2004; Horler et al., 1980; Goetz et al., 1983; Kooistra et al., 2003; Kooistra et al., 2004; Schuerger et al., 2003; Schwaller et al., 1983; Sridhar et al., 2007).

Given that environmental stress induces modifications in the biochemical composition and physiology of vegetation, information on the degree of soil contamination may be determined by the change in vegetation reflectance spectra (Kooistra et al., 2003). According to Goetz et al. (1983), plant stress induced by heavy metal uptake will influence reflectance spectra at the leaf and canopy level. Traditionally, identification of plant stresses using spectrometry has been based upon changes in individual band intensities or changes in simple band ratios and indices (Schuerger et al., 2003). For example, a study conducted by Horler et al. (1980) applied spectral vegetation indices to investigate changes in plant stress due to soil contamination. Horler et al. (1980) found that as concentrations of heavy metals Cd, Cu, Pb, or Zn increased in plants grown in contaminated soils, leaf reflectance at visible wavelengths (475, 550, and 660 nm) increased and leaf reflectance at infrared wavelengths (850, 1600, and 2200 nm) decreased. This is consistent with studies conducted by Schwaller et al. (1983) and Schuerger et al. (2003).

Vegetation indices can be used to investigate changes in plant stress due to soil contamination (Horler et al., 1980; Kooistra et al., 2004; Schuerger et al., 2003). A vegetation index combines two or more spectral bands to enhance the vegetative signal while minimizing background effects (Kooistra et al., 2004). Canopy cover and chlorophyll content can be measured using the normalized difference vegetation index

(NDVI) or the ratio vegetation index (RVI) defined in Equation 1 and 2 respectively (Jensen, 2000; Schuerger et al., 2003).

$$NDVI = \frac{NIR - Red}{NIR + Red}$$

Where: Red and NIR stand for the spectral reflectance measurements acquired in the red (680 nm) and near-infrared (810 nm) regions.

Equation 1

$$RVI = \frac{R_{750}}{R_{700}}$$

Where: R stands for reflectance.

Equation 2

Typically, as plant stress increases, chlorophyll levels decrease, causing a reduction in NDVI and RVI values (Schuerger et al., 2003). However, plant species vary in their spectral response, and geographical variations such as sources of metal contamination and soil type also have an effect on the correlation between vegetation reflectance and metal concentrations (Horler et al., 1980). A decrease in chlorophyll concentration can often be the result of a combination of other stresses, such as moisture loss and nutrient deficiency (Sridhar et al., 2007). Carter (1993) reported that a decrease in leaf water content generally increased reflectance throughout the entire 350 –2500 nm wavelength region.

For instance, although Schwaller et al. (1983) had consistent results with Horler et al. (1980), they argued that the variations in absorption of heavy metal contaminated vegetation were the result of changes in leaf water content. Schwaller et al. (1983) found that plants treated with excess heavy metals had a tendency to have a lower transpiration rate (higher stomatal resistance) than the same species under control conditions. They suggested that because the leaves of heavy metal treated plants had an increased stomatal

resistance, more water would be present in these leaves than in the leaves of controlled (non-heavy metal treated) plants when there was an abundance of available water. Consequently, results would show a decrease in the near infrared reflectance in the leaves of metal treated plants (Schwaller et al., 1983). In situations where water is limited, stomates of all plants close in response to water deficits, and plants with a better developed root system will be able to absorb and store more available water (Schwaller et al., 1983). A result of heavy metal contamination in vegetation is a poorly developed root system. Thus, Schwaller et al. (1983) proposed that under conditions of water deficits one would expect the leaves of control plants to contain relatively more water as their root system was able to absorb more, and consequently exhibit a lower NIR reflectance than the leaves of metal treated plants. Simply put, the more water in the leaf, the lower the leaf reflectance, due to water absorption of radiation (Schwaller et al., 1983).

To detect the leaf structural changes due to Zn accumulation, Sridhar et al. (2007) found that the ratio index, defined in Equation 3 closely correlated to the leaf structural changes and the content of Zn in vegetation.

$$Leaf\ Structure = \frac{R_{1110}}{R_{810}}$$ Where: R stands for reflectance. **Equation 3**

The index they used was not sensitive to chlorophyll concentration as both wavelengths were away from the red edge and within the spectral region sensitive to internal leaf structure. Sridhar et al. (2007) explained that the closure of stomata (stomatal resistance) associated with a higher Zn accumulation further increased the leaf internal scattering,

leading to a decrease in the NIR (800 – 1300 nm) spectral reflectance. They also concluded that the disintegration and decrease in the number of chloroplasts caused an increase in reflectance in the visible region, particularly around the chlorophyll absorption region. Figure 7 shows canopy *(a)* and leaf *(b)* reflectance spectra of four Zn treated plants and one control plant (T0); ZnT1 through ZnT4 indicate increasing levels of Zn content respectively.

For Zn treated plants, the spectra show a decrease in the 800 – 1300 nm, 1470 – 1850 nm and 2000 – 2400 nm regions. Leaves with high concentrations of Zn showed a decrease in chlorophyll absorption around 680 nm. These values all correlated to the general heavy metal induced plant reflectance values concluded by Horler et al. (1980) and Schwaller et al. (1983).

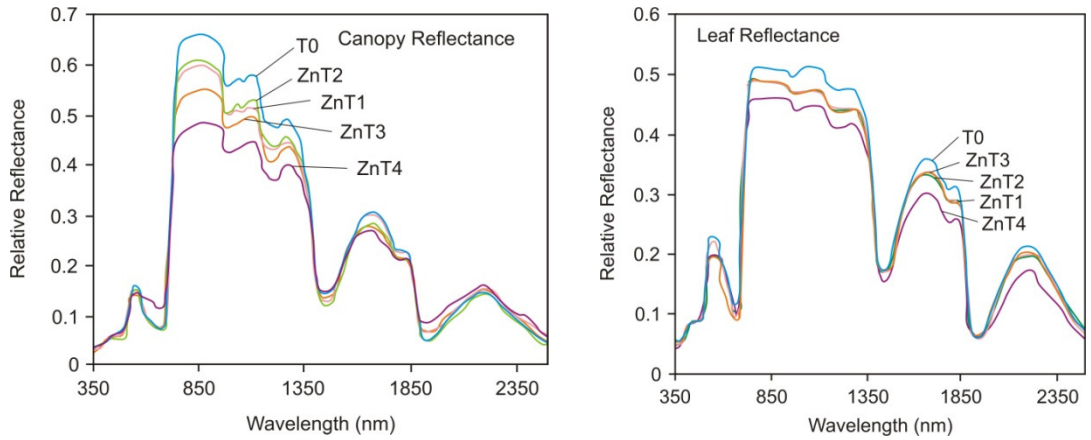

(a) *(b)*

Figure 7 – *(a)* Indicates averaged canopy level spectral reflectance of plants treated with Zn and one control. *(b)* Shows averaged leaf level spectral reflectance (adapted from Sridhar et al., 2007).

Chapter 3 Methodology and Field Study Procedures

3.1 STUDY AREA

In order to explore the influences of soil characteristics on corrosion, data were collected from three sites in the Lower Fraser Valley of south-western British Columbia, Canada. The study locations consist of three steel transmission towers that are all of similar ages, are located in areas with differing soil characteristics, and have common surrounding vegetation species.

The Lower Fraser Valley is characterised by a Pacific Maritime climate. High-pressure systems bring warm-dry conditions during the summer months, and low-pressure systems bring mild, wet weather during the winter (Krzyzanowski et al., 2005). Mean annual precipitation ranges from 850 mm in the west to 2000 mm in the eastern end of the Fraser River Valley and at higher elevations. Less than 10% of the annual precipitation falls as snow at sea level; however, this proportion increases significantly with elevation. The area has a mean annual temperature of 9˚C with a summer mean of 15˚C and a winter mean of 3.5˚C (Ecological Stratification Working Group, 1995).

A selection of study sites were identified by the British Columbia Transmission Corporation based on ease of access, age of transmission towers, and maintenance scheduling. From the selection, three sampling towers were selected along the same transmission line at various locations from Surrey to the Aldergrove area (north of 49˚N and approximately between 122 and 123˚W) in order to ensure that a range of soil types that occur in the Lower Fraser Valley were represented while minimizing variations in tower characteristics.

The research locations are identified as locations B, C and D (Figure 8). The A frame galvanized carbon steel transmission towers were all approximately 50 years old, stand 50 meters high, and each support an estimated 500 kilovolts of electrical transmission line.

A comprehensive assessment of the corrosive soil environments have included the following factors: temperature, pH, moisture content, soil resistivity, overlying plant spectral reflectance, and heavy metal content in both soil and vegetation.

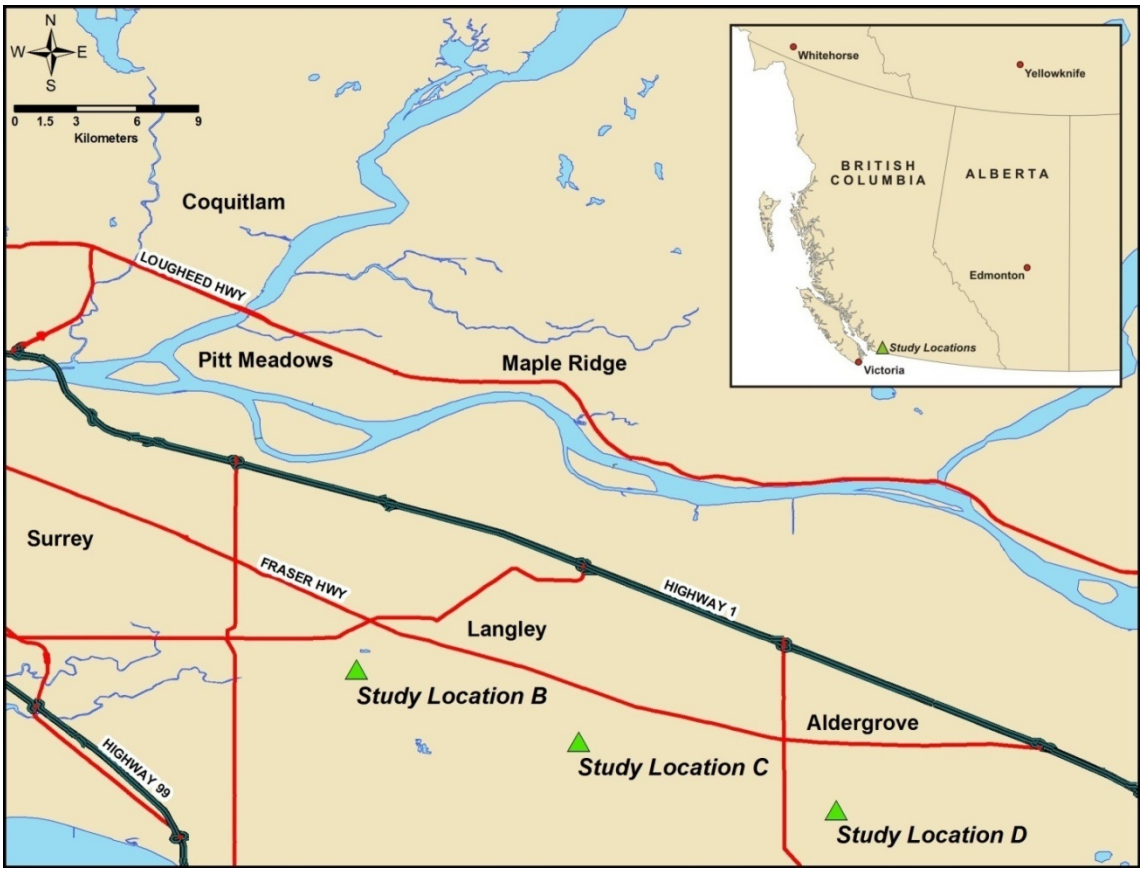

Figure 8 – Transmission tower study locations B, C, and D, Lower Fraser Valley, British Columbia, Canada

3.1.1 Location B – Tower 0153-03, Langley

Location B (Zone 10, 523250mE; 5437750mN; elevation 24 m) is located near the Langley/Surrey border in the residential park of Hi-Knoll off 196th Street. The tower is situated on a near level (0 – 0.5% gradient slope) open area and has a moderately dense mix of native and non-native vegetation with few bare soil areas. Dominant species consist mostly of *Rubus discolour* (Himalayan Blackberry), *Pteridium aquilinum* (Bracken), *Gaultheria shallon* (Salal), and tall overlying grasses.

According to soil survey map information (Luttmerding, 1980) and direct observation, the soil in the study site is classified as an Orthic Humo-Ferric Podzol (Lynden soils) developed from deep, course-textured (sandy) sediments, mainly glaciofluvial and some littoral deposits. The surface textures are generally a red-brown sandy loam, and subsurface textures are a medium to coarse sand with varying amounts of gravel and stone (Kelley & Spilsbury, 1939; Luttmerding, 1980).

Soils at location B are uncultivated, and are well to rapid drained. They have a high porosity, and have low water holding capacity and slow surface runoff (Luttmerding, 1980).

On July 7th, 2008, samples were collected beneath tower 0153-03. Field reconnaissance involved a full range of field data collection including: temperature and pH measurements, soil and vegetation sampling, resistivity measurements, field spectroscopy, and Plant Root Simulator (PRS™) probe placement (discussed below). On August 18th, 2008, after a 42 day burial, the PRS™-probes were unearthed. Resistivity testing was also conducted on November 5th, 2007, for multiple season comparison.

3.1.2 Location C – Tower 0148-02, East Langley

Location C (Zone 10, 530453mE; 5434055mN; elevation 80 m) is located southeast of the city of Langley, and situated directly beside an organic vineyard off 232nd Street. The tower is positioned on a moderately rolling (9 – 15% gradient slope) landscape with a dense mix of native and non-native vegetation. Dominant species consist mostly of *Rubus discolour* (Himalayan Blackberry), *Pteridium aquilinum* (Bracken), *Gaultheria shallon* (Salal), *Acer circinatum* (Vine Maple), *Alnus rubra* (Red Alder), and tall overlying grasses.

The soil in the study site is classified as a Podzol Gray Luvisol according to soil survey map information and direct observation (Luttmerding, 1980). The parent material was developed from moderately fine-textured, compact, glaciomarine deposits with few pebbles and stones, often mixed with variable amounts of silty, aeolian material at the surface (Luttmerding, 1980). The surface textures are generally a reddish-brown silt loam, with some variation to loam or silty clay loam. Subsurface textures are a silt loam or silty clay loam (Kelley & Spilsbury, 1939; Luttmerding, 1980).

Soils at location C are uncultivated, and are moderately well drained. They have a moderate porosity in the surface and subsurface layers, which decreases in the compact subsoil. Podzol Gray Luvisol soils have a high degree of moisture retention, and moderate to slow surface runoff, depending on the slope. A temporary, perched water table usually develops above the compact subsoil during periods of heavy rain. During this time, lateral (Telluric) seepage also occurs along the surface of the compact material. Telluric seepage is groundwater flow moving through the soil nearly parallel with the ground surface above a restricting or confining layer (Luttmerding, 1980).

Samples were collected beneath tower 0148-03 on July 14th, 2008. Field reconnaissance included: temperature and pH measurements, soil and vegetation sampling, resistivity, field spectroscopy, and PRS™-probe placement. After a 42 day burial, on August 25th, 2008, the PRS™-probes were collected.

3.1.3 Location D – Tower 0554-05, Aldergrove

Location D (Zone 10, 538781 mE; 5430754 mN; elevation 116 m) is located in Aldergrove situated on active farm land off 272nd Street. The tower is positioned on an undulating (2 – 5% gradient slope) landscape with a moderately dense mix of native and non-native vegetation. Dominant species consist mostly of *Rubus discolour* (Himalayan Blackberry), *Gaultheria shallon* (Salal), *Alnus rubra* (Red Alder), and tall overlying grasses.

The soil in the study site is classified as a Luvisolic Humo-Ferric Podzol according to soil survey map information and direct observation (Luttmerding, 1980). The parent material was developed from moderately fine to fine textured glaciomarine deposits. This is capped in some areas by up to 50 cm of medium-textured aeolian material. Surface and subsurface textures are a reddish brown silt loam while the subsurface grades to compact, dense, silty clay loam or silty clay. Varying amounts of gravel and stone with some iron concretions are present in the glaciomarine material (Kelley & Spilsbury, 1939; Luttmerding, 1980). Soils directly beneath the tower are uncultivated; however, control sites around the tower were in cultivated soils on active farm land.

Luvisolic Humo-Ferric Podzol soils are moderately well to well drained. They have a moderate porosity in the surface and subsurface, which decreases in the compact subsoil.

The soils also have a high degree of water retention, and slow to moderate surface runoff, depending on the steepness of the slope. Temporary, perched water tables develop above the compact, dense subsoil during periods of heavy precipitation, and lateral (Telluric) seepage occurs in this zone during these periods (Luttmerding, 1980).

Samples were collected beneath tower 0554-05 on July 21st, 2008. Field reconnaissance included: temperature and pH measurements, soil and vegetation sampling, resistivity, field spectroscopy, and PRS™-probe placement. On September 2nd, 2008, after a 43 day burial, the PRS™-probes were collected.

3.2 EXPERIMENTAL DESIGN

A sampling strategy was developed on the assumption that areas closer to the tower legs would invariably have higher concentrations of corrosion by-products (Figure 9).

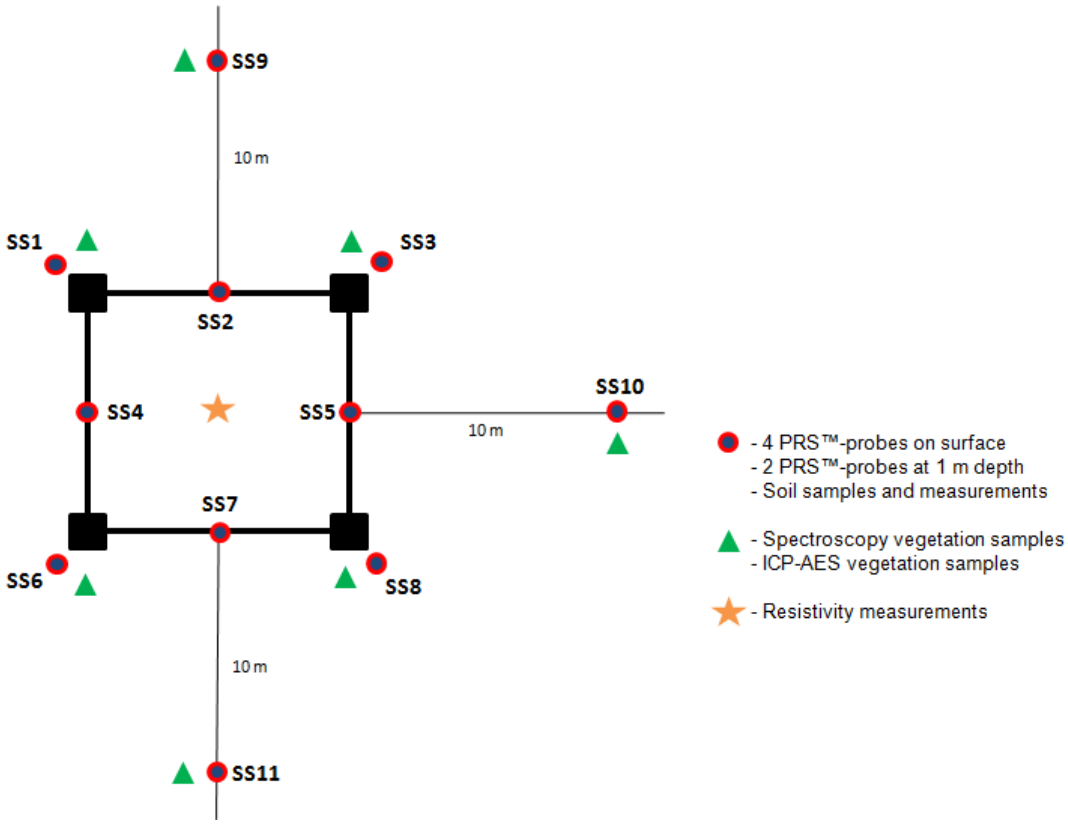

Figure 9 – Sampling diagram for transmission tower study locations B, C, and D

The tower footings stand approximately 7.40 m apart. Vegetation and soil samples were collected along three transects at 10 m originating between the tower footings; two in opposing slope directions, and one for base control perpendicular to the other transects. Samples were also collected beneath the tower, halfway between the footings, and at each tower leg.

At each sample site (SS), soil samples, temperature and pH data were collected at the surface, and at a depth of approximately 1 m. PRS™-probes were also placed at the surface of each site, and at a depth of approximately 1 meter as indicated by the red/blue circles in Figure 9. A common species of vegetation sample was also collected at the

surface of each sample site. At all three locations, *Rubus discolour* (Himalayan Blackberry) was the common plant species.

3.3 SOIL AND VEGETATION ANALYSES

Soil temperature and pH were measured *in situ* at each sample site using a Spectrum Technologies, Inc. IQ 150 pH meter (Plainfield, Illinois, USA). Soil resistivity has a direct impact on the degree of corrosion in an underground environment, and was measured using an AEMC 6470 soil resistance tester (AEMC Instruments, Foxborough, Massachusetts, USA). Lab analysis was conducted on the soil samples for moisture content using the air-dry subtraction method suggested by Tan (2005). Soil samples were oven dried for 24 to 48 hours at 110˚C, then calculated for the percentage of moisture content.

3.3.1 Plant Root Simulator™ Probes

Plant Root Simulator (PRS™) probes (Western Ag Innovations Inc., Saskatoon, Saskatchewan, Canada) equipped with ion-exchange membranes treated with sodium bicarbonate ($NaHCO_3$) were used to assess nutrient supply rates by continuously adsorbing charged ionic species while in soil. A PRS™-probe consists of either an anion or cation exchange resin membrane enclosed in a plastic encasement (Figure 10). The accumulation of nutrients on the ion-exchange membrane during the burial period can be considered as an estimate of the potential nutrient supply rate to an adsorbing surface such as a plant root (Huang & Schoenau, 1996).

The probes are used to make *in situ* measurements of all nutrient ions simultaneously including Fe, Zn, and S as well as many other elements and contaminants. PRS™-probes act as an ion sink to adsorb any ionic species that are supplied by the soil over time, with minimal soil disturbance. They are effective in tracking the active availability of soil nutrients and toxins to plants.

Figure 10 – A PRS™-probe pair consists of one cation (orange) and one anion (purple) probe. Each probe is 15 X 3 cm and has an adsorbing surface area of 17.5 cm^2 (includes both sides).

Anion exchange membranes were used to measure quantities of nitrate (NO_3^-), hydrogen or dihydrogen phosphate (HPO_4^{2-} or $H_2PO_4^-$), sulphate (SO_4^{2-}) and borate (BO_3^-). Cation exchange membranes adsorbed potassium (K^+), calcium (Ca^{2+}), magnesium (Mg^{2+}), and ammonium (NH_4^+) from soil solution. Micronutrient polyvalent cations manganese (Mn^{2+}), iron (Fe^{2+}), nickel (Cu^{2+}), aluminum (Al^{3+}), and zinc (Zn^{2+}) were also measured. Therefore, in addition to $NaHCO_3$, a chelating pre-treatment of the anion membrane was employed with ethylenediaminetetraacetic acid (EDTA). The

chelating agent on the anion exchange membrane is required as the adsorbed agent forms complexes with these metal ions (Western Ag Innovation Inc., 2006).

The longer the probes are left in the soil, the greater the likelihood of measuring highly accurate nutrient availability data (Western Ag Innovations Inc., 2006). Therefore, each probe was left in the soil for the manufacture's recommended period of 42 days, revealing a suitable record of nutrient and toxin concentrations. Once unearthed, the probes were sent back to Western Ag Innovation Inc. for chemical analysis. PRS™-probe analysis provides a complete record of potential vegetation uptake, and can be used as an indicator of soil contaminates. Ion supply rates from the PRS™-probes are measured as the amount of nutrient adsorbed per amount of adsorbing surface area per entire time of burial in the soil (µg ion/10 cm^2/length of burial) (Western Ag Innovations Inc., 2006).

3.3.2 PRS™-probe Protocols and Procedures

The PRS™-probes were vertically inserted into the soil to a depth of approximately 15 cm to ensure complete soil contact with the membrane. At each sample site, two PRS™-probe pairs were installed on the surface, and one PRS™-probe pair was installed at the bottom of an approximately 1 m deep hole. The hole was then covered using a block of wood and surrounding soil to ensure the probes remained undisturbed.

Since plant roots act as a strong sink for nutrients, root competition is a potential problem. Therefore, it is often necessary to use a root exclusion cylinder (REC) such as a PVC or aluminum pipe placed around the PRS™-probes to ensure competition for nutrients is prevented (Western Ag Innovation Inc., 2006). However, the soils in these

areas were often too compact to install root exclusion cylinders. Therefore, as an alternative, a deep slit was cut around the radius of the PRS™-probes to prevent root competition. By using this method, the net mineralization nutrient supply rate can be measured rather than the surplus nutrient supply rate (Western Ag Innovation Inc., 2006).

The buried PRS™-probes were removed then immediately rinsed and scrubbed clean with deionized water to remove adhering soil. After cleaning, the PRS™-probes were placed in clean polyethylene bags, transported on ice to the lab, and stored in a refrigerator until shipment to Western Agriculture Innovation Inc. for analysis.

Thirteen nutrient ions were measured with the PRS™-probes and eluted with a 0.5M HCl extraction. The two PRS™-probe surface pairs (per site) were eluted together, and the same was done for the single PRS™-probe depth pair (per site). The analysis for levels of nitrate (NO_3^-) and ammonium (NH_4^+) was done using an automated colourimetry (FIA Lab 2600). Other nutrients (PO_4^{2-}, SO_4^{2-}-S, BO_3^-, K^+, Ca^{2+}, Mg^{2+}, Fe^{2+}, Mn^{2+}, Al^{2+}, Cu^{2+}, and Zn^{2+}) in the eluate were measured by an inductively coupled plasma spectrophotometer (IRIS Intrepid II XSO, Thermo Scientific) (Western Ag Innovation Inc., 2006).

3.3.3 ICP-AES Analysis

Heavy metal content analysis was conducted on sampled tower vegetation using an Inductively Coupled Plasma Atomic Emission Spectrometer (ICP-AES) by Dr. Doug Maynard at the Chemical Services Laboratory, Pacific Forestry Center, Victoria, British Columbia in May 2009. An ICP-AES is capable of analysing trace multi-elements including a large range of metals and non-metals often at the part per trillion level. The

ICP-AES achieves this level of precision by using inductively coupled plasma to produce excited atoms and ions that emit electromagnetic radiation at wavelengths characteristic of a particular element. The intensity of the wavelength emission corresponds to the concentration of the element within a sample (Newman, 1996).

Three to five healthy, average sized, normal shaped *Rubus discolour* (Himalayan Blackberry) leaves were harvested manually from each sample site. The leaves were then placed in open paper bags, and allowed to air-dry for two months. The samples were then macerated with mortar and pestle and placed in small closed plastic containers. The foliar samples were then oven dried at 70˚C, and 1 mm of material from each sample site was digested using a 1200 watt high throughput microwave digestion method that utilizes nitric acid, hydrogen peroxide, and hydrochloric acid (Kalra et al., 1989; White & Douthit, 1985). Ten elements (Al, B, Ca, Fe, K, Mg, Mn, Na, P, and Zn) were then determined using a Thermo Fisher 6500 DUO Inductively Coupled Plasma Sequential Spectrometer. A LECO CNS-2000 Elemental Analyzer was used to analyze carbon, nitrogen, and sulphur content from the samples.

3.4 SPECTRAL ANALYSES

Using a field spectrometer, reflectance spectra of overlying vegetation beneath the towers were recorded at the sites indicated by a green triangle in Figure 9. Due to the electrical interference on the field spectrometer associated with working beneath a 500 kV electrical transmission tower, vegetation samples were collected and transported to a safer, nearby location for analysis.

Prior to the measurements, the instrument was allowed to warm up for a minimum of 60 minutes. Samples were arranged in bundles to simulate canopy reflectance and placed on a black platform. Each bundle was measured using an Analytical Spectral Devices, Inc. (Boulder, Colorado, USA) full range FieldSpec Pro field spectrometer between 11:00 am and 2:00 pm during clear atmospheric conditions so as to allow for optimal solar illumination (Jensen, 2000). To prevent shadows and maximize sample illumination, the sensor was oriented at an angle of 10 to 15˚ off the vertical, and at a distance of approximately 5 to 6 cm from the sample. Data were recorded throughout the 350 to 2500 nm wavelength range with a spectral resolution of 3 nm at 700 nm, 10 nm at 1400 – 2500 nm, and with a sampling interval of 1.4 nm between 350 and 1050, and 2 nm between 1050 and 2500 nm (ASD Inc., 2008; Murphy et al., 2005; Smith et al., 2004; Zarco et al., 2003). The results were then interpolated by the ASD software to produce readings at every 1 nm. Radiance reflected from each vegetation bundle was divided by radiance reflected from a white reference to compute reflectance. Spectral values were measured ten times for each sample and then averaged to overcome individual variations (Clark, 1999). From these readings, spectra were created for the associated sampling site.

3.4.1 Spectral Processing

A series of spectral analyses were performed on the field spectroscopy data using Microsoft® Excel® 2007 (Microsoft Corp., Redmond, Washington, USA) including: a Normalized Difference Vegetation Index, structural band ratio R_{1110}/R_{810}, water band ratio R_{900}/R_{970}, first order derivative analysis, and a continuum removal.

3.4.1.1 Normalized Difference Vegetation Index

A Normalized Difference Vegetation Index (NDVI) was applied to the acquired spectral data as it is a red-edge based index that is often used to detect healthy green vegetation (Equation 1) (Sridhar et al., 2007). NDVI was used as an indicator of changes in the amount of green biomass and chlorophyll content (Jensen, 2000).

NDVI is sensitive not only to chlorophyll concentration, but also to changes in cellular structure (Sridhar et al., 2007). The red-edge is the region of vegetation spectra where an abrupt reflectance change occurs at 690 to 750 nm. It is produced by the combination of strong absorption of chlorophyll in the red region and strong reflectance in the infrared region due to mesophyll scattering, and the lack of absorption by pigments in the leaf (Dawson & Curran, 1998; Smith et al., 2004; Ustin et al., 1999; Woolley, 1971). The position of the red-edge can be used as an indicator of stress and senescence of vegetation (Dawson & Curran, 1998; Horler et al., 1983; Ustin et al., 1999).

3.4.1.2 Structural Band Ratio R_{1110}/R_{810}

Since high levels of heavy metals often affect internal leaf structure, the ratio index R_{1110}/R_{810} was used to indicate foliar structural changes in the vegetation that have accumulated heavy metals. The reflectance within this range is mainly governed by the internal structure and biochemical composition of the leaf rather than the foliar pigment concentration (Sridhar et al., 2007). For example, according to Sridhar et al. (2007,) higher concentrations of Zn should give higher R_{1110}/R_{810} values.

3.4.1.3 Water Band Ratio R_{900}/R_{970}

The ratio of R_{900}/R_{970} was also used to distinguish differences in water content as suggested by Sims and Gamon (2003). The vegetation with higher concentrations of heavy metals should show a decrease in this ratio compared to the control (Sridhar et al., 2007).

3.4.1.4 First Order Derivative Analysis

First order derivative spectra from 400 to 780 nm were calculated using 1 nm intervals. Several studies have documented the usefulness of derivative spectra for estimating chlorophyll content and plant stress in vegetation (Blackburn, 1999; Demetriades-Shah et al., 1990; Horler et al., 1983; Kochubey & Kazantsev, 2006; Murphy et al., 2005; Smith et al., 2004; Tsai & Philpot, 1998). A commonly used approximation of the first derivative is defined in Equation 4 (Dawson & Curran, 1998; Hatchell, 1999). The derivative is the instantaneous rate of change of the reflectance with respect to wavelength. Derivatives often highlight changes in position and amplitude of the reflectance spectra, and are useful for separating out peaks of overlapping bands (Elvidge & Chen, 1995; Hatchell, 1999; Penuelas et al., 1994).

$$D_{\lambda(i)} = \frac{R_{\lambda(j+1)} - R_{\lambda(j)}}{\Delta\lambda}$$

Where: $D_{\lambda(i)}$ is the first-difference transformation at a wavelength *i* midpoint between bands *j* and *j+1*. $R_{\lambda(j)}$ is the reflectance at the *j* band, $R_{\lambda(j+1)}$ is the reflectance at the *j +1* band and $\Delta\lambda$ is the difference in wavelengths between *j* and *j+1*.

Equation 4

Derivatives can be used to facilitate the location of critical wavelengths such as the red-edge (see above) (Dawson & Curran, 1998; Demetriades-Shah et al., 1990). The red-

edge is the area where there is a sharp change in reflectance between wavelengths 690 and 750 nm. This reflectance region characterises the boundary between strong absorption of red light by chlorophyll, and high scattering of radiation in leaf mesophyll (Smith et al., 2004). When the first order derivative analysis is applied, the red-edge shows a peak or inflection point which can be used to describe changes due to stress (Horler et al., 1983; Murphy et. al, 2005; Smith et al., 2004; Tsai & Philpot, 1998). This red-edge inflection point (REIP) is the wavelength of maximal slope in reflectance between the red and NIR wavelengths. It has been documented to be highly correlated with chlorophyll content in individual leaves and at the canopy level (Blackburn, 1999; Murphy et al., 2005). There is a broadening and deepening of chlorophyll absorption centred at approximately 680 nm as the amount of chlorophyll increases. This causes the REIP to shift to longer wavelengths (Lamb et al., 2002; Murphy et al., 2005). Using the first order derivative, the REIP can be obtained by identifying the position of the wavelength peak between 680 nm and 750 nm in the derivative reflectance (Horler et al., 1983).

3.4.1.5 Continuum Removal

Since chlorophyll absorption occurs at 430 – 460 and 650 – 660 nm, continuum removal was applied on the Himalayan Blackberry spectra between 400 and 550 nm and between 550 and 750 nm (Clark, 1999; Gao & Goetz, 1994; Noomen et al., 2006). The continuum removal was conducted in these spectral regions utilizing the equations explained below.

There are two components of absorption in a spectrum: individual features and continuum. The continuum refers to the background absorption signal unrelated to specific absorption features of interest (Clark, 1999). This background absorption or continuous spectrum is the result of a combination of all the scattering and absorbing characteristics of a material under study (Ustin et al., 1999). By creating a common baseline, the continuum removal process normalizes reflectance spectra in order to allow comparison of individual absorption features (Clark, 1999; Ustin et al., 1999). An analysis of continuum removed radiance spectra may illustrate minute differences in stressed vegetation samples (Ustin et al., 1999). Continuum removed spectra have been used in the detection of plant stress and species mapping, leaf water content analysis, mineral comparison, and vegetation contamination (Clark, 1999; Curran et al., 2001; Kokaly & Clark, 1999; Noomen et al., 2006; Ustin et al., 1999).

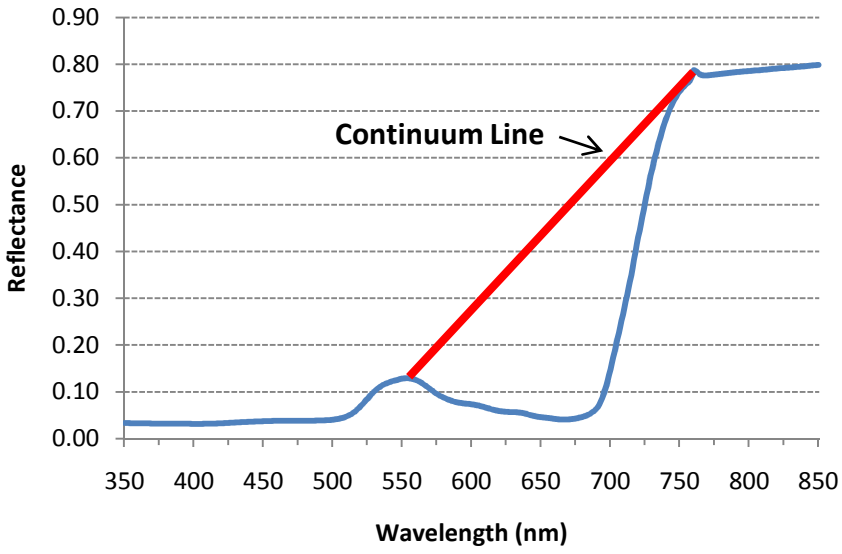

Figure 11 – Continuum removal on the red absorption region

To establish a continuum line, a convex hull is fitted over top of a spectrum to connect local spectrum maximum (Figure 11) (Kokaly & Clark, 1999; Ustin et al., 1999). By dividing the original reflectance values in the absorption pit ($R_{(\lambda)}$) by the value of the hull or continuum line ($Rc_{(\lambda)}$) at that wavelength, a relative continuum removed reflectance value for the absorption between 0 and 1 can be obtained (Equation 5) (Clark & Roush, 1984; Kokaly & Clark, 1999; Noomen et al., 2006).

$$R'_{(\lambda i)} = \frac{R_{(\lambda i)}}{Rc_{(\lambda i)}}$$

Where: $R'_{(\lambda i)}$ is the continuum removed reflectance at i wavelength, $R_{(\lambda i)}$ is the original reflectance values in the absorption pit, and $Rc_{(\lambda i)}$ is the continuum line (convex hull). **Equation 5**

After the continuum removal is applied, the continuum removed reflectance ($R'_{(\lambda)}$) is subtracted from 1 to calculate the band depth ($BD_{(\lambda)}$) at each wavelength in the absorption feature (Equation 6) (Kokaly & Clark, 1999; Noomen et al., 2006). The band depth implies the amount of light absorbed by the reflectance feature under study (Clark & Roush, 1984). Noomen et al. (2006) found that lower chlorophyll concentrations caused higher reflectance, and a decrease in band depth in the red region.

$$BD_{(\lambda i)} = 1 - R'_{(\lambda i)}$$

Where: $R'_{(\lambda i)}$ is the continuum removed reflectance at i wavelength and $BD_{(\lambda i)}$ is the band depth. **Equation 6**

Once the band depth is calculated, a normalization procedure using band ratios can be done to minimize the effects of atmospheric absorptions, leaf absorption features (such as water), and even soil background. Normalization also enhances differences in the shape

of the absorption features (Noomen et al., 2006). The normalized band depth ratio ($BDR_{(\lambda)}$) is calculated by dividing the band depth ($BD_{(\lambda)}$) at a certain wavelength by the band center or maximum depth from that absorption feature (D_c) (Equation 7) (Kokaly & Clark, 1999; Noomen et al., 2006).

$$BDR_{(\lambda i)} = \frac{BD_{(\lambda i)}}{D_c}$$

Where: $BDR_{(\lambda i)}$ is the normalized band depth at i wavelength, $BD_{(\lambda i)}$ is the band depth, and D_c is the band center or maximum depth in the absorption feature. **Equation 7**

From the continuum removal, several key geometric absorption variables can be derived including: band symmetry, total area of absorption, left area, right area, and band depth center. While these variables contain important absorption information, they are also highly correlated which may cause statistical confusion in the differentiation of some spectral features. This is further discussed in the next section.

3.5 STATISTICAL ANALYSES

Statistical analyses were performed using SPSS version 13.0 software (SPSS Inc., Chicago, Illinois, USA, 2004). A lower significance value decreases the probability of making any Type II errors. Therefore, all tests were conducted using a confidence interval of 95%, or $\alpha = 0.05$, and the critical region is divided equally between two tails of the test statistic.

3.5.1 Soil Statistical Analysis

Soil statistical analysis focussed on fifteen variables from soil data collected at each study location. Table 6 outlines the variables included in each location data set.

Table 6 – Variables included in soil analysis of transmission tower corrosion

Variable	Description
Depth	Sample designation for surface and 1 metre depth. Samples on the surface are labelled with a 1, and samples at a 1 metre depth are labelled with a 0.
Site	Tower site versus control site designation. Samples located directly beneath the transmission tower are labelled with a 1, and samples taken from the control areas are labelled with a 0.
MC	Moisture Content (%) was collected through laboratory analysis conducted on soil samples using an air-dry subtraction method suggested by Tan (2005).
Temp_Avg	Temperature (˚C) was measured *in situ* using a Spectrum Technologies, Inc. IQ 150 pH meter. Three values were collected at each sample site and an average was calculated.
pH_Avg	pH was measured *in situ* using a Spectrum Technologies, Inc. IQ 150 pH meter. Three values were collected at each sample site and an average was calculated.
Zn, Tot_N, NO3, Ca, Mg, K, P, Fe, Mn, B, S, and Al	Zinc (Zn), Total Nitrogen (Tot_N), Nitrate (NO3), Calcium (Ca), Magnesium (Mg), Potassium (K), Phosphorus (P), Iron (Fe), Manganese (Mn), Boron (B), Sulphur (S), and Aluminum (Al) levels were collected using PRS™-probes (µg ion/10 cm^2/42 days).

To better understand the complex data interactions, data sets from each study location can be broken down into four different segments. For example, consider the data set from location B seen in Table 7. The blue highlighted section indicates the study sites from directly beneath the tower. The orange highlighted section indicates the control sites. The red highlighted areas indicate the study sites located on the surface, and the non-highlighted areas indicate the study sites located at a depth of approximately 1 metre.

Table 7 – Location B data set

Sample	Depth	Site	MC	Zn	Tot_N	NO3	Ca	Mg	K	P	Fe	Mn	B	S	Al	Temp _Avg	pH_ Avg
SS1	1	1	17.96	222.20	71.00	71.00	858.60	241.20	570.40	2.80	7.00	.80	1.20	8.80	51.80	19.77	5.85
SS1	0	1	8.10	3.20	4.00	4.00	131.60	30.60	221.40	1.60	5.80	.60	.80	6.60	55.00	17.27	5.64
SS2	1	1	17.08	273.40	71.20	71.20	234.20	38.40	166.60	4.00	5.20	1.00	2.20	16.60	54.00	18.70	5.40
SS2	0	1	8.53	25.60	3.20	3.20	60.60	3.00	36.60	2.00	7.80	.60	.80	8.80	62.20	16.20	5.35
SS3	1	1	12.84	453.60	540.20	540.20	871.00	237.40	474.60	2.60	8.00	4.40	.80	123.00	64.20	20.63	5.56
SS3	0	1	13.65	19.40	51.20	51.20	135.20	20.00	158.00	2.40	7.00	.40	1.80	8.40	64.60	17.53	5.61
SS4	1	1	20.82	286.20	181.80	181.80	465.20	129.20	848.20	7.00	5.20	3.40	1.20	29.40	51.00	19.93	5.67
SS4	0	1	9.79	31.20	41.60	41.60	129.00	7.20	68.00	3.00	10.20	.80	.80	21.40	79.20	16.50	5.54
SS5	1	1	21.54	392.80	408.80	408.80	714.60	88.60	207.60	5.80	12.00	3.80	1.20	18.60	66.00	20.20	5.35
SS5	0	1	10.13	42.40	19.00	19.00	152.40	14.40	29.80	3.00	8.40	.80	.80	7.20	54.60	16.80	5.47
SS6	1	1	23.63	103.80	78.20	78.20	1053.40	244.20	265.40	4.80	5.80	1.40	1.60	14.00	57.60	18.77	5.53
SS6	0	1	9.43	10.00	16.60	16.60	154.40	16.00	55.40	2.20	5.60	.60	.80	6.80	54.60	16.57	5.78
SS7	1	1	16.38	134.60	60.60	60.60	282.60	42.80	77.20	3.60	4.00	.80	1.00	22.00	40.60	21.00	5.50
SS7	0	1	8.54	50.40	18.00	18.00	128.80	12.00	38.60	2.40	7.60	.60	.80	14.00	61.60	17.27	5.54
SS8	1	1	10.41	56.80	32.60	32.60	388.80	99.80	158.80	1.40	4.00	.60	1.00	9.80	53.80	20.60	5.58
SS8	0	1	10.73	14.40	7.20	7.20	169.20	15.80	95.20	1.40	7.80	.60	1.40	9.20	79.60	17.03	5.45
SS9	1	0	6.05	.80	17.00	17.00	296.40	24.20	145.60	1.60	7.00	1.80	1.40	44.00	71.40	24.93	5.79
SS9	0	0	6.47	.60	8.20	8.20	62.60	4.20	16.20	2.80	9.20	.40	.60	7.80	71.80	19.23	5.48
SS10	1	0	20.86	10.00	1.60	1.60	588.60	171.00	645.60	1.80	5.20	1.40	1.20	14.20	51.20	19.40	5.75
SS10	0	0	7.77	1.20	3.00	3.00	122.60	7.40	41.40	2.00	8.60	.80	2.60	10.80	69.40	15.27	5.67
SS11	1	0	15.90	4.40	165.40	165.40	566.60	159.40	194.00	2.00	5.40	2.60	1.40	31.20	49.20	19.37	5.85
SS11	0	0	9.18	1.00	41.40	41.40	209.00	31.80	92.00	1.40	5.60	.60	.40	7.00	53.60	15.37	5.42

For the analysis to produce significant results, the relationship between tower and control segments, and surface and depth segments, needed to be examined. To achieve this, appropriate statistical methods that take the segments into account were applied.

If the populations of a data set under investigation violate one or more assumptions of a particular statistical method, the results of an analysis may be incorrect or misleading (Ritchey, 2008). Therefore, when evaluating the relationship between tower and control sites and surface and depth levels, independence, sampling techniques, distribution, and variance must be considered. For instance, although the tower sites and control sites are

technically independent of each other, they do not have equal sample sizes, and were not selected randomly. It is also assumed that the surface and depth samples are independent of each other to better distinguish the location between above ground and subsurface corrosion. The study sites below the transmission towers have 8 samples on the surface and 8 at depth for a total of 16 samples below each tower. The control sites consist of 3 samples on the surface and 3 at depth for a total of 6 samples. Violating statistical test assumptions may cause incorrect conclusions, and proper statistical methods must be selected accordingly.

To check for normality, the Kolmogorov-Smirnov (KS) Goodness-of-Fit test was conducted on the data (McGrew & Monroe, 2000). The results of the KS test show a departure of normality for several of the variables. To examine variance, a Levene's test was used (SPSS Inc., 2004; Ritchey, 2008). This test indicated unequal variances for several of the variables under study. Results of these two tests can be found in Appendix C.

Therefore to account for the lack of normality, the unequal sample sizes, and the unequal variance from the soil data, a non-parametric Mann-Whitney *U* statistic was performed using SPSS as an indicator of statistical difference (Mann & Whitney, 1947). Non-parametric tests provide an alternative series of statistical methods that require no or very limited assumptions about the data (Ritchey, 2008). The Mann-Whitney *U* test is one of the most commonly used non-parametric alternatives to the parametric two-sample difference of means test (McGrew & Monroe, 2000). However, the Mann-Whitney *U* test does not make any assumptions on the nature of the underlying distribution (except continuity). It is also especially useful for problems with small sample sizes that are not

necessarily normally distributed. This technique is possible because instead of using parameters like mean and variance, the Mann-Whitney *U* test uses ranks of sample observations to measure the magnitude of the differences in the ranked positions or locations between the two sets of samples (McGrew & Monroe, 2000). In addition, an independent samples t-test was used as a parametric indicator of statistical difference. Despite the possibility of Type I or II errors, the independent samples t-test was recorded as a contrast to the non-parametric Mann-Whitney *U* statistic.

3.5.2 ICP-AES Vegetation Statistical Analysis

Unlike the soil data, the thirteen variables (shown in Table 8) in the ICP-AES data set were found to be normally distributed after the Kolmogorov-Smirnov Goodness-of-Fit test. However, since the samples sizes are still unequal, the Mann-Whitney *U* statistic was also performed on the data set using SPSS. It is important to note that, since the ICP-AES data were collected from vegetation growing at the surface, only the relationship between tower and control segments can be examined.

Table 8 – Variables included in ICP-AES statistical analysis of transmission tower corrosion

Variable	Description
Site	Tower site versus control site designation. Samples located directly beneath the transmission tower are labelled with a 1, and samples taken from the control areas are labelled with a 0.
C, N, S, Al, B, Ca, Fe, K, Mg, Mn, Na, P, and Zn	Carbon (C), Nitrogen (N), and Sulphur (S) in percent (%). Aluminum (Al), Boron (B), Calcium (Ca), Iron (Fe), Potassium (K), Magnesium (Mg), Manganese (Mn), Sodium (Na), Phosphorus (P), and Zinc (Zn) levels in µg/g.

3.5.3 Spectroscopy Statistical Analysis

To determine if a relationship exists between Zn levels and vegetation spectral response, a series of correlation and regression analyses as well as an independent samples t-test and a Mann-Whitney *U* test were applied to NDVI, leaf structural spectral band ratio R_{1110}/R_{810}, water content spectral band ratio R_{900}/R_{970}, and Zn levels from both PRS™-probes and the ICP-AES. The five variables (NDVI, leaf structure, water content ratio, Zn PRS™-probe, and Zn ICP-AES) were found to be normally distributed after the Kolmogorov-Smirnov Goodness-of-Fit test. Bivariate Pearson correlation was used to distinguish a relationship between Zn levels from the PRS™-probes and the ICP-AES. Correlation makes no assumption as to whether one variable is dependent on the other, and is not concerned with the relationship between variables. Correlation gives an estimate as to the degree of association between variables (McGrew & Monroe, 2000; Ritchey, 2008). In contrast, since Zn levels affect leaf structural changes and therefore water content and NDVI, a causal relationship may exist. Therefore, a regression was used to distinguish a relationship between Zn levels and NDVI, leaf structure, and water content ratio. A regression attempts to describe the dependence of a variable on one (or more) explanatory variables and assumes that there is a one-way causal effect (Ritchey, 2008). In addition, a correlation analysis was conducted to determine if there was a relationship between water content spectral band ratio R_{900}/R_{970}, soil moisture content, and leaf structural spectral band ratio R_{1110}/R_{810}.

Since the geometric absorption variables derived from the continuum removal are highly correlated, a Principal Component Analysis (PCA) (discussed below) was utilized to overcome this correlation and characterize the similarity among the absorption

features. A regression was then calculated to find the relationship between the resulting principal component factor scores and the ICP-AES Zn levels. A Mann-Whitney *U* test was also conducted on the geometric variables as an indicator of statistical difference between tower and control sites.

3.5.3.1 Principal Component Analysis

Principal Component Analysis (PCA) is a statistical technique used to reduce the dimensionality of a data set while retaining as much information as possible (Smith et al., 1985; Dunteman, 1989; Munyati, 1994; Galvão & Vitorello, 1995; Galvão et al., 2003; Yesilnacar & Süzen, 2006). PCA is also an important exploratory tool that can be used to uncover any unknown trends in the data.

PCA linearly transforms an original set of possibly correlated variables into a smaller number of uncorrelated variables called principle components. PCA is computed iteratively in such a way that the first principal component accounts for as much of the variability in the data as possible, and each subsequent component accounts for as much of the remaining variability (Dunteman, 1989).

Three computational steps are involved in principal component transformation. The first is the calculation of a covariance or correlation matrix using input data sets, the second is the calculation of eigenvalues and eigenvectors, and the third is the calculation of the principal components (Eklundh & Singh, 1993). The principal components calculated using the covariance matrix are referred to as unstandardised principal components, whereas those calculated using the correlation matrix are referred to as standardised principal components (Eklundh & Singh, 1993; Munyati, 1994). Generally,

the use of a correlation matrix scales the axes so that each feature has a unit variance (Eklundh & Singh, 1993). This normalisation process is useful in preventing certain features from dominating the analysis due to large numerical values (Eklundh & Singh, 1993; Munyati, 1994). Standardised PCA was used in this study since it has been found to show significant improvements in comparison to unstandardised PCA (Eklundh & Singh, 1993). A description of PCA and examples of the mathematical procedures used to obtain the resulting data can be found in Dunteman (1989).

All three locations were combined and a PCA was conducted on band symmetry, total area of absorption, left area, right area, and band depth center from the continuum removed output between 400 and 550 nm and 550 and 750 nm. The results of the PCA can be found in Appendix G.

Chapter 4 Results

4.1 SOIL CHARACTERISTICS

4.1.1 Soil Temperature and pH

Results from the IQ 150 pH meter from locations B, C, and D are displayed in Appendix A. To better represent the data across all three study locations, temperature and pH averages are illustrated in Figures 12 and 13 respectively.

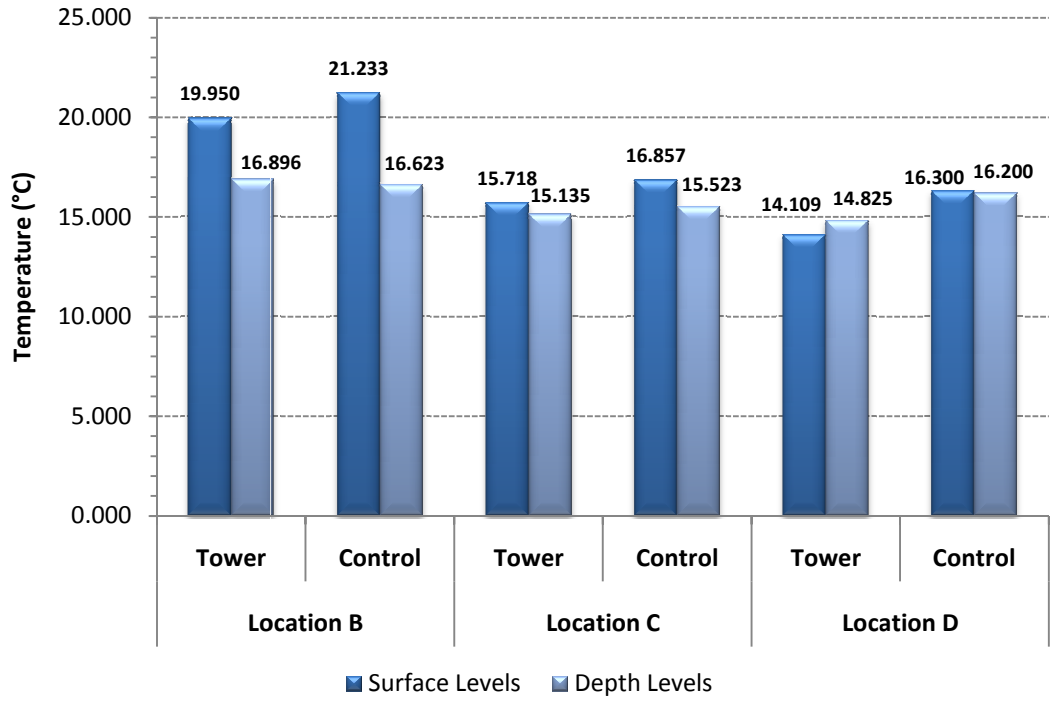

Figure 12 – Average surface and 1 m depth temperature results for tower and control sites at locations B, C, and D

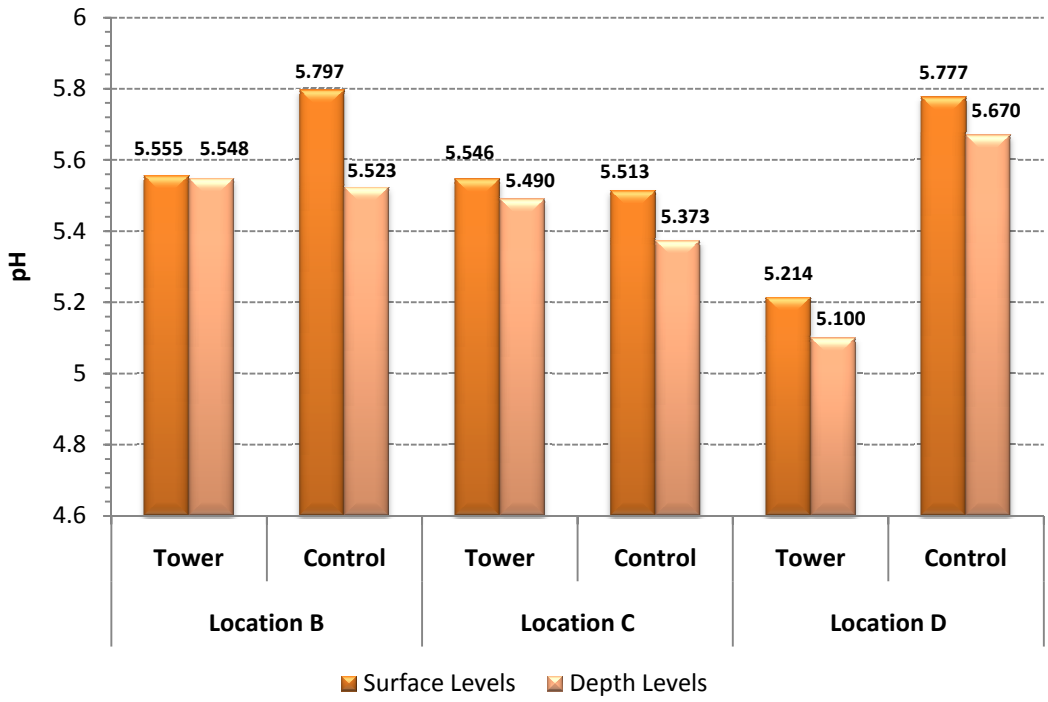

Figure 13 – Average surface and 1 m depth pH results for tower and control sites at locations B, C, and D

4.1.2 Soil Percent Moisture Content

Percent moisture content results for all three locations are displayed in Appendix B and average surface and 1 m depth percent moisture content levels are illustrated in Figure 14.

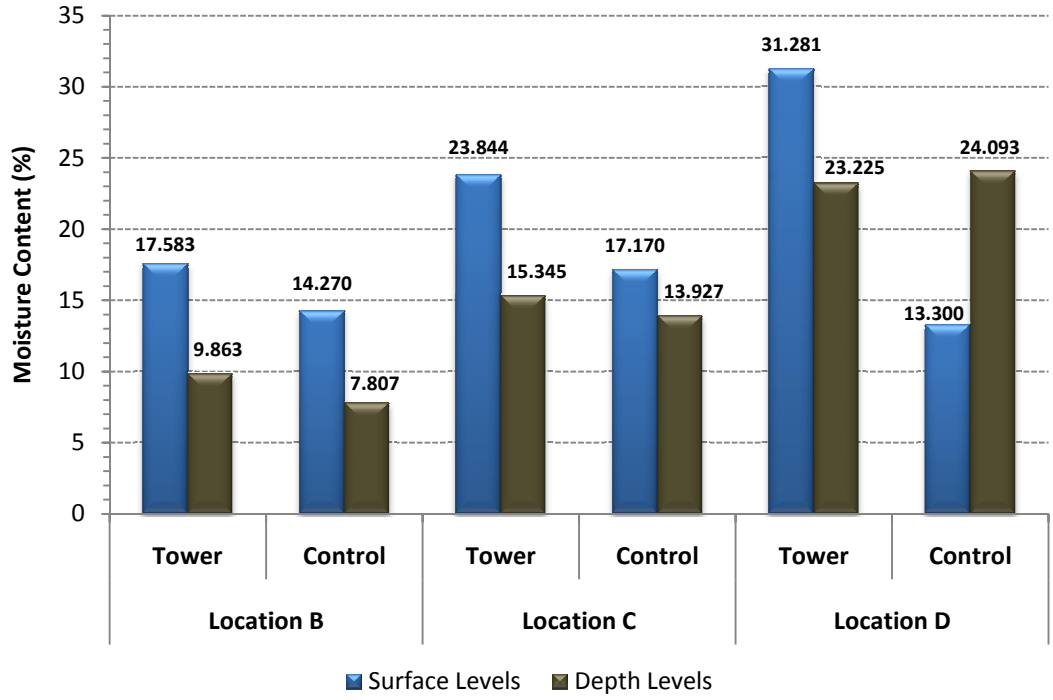

Figure 14 – Average surface and 1 m depth percent moisture content levels at transmission tower sampling locations B, C, and D

4.1.3 Soil Resistivity

An AEMC 6470 soil resistance tester was used to acquire resistivity measurements at locations B, C, and D which are presented in Figure 15.

4.1.3.1 Location B

Resistivity testing was conducted on November 5th, 2007, at location B, and revealed an average value of 44,760.00 Ohm-cm at a depth of 1 meter. Based on Table 3 by Waters (1952), this initial value indicates that tower 0153-03 is located in a "very mild" corrosive environment. Location B was reassessed for resistivity on August 18th, 2008, which revealed an average value of 76,560.00 Ohm-cm at a depth of 1 meter. Based on

Table 3 by Waters (1952), this value also indicates that tower 0153-03 is located in a "very mild" corrosive environment.

4.1.3.2 Location C

Resistivity measurements were conducted on August 25th, 2008, at location C and revealed an average value of 28,480.00 Ohm-cm at a depth of 1 meter. Based on Table 3 by Waters (1952), this value indicates that tower 0148-03 is located in a "very mild" corrosive environment.

4.1.3.3 Location D

Resistivity measurements were conducted on September 2nd, 2008, at location D and revealed an average value of 850.20 Ohm-cm at a depth of 1 meter. Based on Table 3 by Waters (1952), this value indicates that tower *0554-05* is located in a "very severe" corrosive environment.

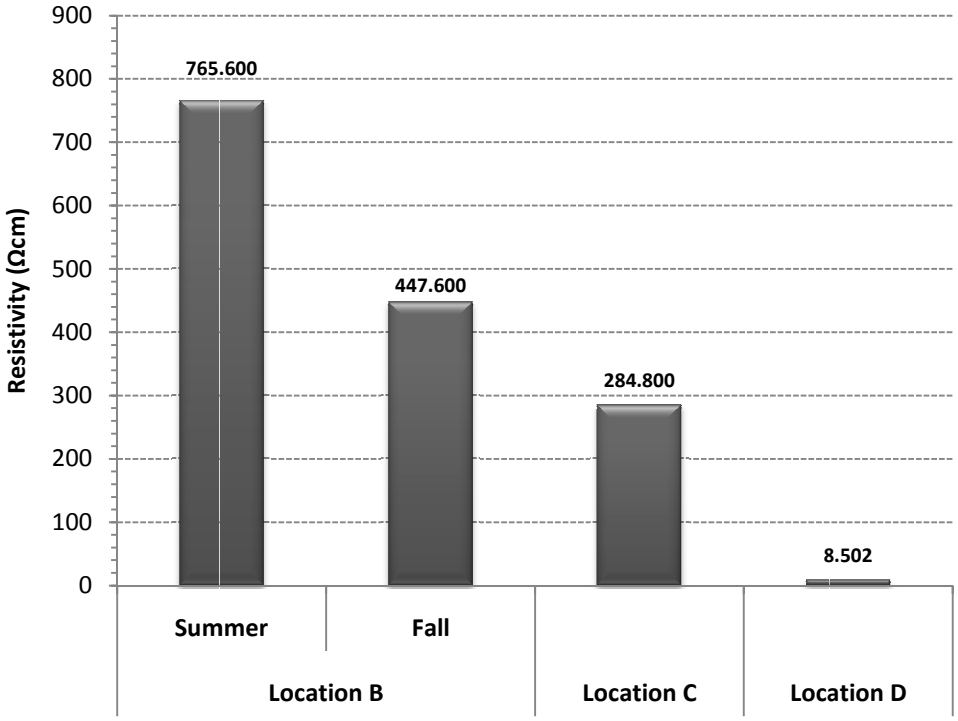

Figure 15 – Soil resistivity at a 1 m depth at locations B, C, and D

4.1.4 PRS™-probes

Since Zn levels directly correspond to the corrosion process, average Zn levels recorded from the PRS™-probes at each location are illustrated in Figure 16. Individual PRS™-probe Zn concentrations for locations B, C, and D are presented in Appendix F, Figures 48 through 50 respectively. Unfortunately, due to farm activity at location D, several issues did arise with respect to data collection. Two of the three control sites were ploughed over and several probes were lost, thereby reducing the accuracy of the PRS™-probe comparison.

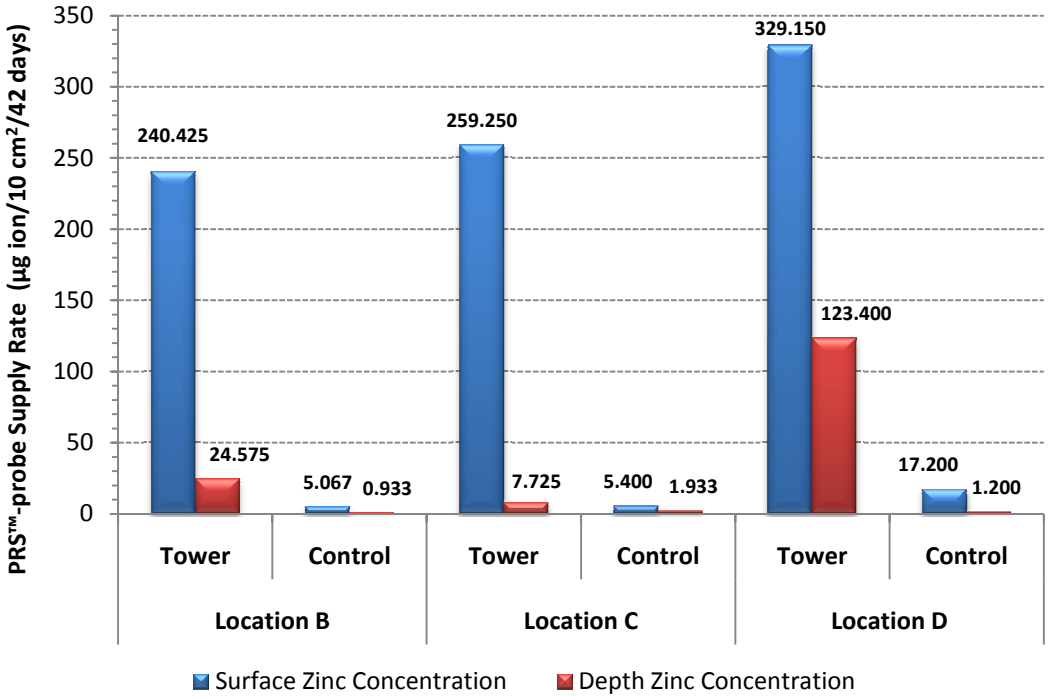

Figure 16 – PRS™-probe average surface and 1 m depth Zn concentrations at transmission tower sampling locations B, C, and D

4.1.5 Soil Statistics

4.1.5.1 Location B

Summary statistics for soil variables from location B are presented in Appendix C (Tables 18 and 19). According to the Kolmogorov-Smirnov test, 11 of the 16 soil variables from location B are normally distributed, and 5 variables show a departure from normality. Among these five variables are: Zn ($p = 0.041$), total nitrogen ($p = 0.015$), nitrate ($p = 0.015$), Mn ($p = 0.033$), and S ($p = 0.043$).

The results of the independent samples t-test indicate that between tower and control sites, the only significant difference ($p \leq 0.050$) was found in Zn levels ($p = 0.003$). That is, the levels of Zn at the tower sites ($M = 132.500$, $SD = 146.959$) are significantly different from that of the control sites ($M = 3.000$, $SD = 1.514$). In this case, the

Levene's test indicates that equal variances are not assumed, and the condition of homogeneity of variance has not been satisfied. Therefore, Zn levels violate the assumption of equal variances. However, the results of the non-parametric Mann-Whitney *U* test (p = 0.001) coincide with those of independent samples t-test.

When depth is taken into consideration, the Levene's test indicates that Zn, moisture content, total nitrogen, nitrate, Ca, Mg, K, P, Mn, and S levels all violate the assumption of equal variances. The independent samples t-test indicates a statistical difference between surface and depth levels in moisture content (p = 0.001), total nitrogen (p = 0.034), nitrate (p = 0.034), Zn (p =0.008), Ca (p = 0.000), Mg (p = 0.001), K (p = 0.006), Mn (p = 0.007), Al (p = 0.039), and average temperature (p= 0.000). The depth results of the Mann-Whitney *U* test were similar, although there was a statistical difference between surface and depth levels when considering Fe (p = 0.030) and S (p = 0.001). The p values can be found in Table 19 of Appendix C. The distribution of values indicates that the majority of surface means are higher than those at a depth of 1 m. Means that are higher at depth included Fe and Al.

4.1.5.2 Location C

Summary statistics for soil variables from location C are presented in Appendix C (Tables 20 and 21). According to the Kolmogorov-Smirnov test, 13 of the 16 soil variables from location C are normally distributed, and three variables show a departure from normality including: Zn (p = 0.016), Fe (p = 0.040), and S (p = 0.032). The results of the Levene's test indicate that when considering control versus tower sites, Zn, pH, P, and Fe values violate the assumption of equal variances. The independent samples t-test

indicates that between tower and control sites, a significant difference ($p \leq 0.050$) was found among Zn levels ($p = 0.011$) and P levels ($p = 0.009$). That is, the levels of Zn (M = 133.488, SD = 178.048) and P (M = 3.300, SD = 1.133) at the tower sites are significantly different from that of the control sites (Zn - M = 3.667, SD = 3.410; P - M = 2.875, SD = 0.327). The Mann-Whitney *U* test results coincide with those of the independent samples t-test (Zn, $p = 0.006$; P, $p = 0.012$).

When considering depth, the Levene's test indicates that Zn, total nitrogen, nitrate, Ca, K, P, Fe, and S levels all violate the assumption of equal variances. The independent samples t-test indicates a statistical difference between surface and depth levels in Zn ($p = 0.009$), moisture content ($p = 0.030$), total nitrogen ($p = 0.003$), nitrate ($p = 0.003$), Ca ($p = 0.000$), Mg ($p = 0.000$), K ($p = 0.001$), P ($p = 0.032$), Mn ($p = 0.025$), and S ($p = 0.046$). The depth results of the Mann-Whitney *U* test parallel those of the independent samples t-test. The p values can be found in Table 21 of Appendix C. Similar to location B, the distribution of values indicates that the surface means are generally higher than those at a depth of 1 m. Fe was the only element found to be higher at depth.

4.1.5.3 Location D

Summary statistics for soil variables from location D are presented in Appendix C (Tables 22 and 23). According to the Kolmogorov-Smirnov test, all of the 16 soil variables at location D are normally distributed. When considering control versus tower sites, the Levene's test indicates that Zn, Ca, P, and Al values violate the assumption of equal variances. According to the independent samples t-test, between tower and control sites, a significant difference ($p \leq 0.050$) exists in Zn ($p = 0.000$), moisture content ($p =$

0.007), pH (p = 0.000), and temperature (p = 0.000). That is, the levels of Zn (M = 226.275, SD = 171.020), moisture content (M = 27.253, SD = 4.928), pH (M = 5.157, SD = 0.261), and temperature (M = 14.467, SD= 0.5979) at the tower sites are significantly different from that of the control sites (Zn - M = 9.200, SD = 11.314; moisture content - M = 18.697, SD = 8.393; pH - M = 5.750, SD = 0.1897; temperature - M = 16.275, SD = 0.654). The Mann-Whitney *U* test results coincide with those of the independent samples t-test (Zn, p = 0.049; moisture content, p = 0.012; pH, p = 0.002; temperature, p = 0.002).

When considering depth, the Levene's test indicates that moisture content, Mg, and B levels violate the assumption of equal variances. The independent samples t-test indicates a statistical difference between surface and depth levels in Zn (p = 0.020), total nitrogen (p = 0.028), nitrate (p = 0.028), Mg (p = 0.041), K (p = 0.046), and Fe (p = 0.048). The depth results of the Mann-Whitney *U* test indicate a statistical difference between surface and depth levels in Zn (p = 0.047), total nitrogen (p = 0.024), nitrate (p = 0.024), Fe (p = 0.024), and S (p = 0.047).

Similar to locations B and C, the distribution of values indicates that the majority of surface means are higher than those at a depth of 1 m. Means that are higher at depth include: Mg, Fe, B, and average temperature.

4.2 ICP-AES VEGETATION ANALYSIS

Since Zn values are directly related to transmission tower corrosion, the ICP-AES average vegetation Zn concentrations at locations B, C, and D are illustrated in Figure 17.

Individual ICP-AES Zn concentrations for locations B, C, and D are presented in Appendix F, Figures 51, 52, and 53 respectively.

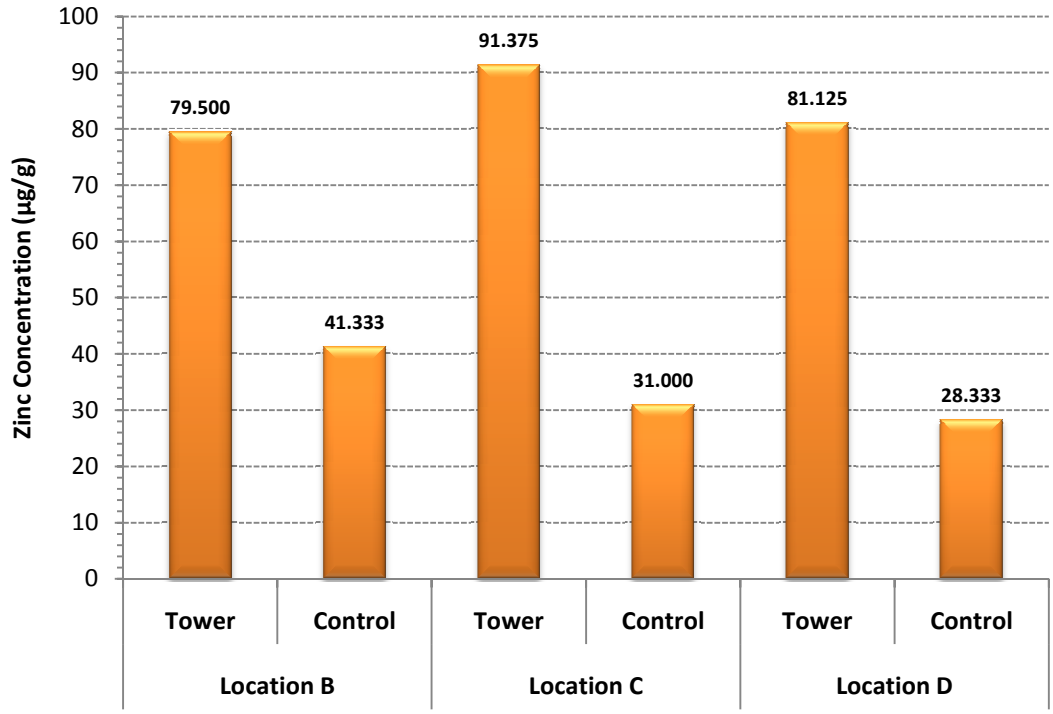

Figure 17 – ICP-AES average Zn concentrations at transmission tower sampling locations B, C, and D

4.2.1 ICP-AES Statistics

4.2.1.1 Location B

Summary statistics for ICP-AES variables from location B are presented in Appendix D (Tables 24 and 25). The results of the Kolmogorov-Smirnov test indicate that all of the location B ICP-AES variables are normally distributed. The Levene's test shows that B is the only variable that violates the assumption of equal variances. According to the independent samples t-test, none of the variables show a significant difference between

tower and control sites and the Mann-Whitney *U* test parallels these results. Zn levels had a p value of 0.066.

4.2.1.2 Location C

Summary statistics for ICP-AES variables from location C are presented in Appendix D (Tables 26 and 27). According to the Kolmogorov-Smirnov test, all of the 13 ICP-AES variables from location C are normally distributed. The results of the Levene's test indicate that Ca and K levels violate the assumption of equal variances, and the independent samples t-test shows that a significant difference between tower and control sites was found in C ($p = 0.030$) and Zn ($p = 0.046$). However, the Mann-Whitney *U* test indicates that there is a significant difference in Ca ($p = 0.041$), Fe ($p = 0.041$), Na ($p = 0.050$), and Zn ($p = 0.014$) between tower and control sites.

4.2.1.3 Location D

Summary statistics for ICP-AES variables from location D are presented in Appendix D (Tables 28 and 29). According to the Kolmogorov-Smirnov test, all of the 13 ICP-AES variables from location D are normally distributed. The Levene's test indicates that Al, Fe, and Na levels violate the assumption of equal variances. The independent samples t-test shows that a significant difference between tower and control sites was found in B ($p = 0.000$). However, the Mann-Whitney *U* test indicates that there is a significant difference in Al ($p = 0.014$), B ($p = 0.016$), Fe ($p = 0.014$), Na ($p = 0.023$), and Zn ($p = 0.041$) levels between tower and control sites.

4.3 SPECTROSCOPY

4.3.1 Location B

Sample site Himalayan Blackberry reflectance spectra over the 350 to 2500 nm spectral region are presented in Figure 18. Figure 19 presents the average reflectance spectra of the tower and control sites.

The spectra of vegetation grown in Zn contaminated soils beneath the tower vary considerably, and show little difference from the controlled samples. As indicated in Figure 18, the vegetation spectra from the control sites (SS9, SS10, and SS11) do not specifically correspond to highs or lows in reflectance. Throughout the visible wavelengths (400 – 700 nm), vegetation reflectance from SS6 (tower) and SS11 (control) have generally the highest reflectance, whereas SS3 (tower) has the lowest. When comparing reflectance values to actual Zn content, PRS™-probes do have the highest levels of Zn at SS3. However, this is inconsistent with the ICP-AES results where SS2 has the highest levels of Zn (Figures 48 and 51, Appendix F). The PRS™-probe results at SS5 have the second highest levels of Zn, but are generally neither high nor low in reflectance. Similar inconsistencies occur in the infrared which do not correspond to the measured Zn values from the PRS™-probes or the ICP-AES results.

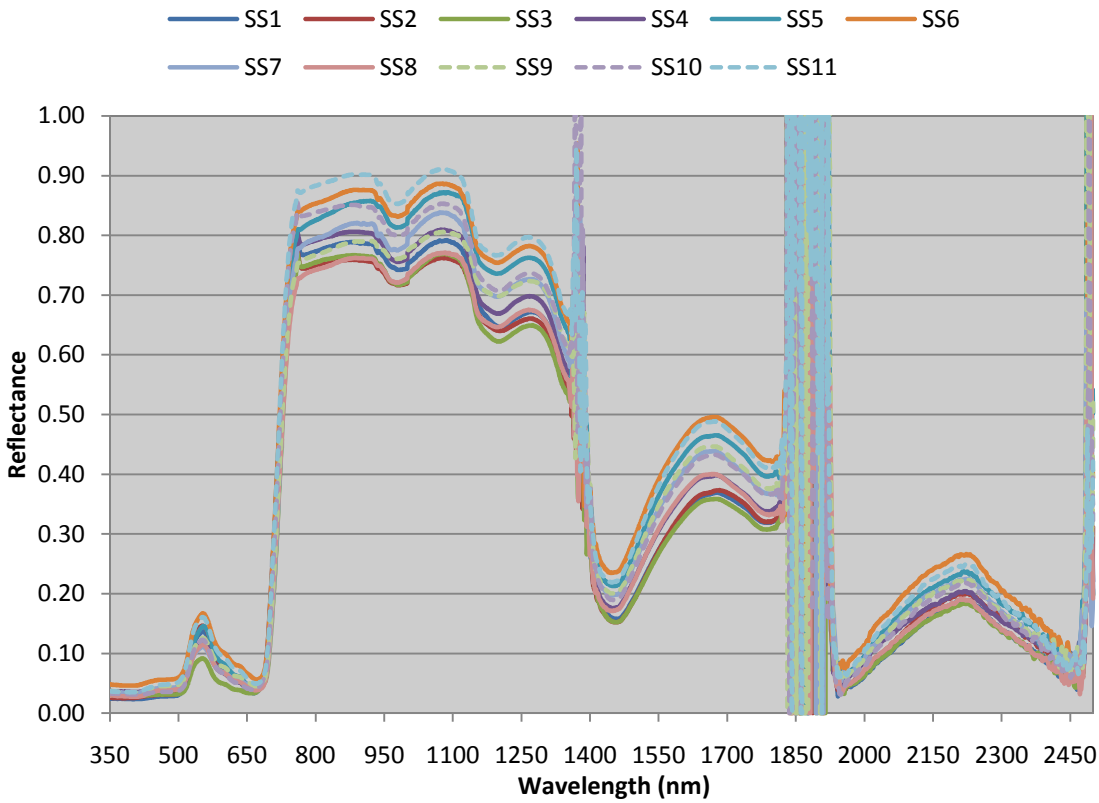

Figure 18 – Sample site reflectance spectra of Himalayan Blackberry at location B, Langley, British Columbia measured on July 7th, 2008. The dashed lines indicate control sites. The gaps in the spectra are noise regions affected by atmospheric water vapour.

Figure 19 – Average tower and control sample reflectance spectra of Himalayan Blackberry at location B, Langley, British Columbia measured on July 7th, 2008. The gaps in the spectra are noise regions affected by atmospheric water vapour.

4.3.1.1 NDVI

The NDVI results are shown in Figure 20. As illustrated, the sampling sites with high Zn concentrations are indistinguishable from the control. The control samples (SS9, SS10, SS11) are highly variable, and give no indication that the concentration of Zn has had an influence on the NDVI. Higher concentrations of Zn in vegetation should decrease the NDVI value as the vegetation becomes stressed. According to the independent samples t-test and the Mann-Whitney *U* test, there is no statistical difference between tower and control sites when considering NDVI (see Table 30, Appendix E for summary statistics).

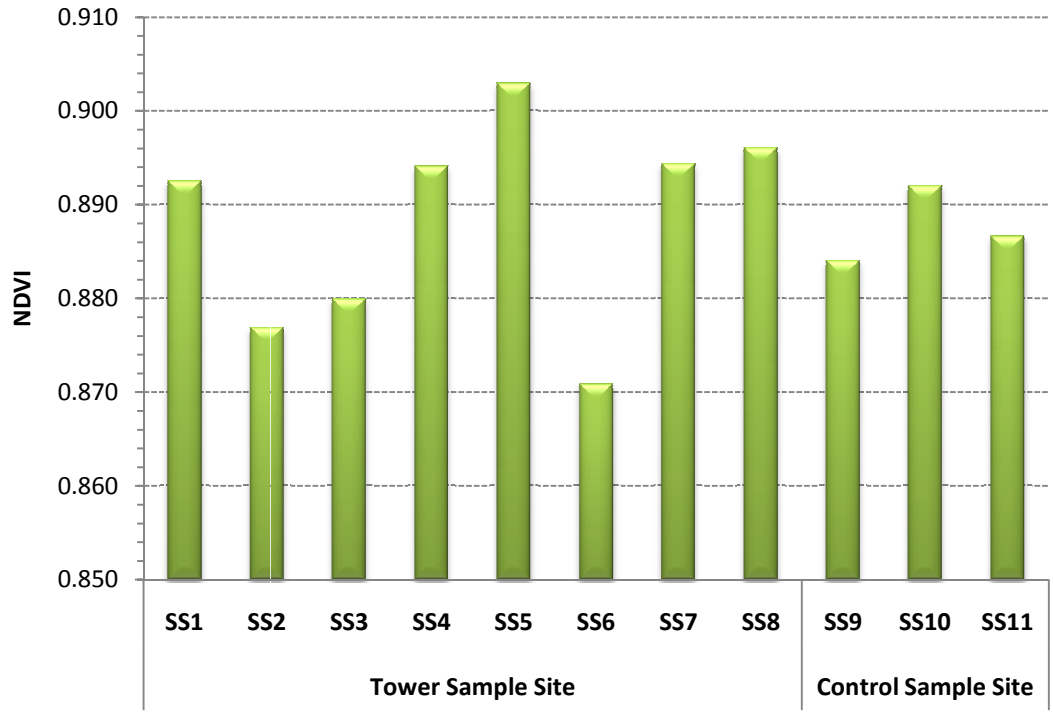

Figure 20 – NDVI results for tower and control sample sites at location B

4.3.1.2 Structural Band Ratio R_{1110}/R_{810}

The structural band ratio R_{1110}/R_{810} results are shown in Figure 21. According to Sridhar et al. (2007), higher concentrations of Zn should give higher R_{1110}/R_{810} values. However, there is no trend when compared to actual Zn levels that would indicate that Zn has had a negative influence on leaf structure (Figures 48 and 51, Appendix F). According to the independent samples t-test and the Mann-Whitney *U* test, there is no statistical difference between tower and control sites when considering the ratio index R_{1110}/R_{810} (see Table 30, Appendix E for summary statistics).

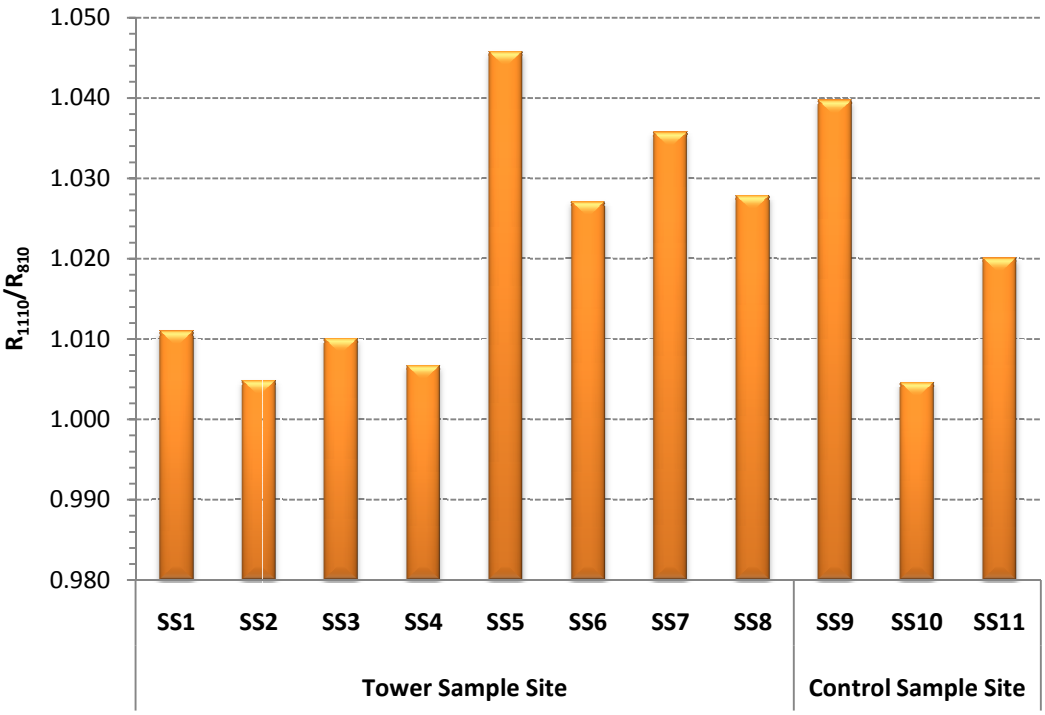

Figure 21 – R_{1110}/R_{810} band ratio results for tower and control sample sites at location B

4.3.1.3 Water Band Ratio R_{900}/R_{970}

The water band ratio R_{900}/R_{970} results are shown in Figure 22. The vegetation with higher concentrations of Zn should show a decrease in this ratio compared to the control (Sridhar et al., 2007). However, variation is high, and does not correspond to the tested Zn concentration from both the PRS™-probes and the ICP-AES at the sample sites (Figures 48 and 51, Appendix F). According to the independent samples t-test and the Mann-Whitney *U* test, there is no statistical difference between tower and control sites when considering the ratio index R_{900}/R_{970} (see Table 30, Appendix E for summary statistics). It was also found that there was no correlation between water content R_{900}/R_{970} and soil moisture content ($R^2 = 0.225$, $r = 0.474(9)$, $p\ (0.140) > 0.05$).

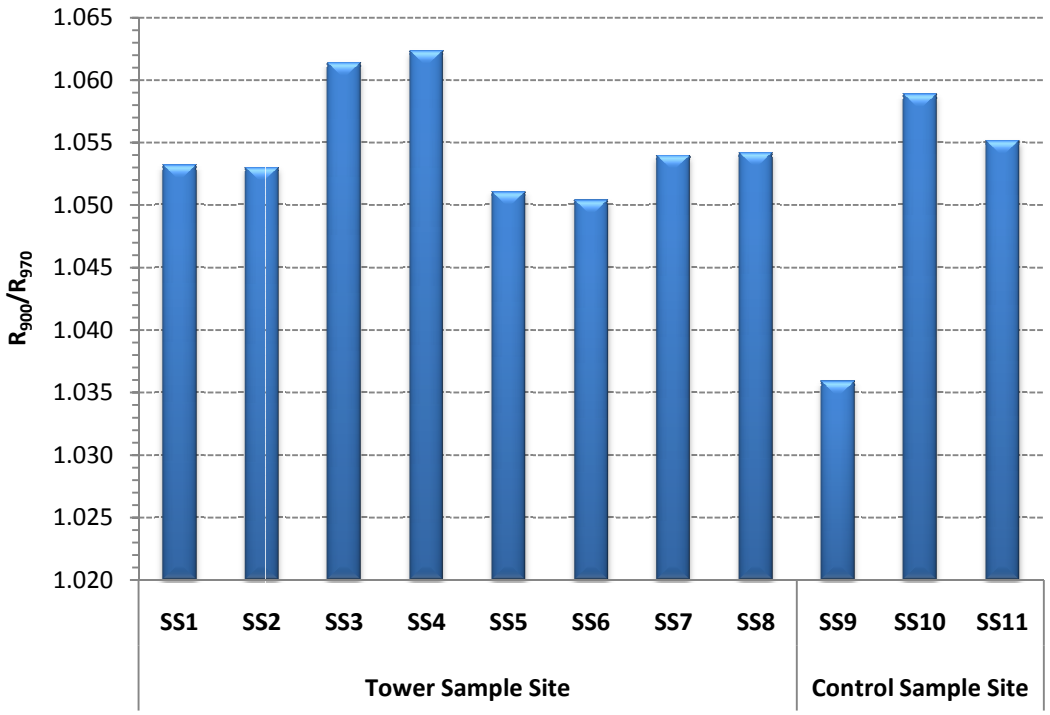

Figure 22 – R_{900}/R_{970} band ratio results for tower and control sample sites at location B

4.3.1.4 First Order Derivative

Average first order derivative spectra from 400 to 780 nm were calculated using 1 nm intervals presented in Figure 23. The derivative analysis shows that the red-edge (690 – 750) is comprised of an asymmetric peak with one distinct maximum and two secondary features. The first peak for both the tower and control derivatives is located at 717 nm, and the second at 723 nm. A small peak or shoulder can also be seen at around 699 nm. The first peak in reflectance at 717 nm indicates the wavelength position of the REIP.

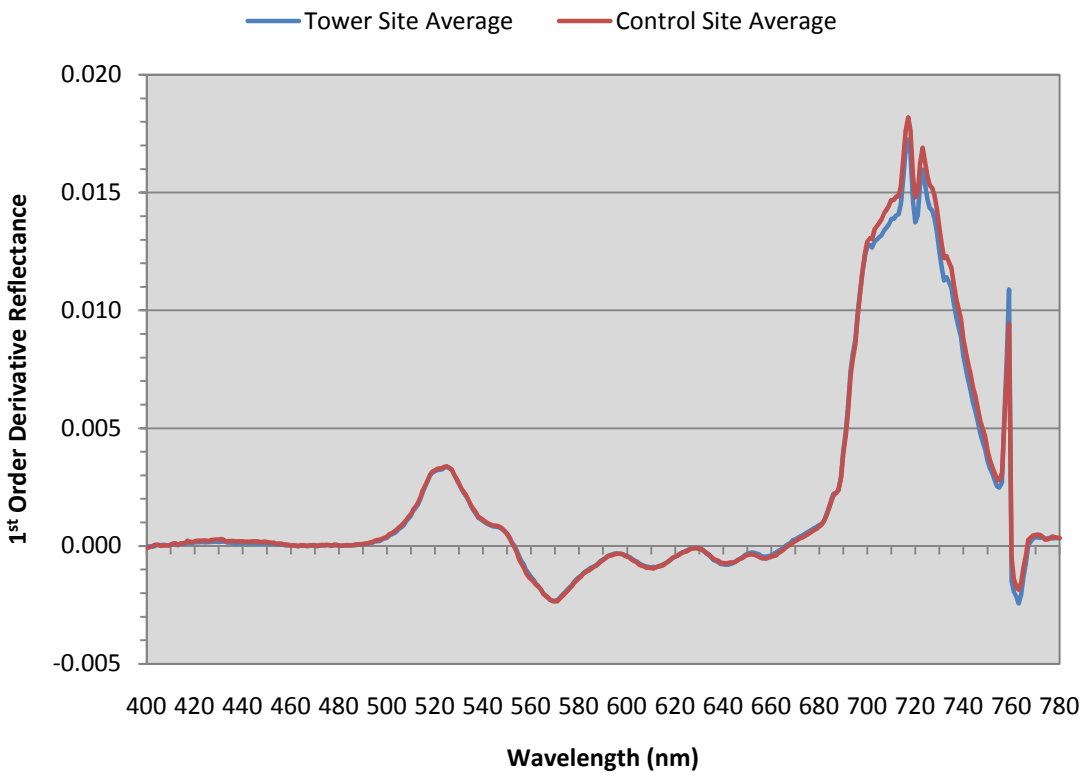

Figure 23 – Average first order derivative Himalayan Blackberry reflectance spectra for tower and control sites at location B

4.3.1.5 Continuum Removal

Since chlorophyll absorption occurs at 430 – 460 nm and 650 – 660 nm, continuum removal was applied between 400 and 550 nm and between 550 and 750 nm (Clark, 1999; Gao & Goetz, 1994; Noomen et al., 2006). Continuum removal of the 400 – 550 nm region (Figure 24) and the 550 and 750 nm region (Figure 25) does not result in any apparent differences between the control and tower sites. According to the Mann-Whitney *U* test, there is no statistical difference between tower and control sites when considering band symmetry ($p = 0.838$; $p = 1.000$), total area of absorption ($p = 0.838$; $p = 0.683$), left area ($p = 0.838$; $p = 1.000$), right area ($p = 0.307$; $p = 0.838$), or band depth center ($p = 0.838$; $p = 0.414$) at 400 to 550 nm and 550 to 750 nm respectively.

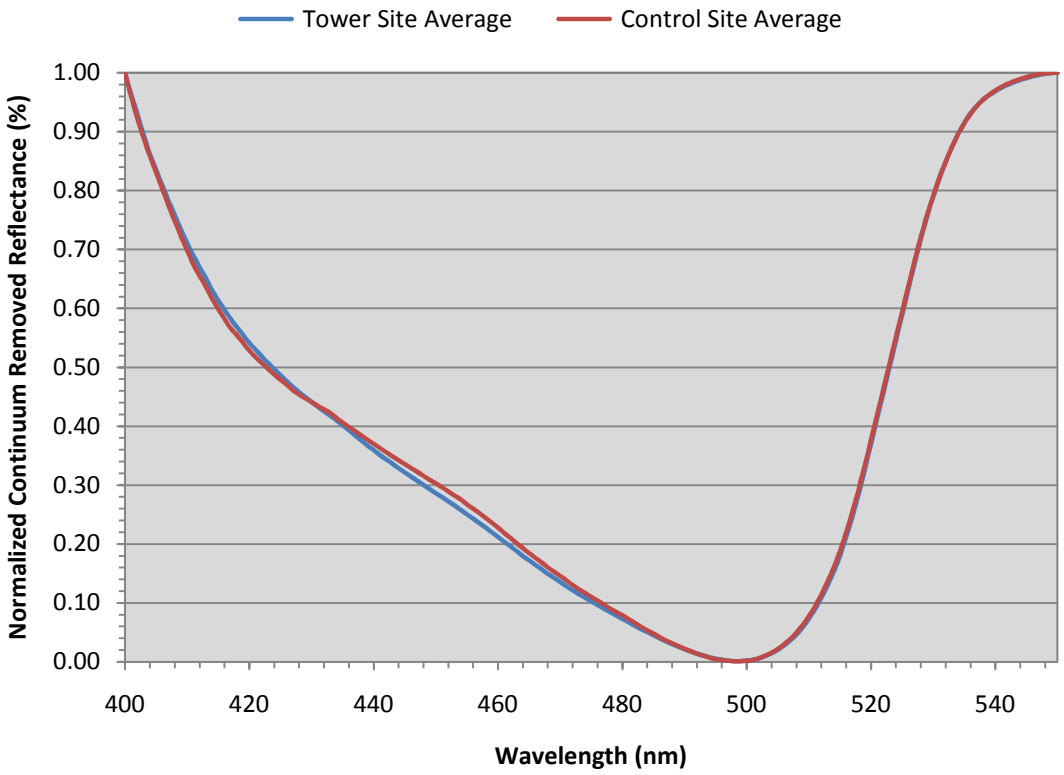

Figure 24 – Normalized continuum removed reflectance ($R_{400-550}$) of Himalayan Blackberry at location B

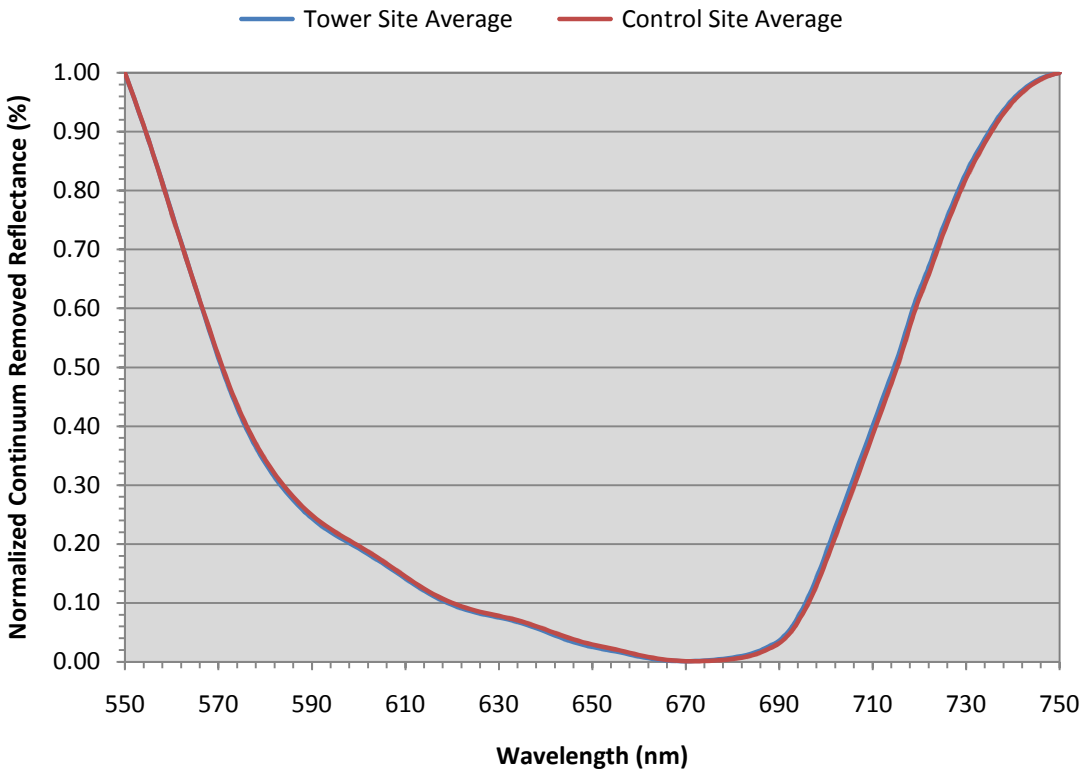

Figure 25 – Normalized continuum removed reflectance ($R_{550-750}$) of Himalayan Blackberry at location B

4.3.2 Location C

Sample site Himalayan Blackberry reflectance spectra over the 350 to 2500 nm spectral region are presented in Figure 26. Figure 27 presents the average reflectance spectra of the tower and control sites.

The spectra of vegetation grown in Zn contaminated soils beneath the tower vary considerably, and show little difference from the controlled samples around the tower. As illustrated in Figure 26, the vegetation spectra from the control sites (SS9, SS10, and SS11) are not consistently specific to highs or lows in reflectance. Throughout the visible wavelengths (400 – 700 nm), vegetation reflectance from SS6 (tower) and SS7 (tower) have generally the highest reflectance, whereas SS10 (control) has the lowest. In

this case, given the high values of Zn in tower sites, a higher visible green reflectance from control samples would be expected. When comparing reflectance values to actual Zn content, PRS™-probes have the highest levels of Zn at SS6 and SS8, however, this is inconsistent with the ICP-AES results where SS7 and SS2 have the highest levels of Zn (Tables 49 and 52, Appendix F). Similar inconsistencies occur in the infrared which do not correspond to the measured Zn values from the PRS™-probes or the ICP-AES results.

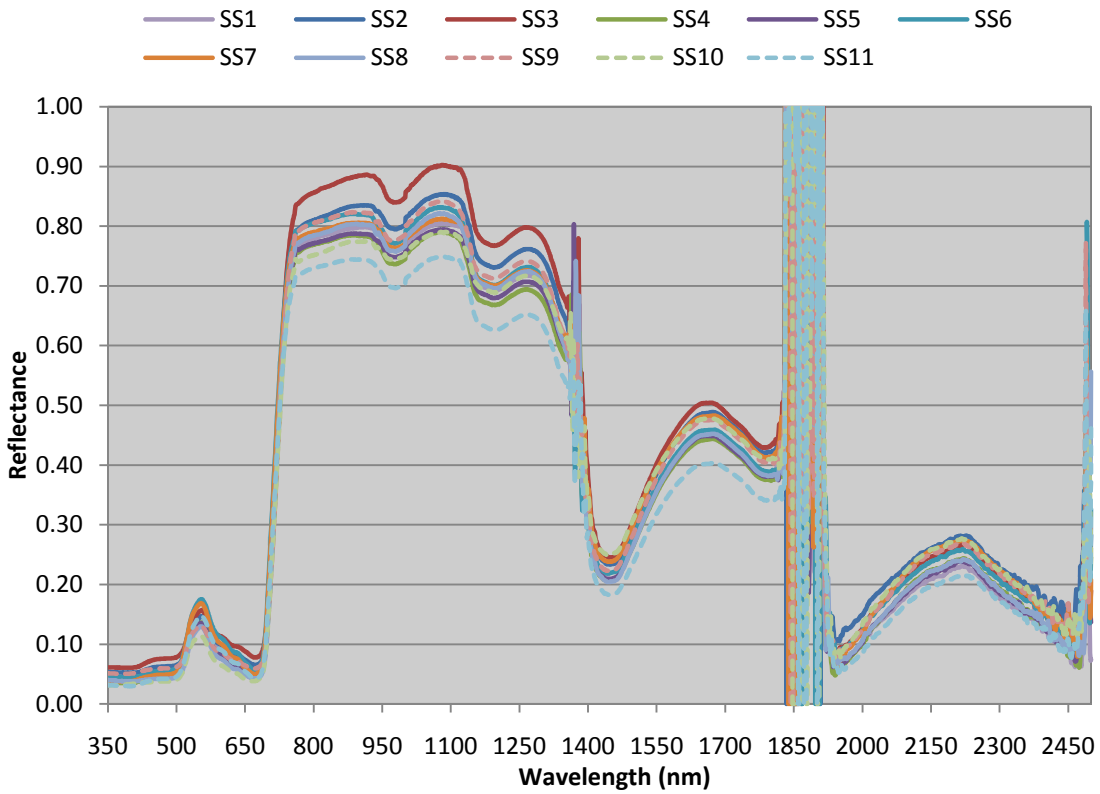

Figure 26 – Sample site reflectance spectra of Himalayan Blackberry at location C, Langley, British Columbia measured on July 14th, 2008. The dashed lines indicate control sites. The gaps in the spectra are noise regions affected by atmospheric water vapour.

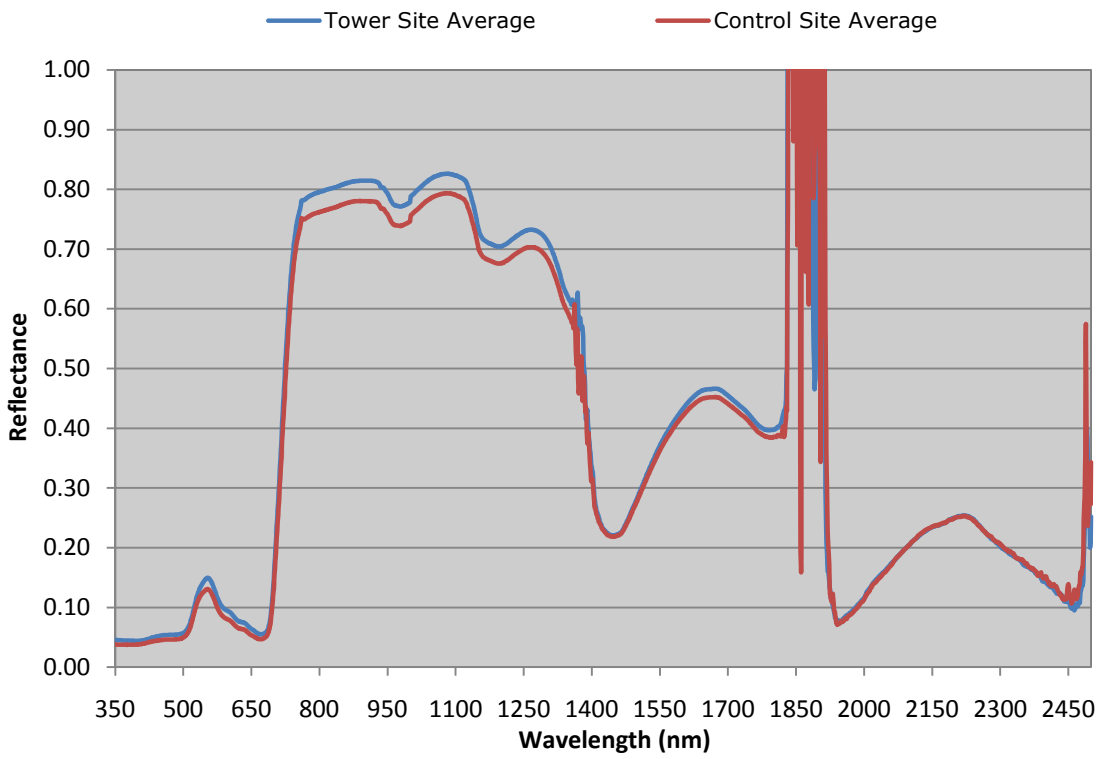

Figure 27 – Average tower and control sample reflectance spectra of Himalayan Blackberry at location C, Langley, British Columbia measured on July 14th, 2008. The gaps in the spectra are noise regions affected by atmospheric water vapour.

4.3.2.1 NDVI

The NDVI results are presented in Figure 28. Similar to the location B data, the sampling sites with high Zn concentrations are indistinguishable from the control. The control samples (SS9, SS10, SS11) are highly variable, and give no indication that the concentration of Zn has had an influence on the NDVI. Since higher concentrations of Zn in vegetation should decrease the NDVI value as the vegetation becomes stressed, there should be a low NDVI value at SS8 (PRS™-probes) or SS7 (ICP-AES) where Zn levels are at their highest (Figures 49 and 52, Appendix F). According to the independent samples t-test and the Mann-Whitney *U* test, there is no statistical difference between

tower and control sites when considering NDVI (see Table 31, Appendix E for summary statistics).

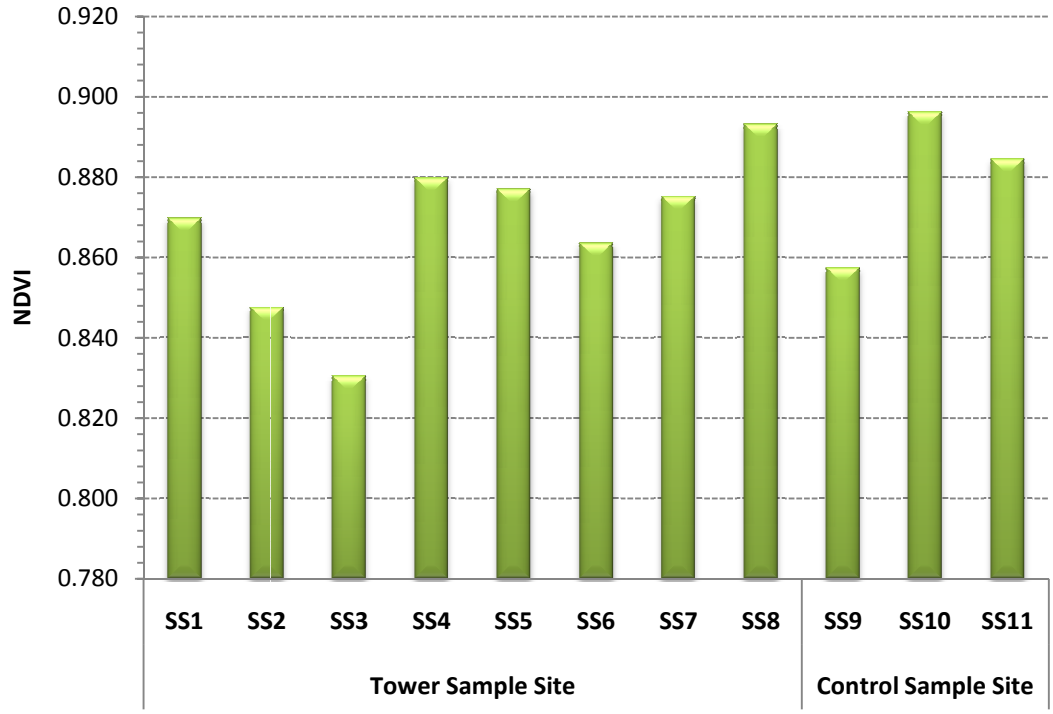

Figure 28 – NDVI results for tower and control sample sites at location C

4.3.2.2 Structural Band Ratio R_{1110}/R_{810}

The R_{1110}/R_{810} results are presented in Figure 29. According to Sridhar et al. (2007), higher concentrations of Zn should give higher R_{1110}/R_{810} values. However, there is no trend when compared to actual Zn levels that would indicate that Zn has had a negative influence on leaf structure (Figures 49 and 52, Appendix F). According to the independent samples t-test and the Mann-Whitney *U* test, there is no statistical difference between tower and control sites when considering the ratio index R_{1110}/R_{810} (see Table 31, Appendix E for summary statistics).

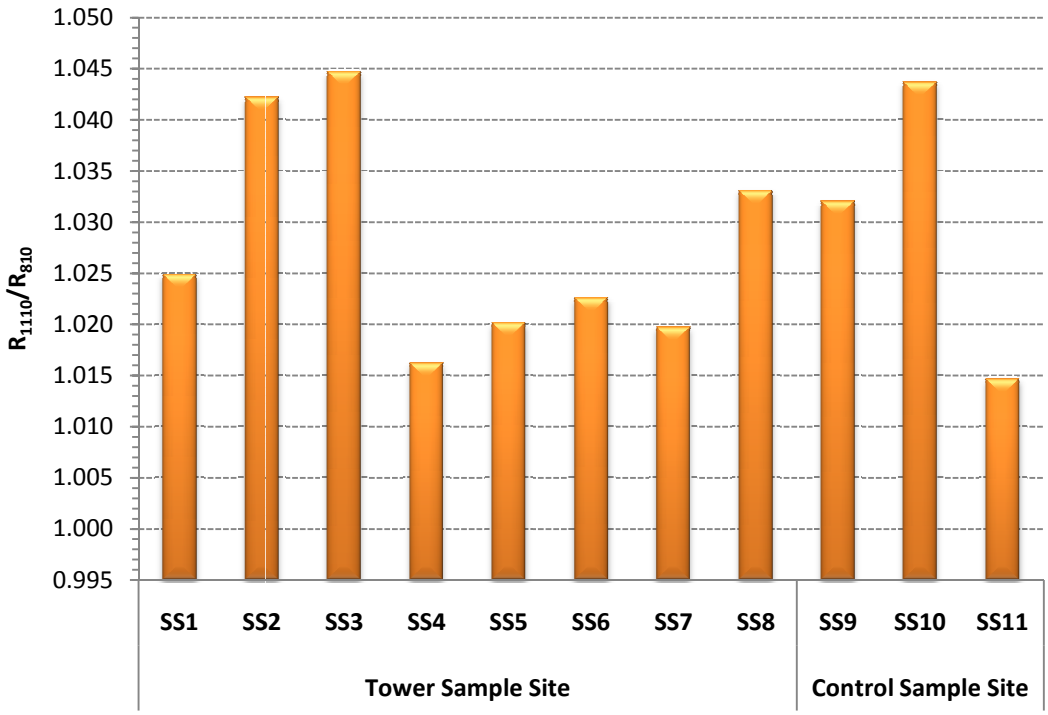

Figure 29 – R_{1110}/R_{810} band ratio results for tower and control sample sites at location C

4.3.2.3 Water Band Ratio R_{900}/R_{970}

The water band ratio R_{900}/R_{970} results are presented in Figure 30. The vegetation with higher concentrations of Zn should show a decrease in this ratio compared to the control (Sridhar et al., 2007). Similar to location B, variation is high, and does not correspond to the tested Zn concentration from both the PRS™-probes and the ICP-AES at the sample sites (Figures 49 and 52, Appendix F). According to the independent samples t-test and the Mann-Whitney *U* test, there is no statistical difference between tower and control sites when considering the ratio index R_{900}/R_{970} (see Table 31, Appendix E for summary statistics). It was also found that there is no correlation between water content R_{900}/R_{970} and soil moisture content ($R^2 = 0.075$, $r = 0.275(9)$, $p\ (0.414) > 0.05$).

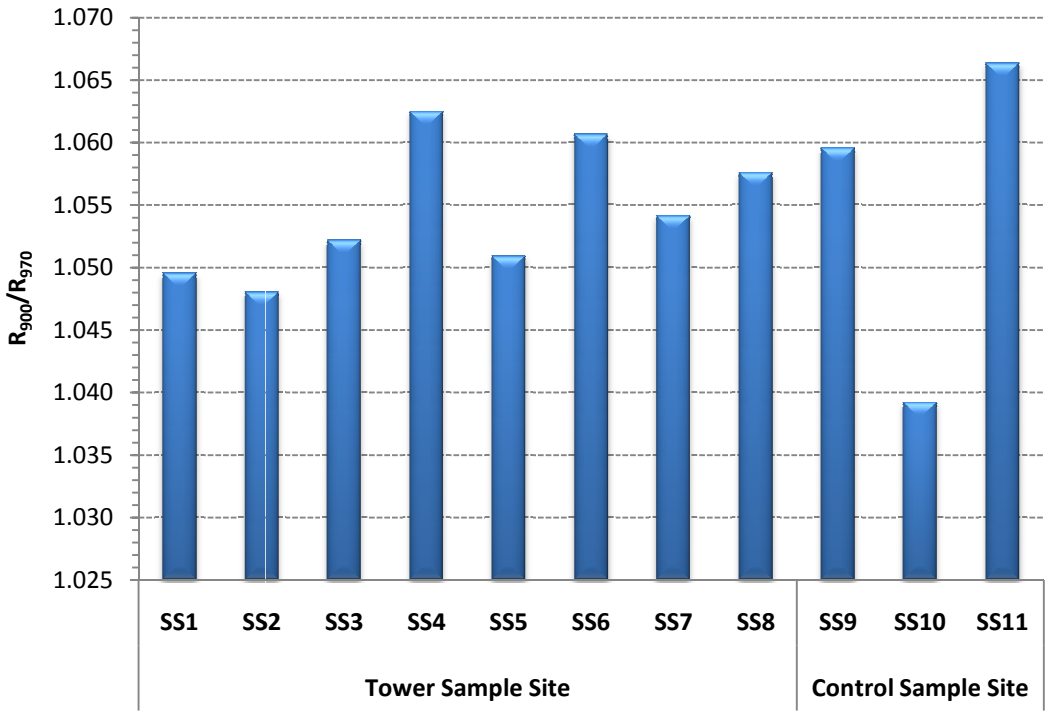

Figure 30 – R_{900}/R_{970} band ratio results for tower and control sample sites at location C

4.3.2.4 First Order Derivative

Average first order derivative spectra for location C from 400 to 780 nm were calculated using 1 nm intervals presented in Figure 31. The shape of the red-edge for the control and tower samples has little variation. Similar to the location B derivatives, location C exhibits the same REIP at 717 nm and secondary peak at 723 nm. A small peak or shoulder can be seen around 700 nm where there is a change in magnitude between the control and tower derivatives.

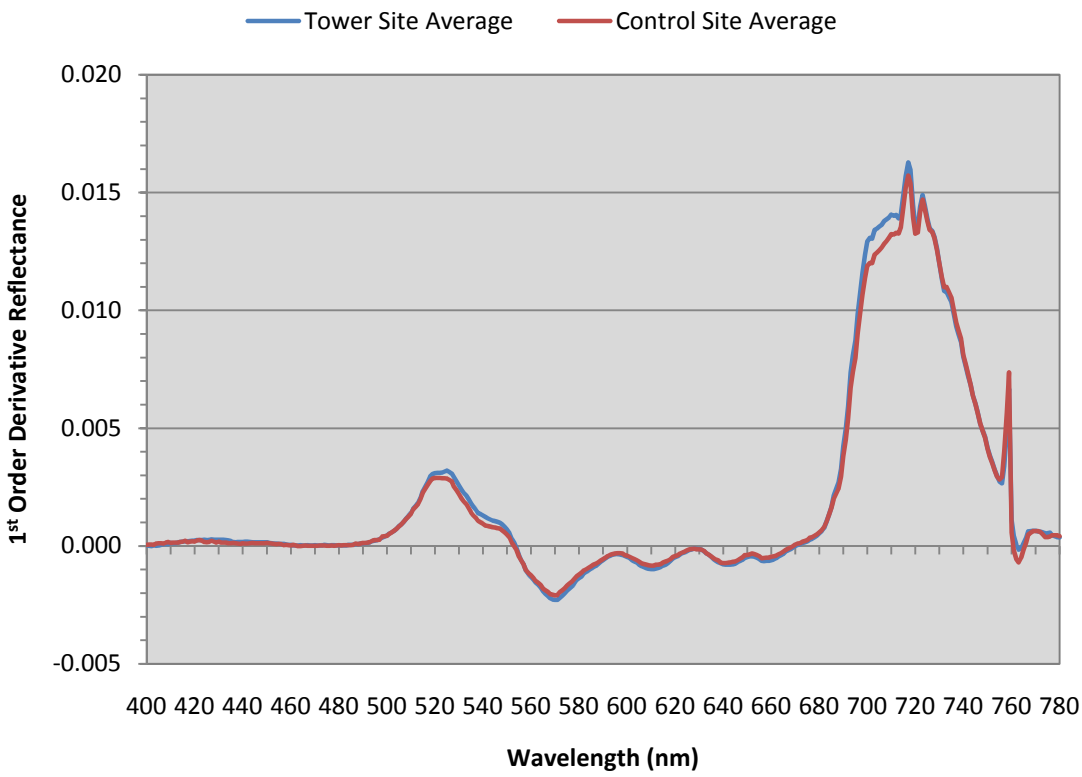

Figure 31 – Average first order derivative Himalayan Blackberry reflectance spectra for tower and control sites at location C

4.3.2.5 Continuum Removal

Normalized continuum removed reflectance at location C indicates that the tower reflectance has a small shift of 2 to 3 nm toward longer wavelengths in the blue absorption feature (400 – 550 nm, Figure 32), and a slight shift of 1 to 2 nm between 560 and 660 nm in the red (Figure 33). According to the Mann-Whitney *U* test, there is no statistical difference between tower and control sites when considering band symmetry ($p = 0.838$; $p = 0.683$), total area of absorption ($p = 0.683$; $p = 0.307$), left area ($p = 0.838$; $p = 0.540$), right area ($p = 0.102$; $p = 0.221$), or band depth center ($p = 0.683$; $p = 0.307$) at 400 to 550 nm and 550 to 750 nm respectively.

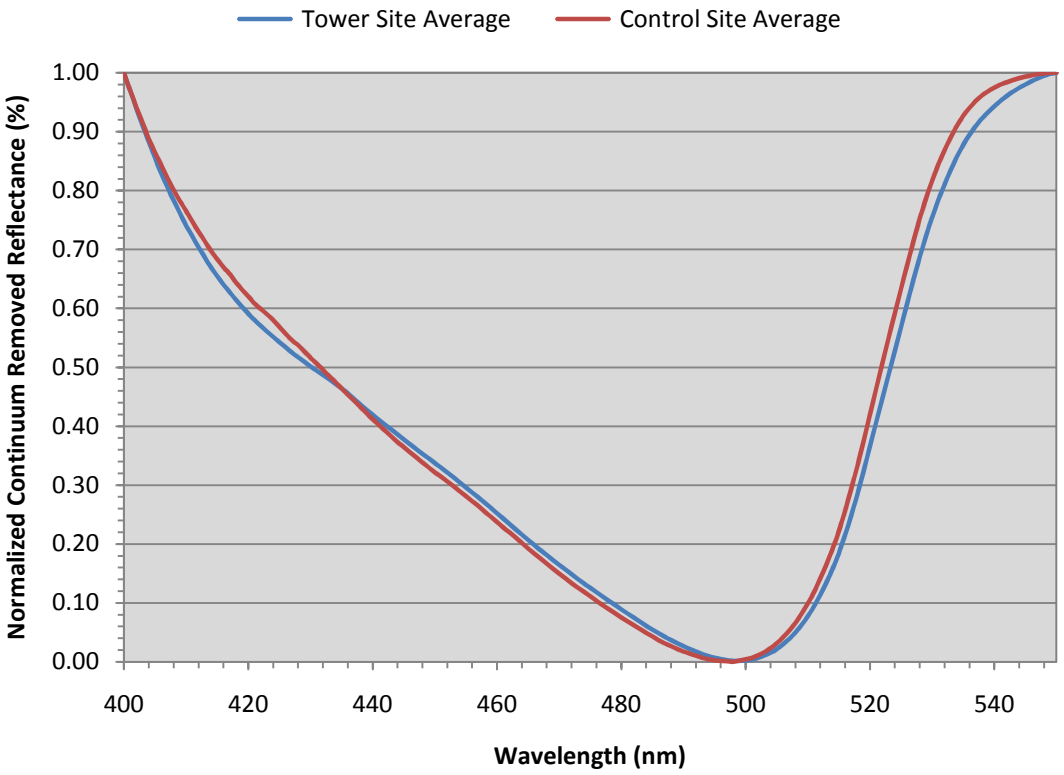

Figure 32 – Normalized continuum removed reflectance ($R_{400-550}$) of Himalayan Blackberry at location C

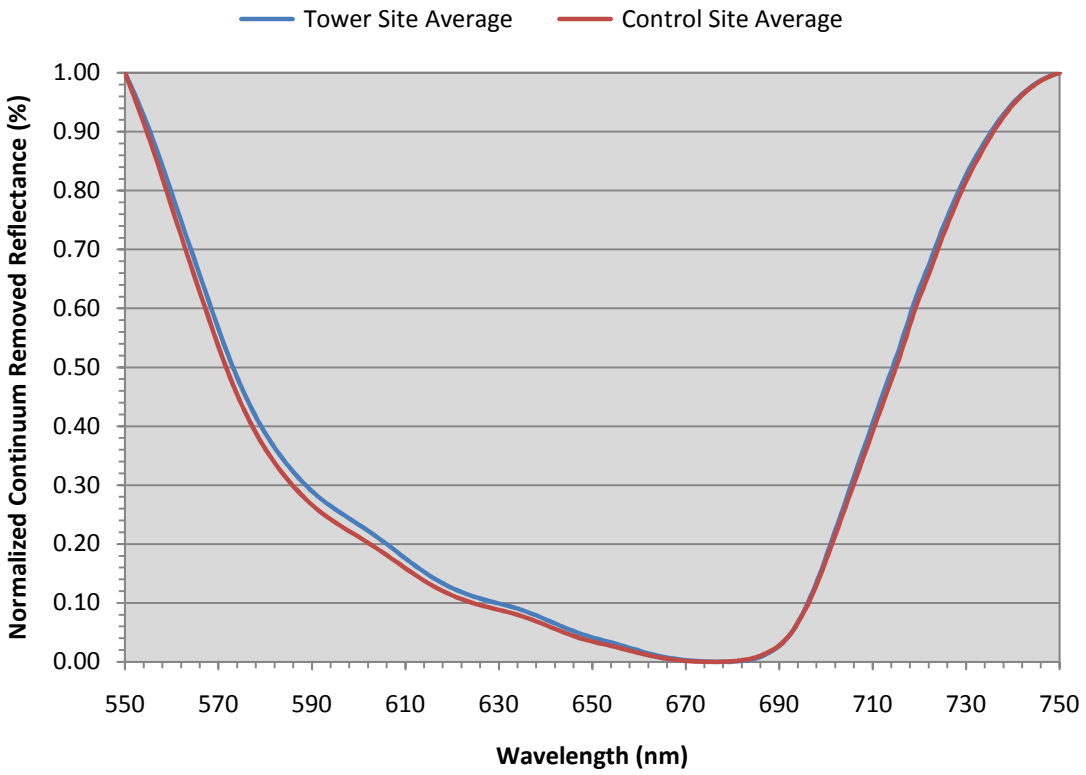

Figure 33 – Normalized continuum removed reflectance ($R_{550-750}$) of Himalayan Blackberry at location C

4.3.3 Location D

Sample site Himalayan Blackberry reflectance spectra over the 350 to 2500 nm spectral region are presented in Figure 34. Figure 35 presents the average reflectance spectra of the tower and control sites.

The spectra of vegetation grown in Zn contaminated soils beneath the tower vary considerably, and show little difference from the controlled samples around the tower. As illustrated in Figure 34, the vegetation spectra from the control sites (SS9, SS10, and SS11) are not consistently specific to highs or lows in reflectance. Throughout the visible wavelengths (400 – 700 nm), vegetation reflectance from SS7 (tower) generally has the highest reflectance, whereas SS6 (tower) has the lowest. In this case, given the

high values of Zn in tower sites, one would expect a higher visible green reflectance from control samples. When comparing reflectance values to actual Zn content, PRS™-probes have the highest levels of Zn at SS3 and SS8. However, this is inconsistent with the ICP-AES results where SS1 and SS4 have the highest levels of Zn (Tables 50 and 53, Appendix F). Similar inconsistencies occur in the infrared which do not correspond to the measured Zn values from the PRS™-probes or the ICP-AES results.

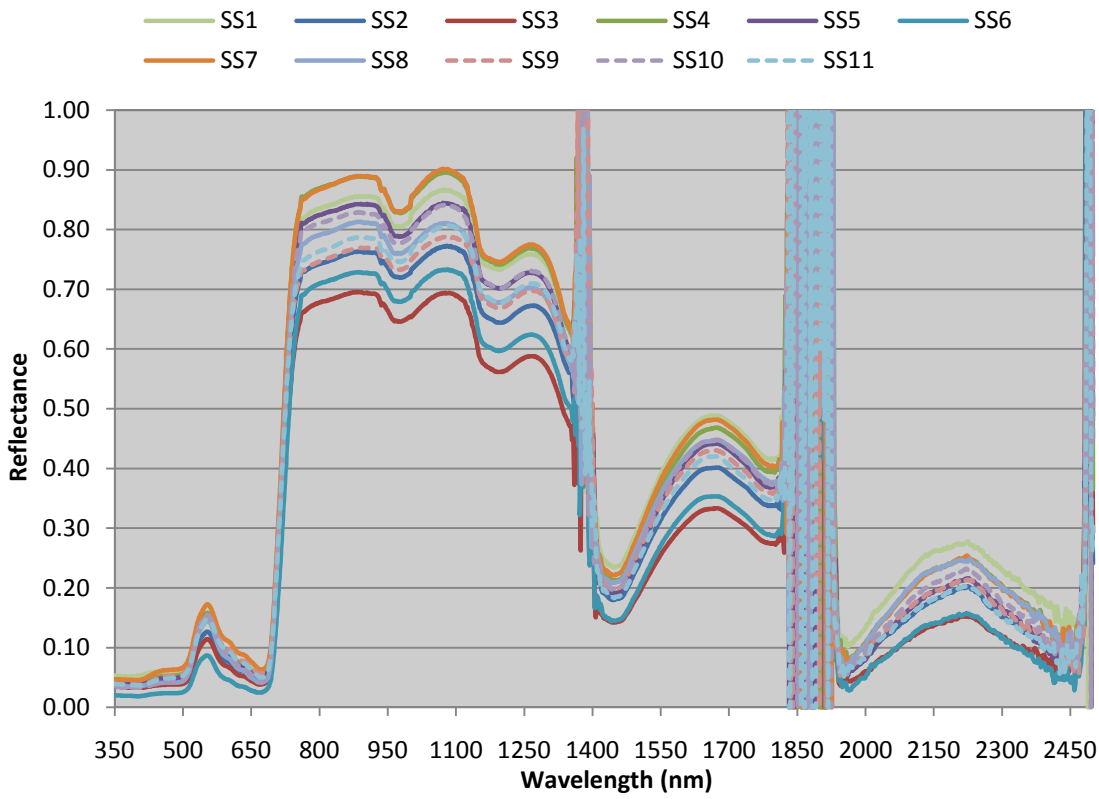

Figure 34 – Sample site reflectance spectra of Himalayan Blackberry at location D, Aldergrove, British Columbia measured on July 21st, 2008. The dashed lines indicate control sites. The gaps in the spectra are noise regions affected by atmospheric water vapour.

Figure 35 – Average tower and control sample reflectance spectra of Himalayan Blackberry at location D, Aldergrove, British Columbia measured on July 21st, 2008. The gaps in the spectra are noise regions affected by atmospheric water vapour.

4.3.3.1 NDVI

The NDVI results are presented in Figure 36. Similar to the location B and C data, the sampling sites with high Zn concentrations are completely indistinguishable from the control. The control samples (SS9, SS10, SS11) are highly variable, and give no indication that the concentration of Zn has had an influence on the NDVI. Since higher concentrations of Zn in vegetation should decrease the NDVI value as the vegetation becomes stressed, there should be a low NDVI value at SS8 (PRS™-probes) or SS4 (ICP-AES) where Zn levels are at their highest (Figures 50 and 53, Appendix F). According to the independent samples t-test and the Mann-Whitney *U* test, there is no

statistical difference between tower and control sites when considering NDVI (see Table 32, Appendix E for summary statistics).

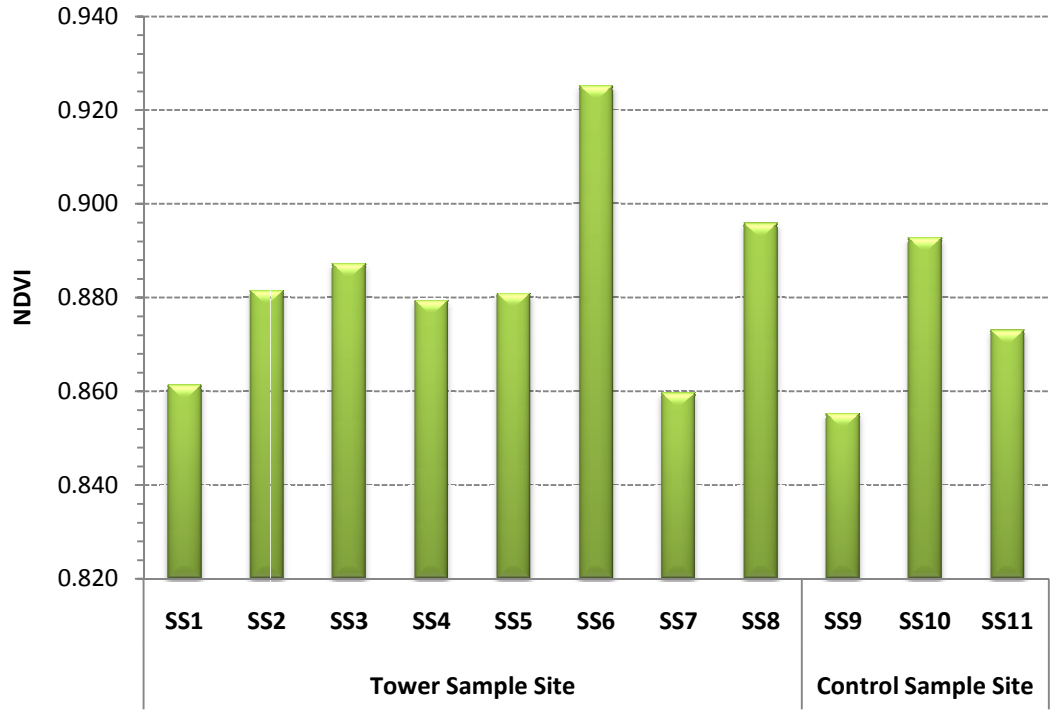

Figure 36 – NDVI results for tower and control sample sites at location D

4.3.3.2 Structural Band Ratio R_{1110}/R_{810}

The R_{1110}/R_{810} results are presented in Figure 37. According to Sridhar et al. (2007), higher concentrations of Zn should give higher R_{1110}/R_{810} values. In this case, the control samples with the lowest levels of Zn concentration appear to have the highest R_{1110}/R_{810} values. However, there was no distinct trend when compared to actual Zn levels that would indicate that Zn has had a negative influence on leaf structure (Figures 50 and 53, Appendix F). According to the independent samples t-test and the Mann-Whitney *U* test, there is a statistical difference ($p \leq 0.05$) between tower and control sites when

considering the ratio index R_{1110}/R_{810} ($p = 0.007$, $p = 0.025$ respectively) (see Table 32, Appendix E for summary statistics).

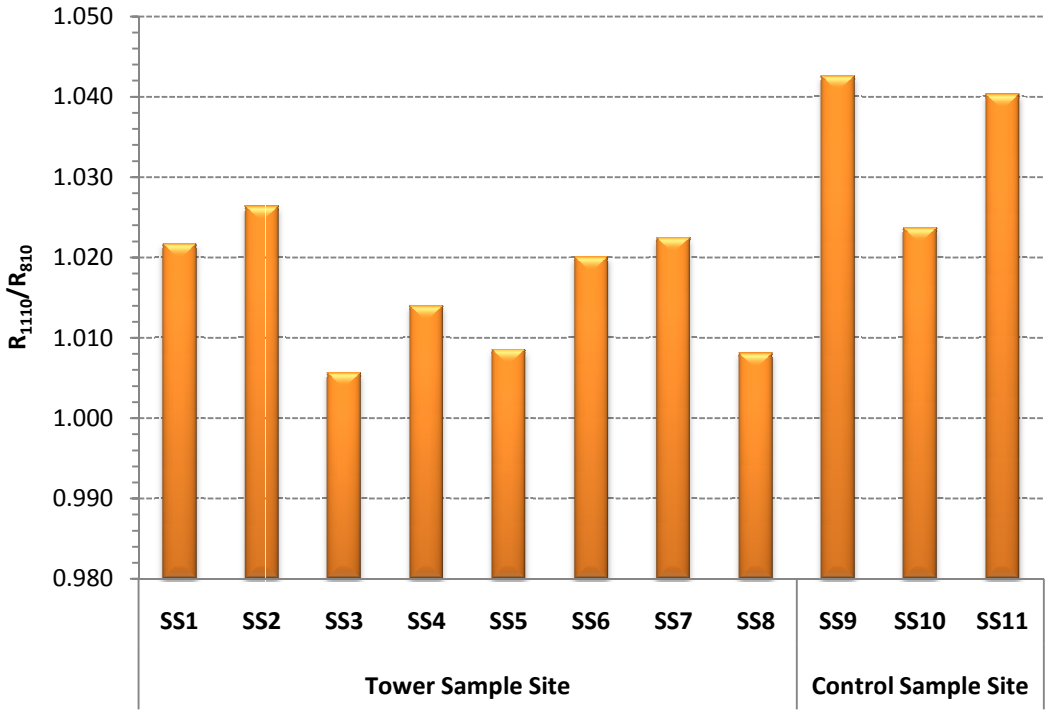

Figure 37 – R_{1110}/R_{810} band ratio results for tower and control sample sites at location D

4.3.3.3 Water Band Ratio R_{900}/R_{970}

The water band ratio R_{900}/R_{970} results are presented in Figure 38. The vegetation with higher concentrations of Zn should show a decrease in this ratio compared to the control (Sridhar et al., 2007). In this case, the control samples with the lowest levels of Zn concentration appear to have the lowest R_{900}/R_{970} values. However, there was no distinct trend when compared to actual Zn levels that would indicate that Zn has had a negative influence on the water band ratio (Figures 50 and 53, Appendix F). According to the independent samples t-test and the Mann-Whitney *U* test, there is a statistical difference ($p \leq 0.05$) between tower and control sites when considering the ratio index R_{900}/R_{970} ($p =$

0.007, p = 0.025 respectively) (see Table 32, Appendix E for summary statistics). There was also a strong positive correlation between water content R_{900}/R_{970} and soil moisture content (R^2 = 0.527, r = 0.726(9), p (0.011) < 0.05).

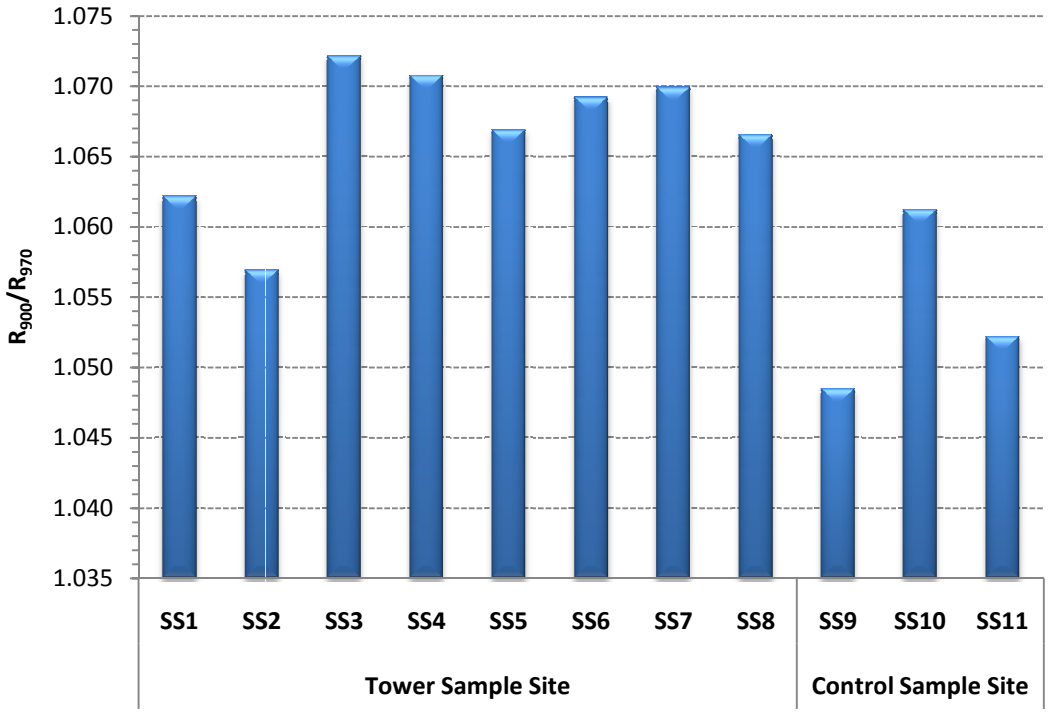

Figure 38 – R_{900}/R_{970} band ratio results for tower and control sample sites at location D

4.3.3.4 First Order Derivative

First order derivative spectra for location D from 400 to 780 nm were calculated using 1 nm intervals presented in Figure 39. The shape of the red-edge for the control and tower samples has little variation. Similar to the location B and C derivatives, location D exhibits the same REIP at 717 nm and secondary peak at 723 nm. However, location D has little changes in magnitude at those peaks. A small peak or shoulder can be seen around 699 nm where there is a change in magnitude between the control and tower derivatives.

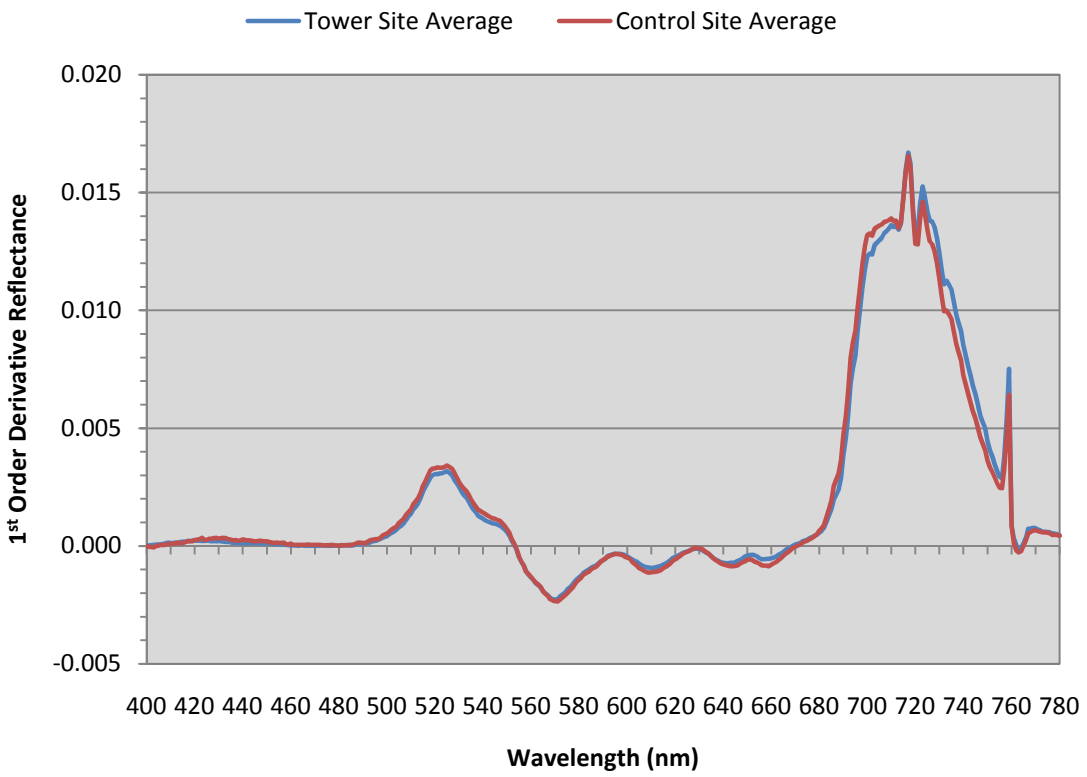

Figure 39 – Average first order derivative Himalayan Blackberry reflectance spectra for tower and control sites at location D

4.3.3.5 Continuum Removal

Normalized continuum removed reflectance at location D indicates that the tower reflectance has a large shift between 405 and 450 nm of 1 to 10 nm toward longer wavelengths in the blue absorption feature (400 – 550 nm, Figure 40). There is also a slight shift of 1 to 2 nm in tower reflectance between 560 and 660 nm toward shorter wavelengths, and a small shift to longer wavelengths between 690 and 745 nm (Figure 41). According to the Mann-Whitney *U* test, there is no statistical difference between tower and control sites when considering right area ($p = 0.066$) or band depth center ($p = 1.000$) at 400 to 550 nm. However, there is a significant difference between tower and control sites when considering band symmetry ($p = 0.025$), total area of absorption ($p =$

0.025) and left area (p = 0.025) at 400 to 550 nm. There is no statistical difference between tower and control sites when considering band symmetry (p = 0.102) or band depth center (p = 0.414) at 550 to 750 nm. However, there is a significant difference between tower and control sites when considering total area of absorption (p = 0.025), left area (p = 0.025), and right area (p = 0.014) at 550 to 750 nm.

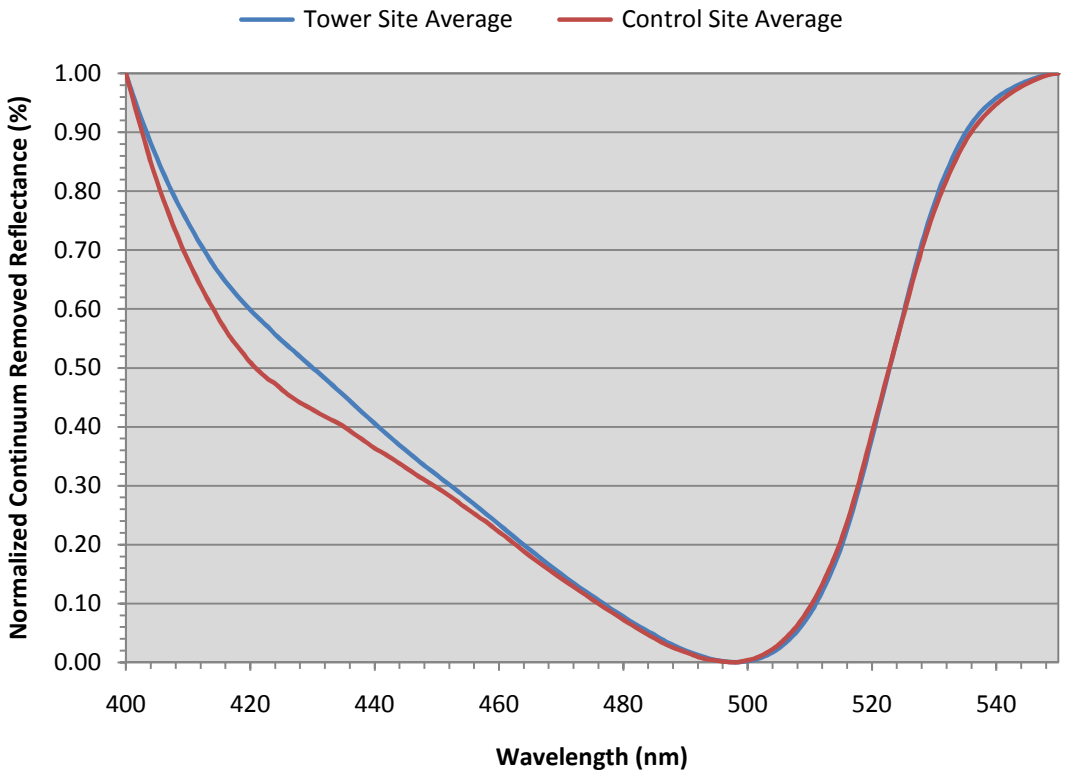

Figure 40 – Normalized continuum removed reflectance ($R_{400-550}$) of Himalayan Blackberry at location D

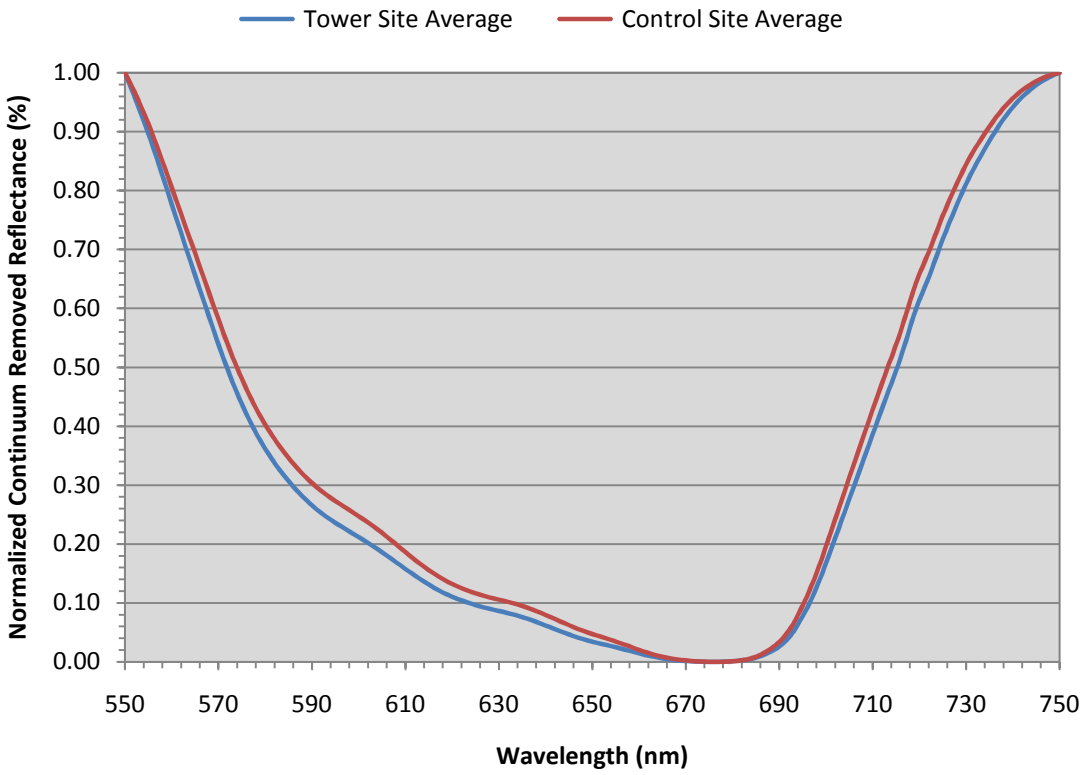

Figure 41 – Normalized continuum removed reflectance ($R_{550-750}$) of Himalayan Blackberry at location D

4.3.4 Spectroscopy Statistics

4.3.4.1 Location B

Results from the regression analysis infer with 95% confidence that Zn (PRS™-probe) ($R^2 = 0.198$, r = 0.445(9), p (0.648) > 0.05) and Zn (ICP-AES) ($R^2 = 0.092$, r = 0.303(9), p (0.869) > 0.05) levels do not explain a significant portion of the variation in structural band ratio R_{1110}/R_{810}, water band ratio R_{900}/R_{970} or NDVI. There is also no statistically significant correlation between Zn (PRS™-probe) and Zn (ICP-AES), r = 0.317(9), p (0.342) > 0.05. However, there is a moderately-strong negative correlation between structural band ratio R_{1110}/R_{810} and water band ratio R_{900}/R_{970}, r = -0.655(9), p (0.029) < 0.05. Figure 42 illustrates this relationship. There is no correlation between NDVI and

structural band ratio R_{1110}/R_{810} (r = 0.290(9), p (0.388) > 0.05) or water band ratio R_{900}/R_{970} (r = 0.162(9), p (0.634) > 0.05). There is also no correlation between water band ratio R_{900}/R_{970} and soil moisture content, r = 0.474(9), p (0.140) > 0.05.

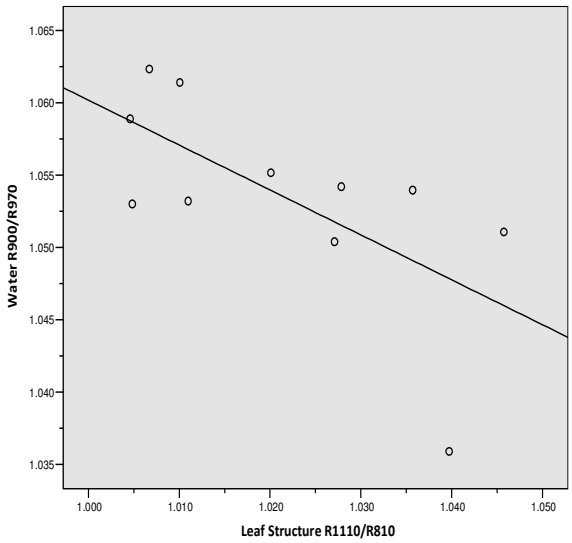

Figure 42 – Relationship between structural band ratio R_{1110}/R_{810} and water band ratio R_{900}/R_{970} of Himalayan Blackberry at location B

4.3.4.2 Location C

Results from the regression analysis infer with 95% confidence that Zn (PRS™-probe) (R^2 = 0.029, r = 0.170(9), p (0.975) > 0.05) and Zn (ICP-AES) (R^2 = 0.106, r = 0.325(9), p (0.841) > 0.05) levels do not explain a significant portion of the variation in structural band ratio R_{1110}/R_{810}, water band ratio R_{900}/R_{970}, or NDVI. There is also no statistically significant correlation between Zn (PRS™-probe) and Zn (ICP-AES), r = 0.365(9), p (0.270) > 0.05. However, there is a strong negative correlation between structural band ratio R_{1110}/R_{810} and water band ratio R_{900}/R_{970}, r = -0.664(9), p (0.026) < 0.05 (Figure 43). There is no correlation between NDVI and structural band ratio R_{1110}/R_{810} (r = -0.395(9),

p (0.226) > 0.05) or water band ratio R_{900}/R_{970} (r = 0.019(9), p (0.956) > 0.05). There is also no correlation between water band ratio R_{900}/R_{970} and soil moisture content, r = 0.275(9), p (0.414) > 0.05.

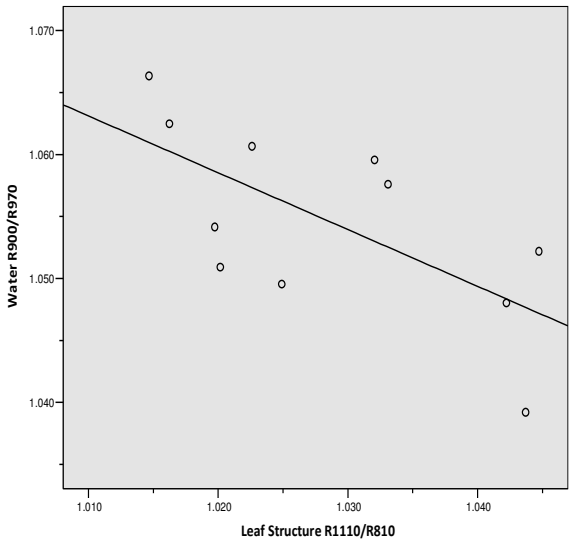

Figure 43 – Relationship between structural band ratio R_{1110}/R_{810} and water band ratio R_{900}/R_{970} of Himalayan Blackberry at location C

4.3.4.3 Location D

Results from the regression analysis infer with 95% confidence that Zn (PRS™-probe) (R^2 = 0.390, r = 0.624(9), p (0.442) > 0.05) and Zn (ICP-AES) (R^2 = 0.421, r = 0.649(9), p (0.253) > 0.05) levels do not explain a significant portion of the variation in structural band ratio R_{1110}/R_{810}, water band ratio R_{900}/R_{970}, or NDVI. There is no statistically significant correlation between Zn (PRS™-probe) and Zn (ICP-AES), r = 0.054(9), p (0.891) > 0.05. There is also no correlation between NDVI and structural band ratio R_{1110}/R_{810} (r = -0.429(9), p (0.187) > 0.05) or water band ratio R_{900}/R_{970} (r = 0.431(9), p (0.186) > 0.05). However, there is a moderately-strong positive correlation between Zn

(ICP-AES) and water band ratio R_{900}/R_{970}, r = 0.610(9), p (0.046) < 0.05 (Figure 44a). There is a strong negative correlation between structural band ratio R_{1110}/R_{810} and water band ratio R_{900}/R_{970}, r = -0.878(9), p (0.000) < 0.01 (Figure 44b). Also, there is a strong positive correlation between water band ratio R_{900}/R_{970} and soil moisture content, r = 0.726(9), p (0.011) < 0.05 (Figure 44c).

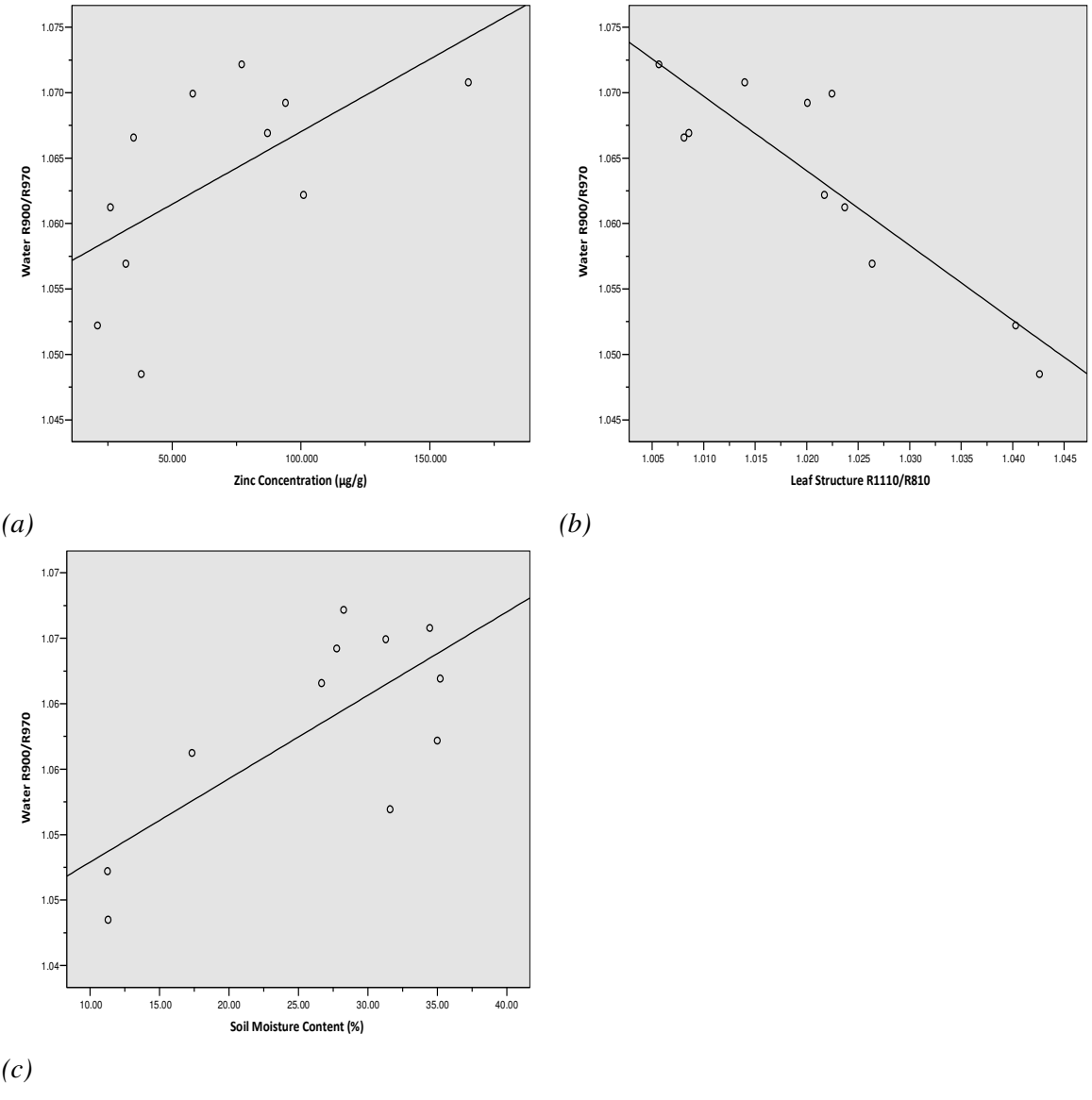

(a) *(b)* *(c)*

Figure 44 – Relationship between (*a*) water band ratio R_{900}/R_{970} and Zn concentration (µg/g); (*b*) structural band ratio R_{1110}/R_{810} and water band ratio R_{900}/R_{970}; and (*c*) and water band ratio R_{900}/R_{970} and soil moisture content (%)of Himalayan Blackberry at location D

Chapter 5 Discussion

5.1 SOIL ANALYSIS

5.1.1 Soil Temperature

Local climate is a major contributor to soil temperature, and the corresponding underground corrosion process. The temperate climate of the Lower Fraser Valley ensures that soil temperatures rarely reach the point of freezing. Freezing temperatures slow the chemical process of corrosion. Therefore, because temperatures rarely go below 0˚C, the underground corrosion process is more likely to occur year round.

The results of the IQ 150 pH meter indicate that average surface temperatures are generally higher than at depth. This is due to the fact that surface temperatures in the upper few centimetres of the soil profile are generally subjected to more direct solar radiation (Brady & Weil, 2002). However, surface and depth temperature levels only differed significantly at location B.

Tower sites generally have lower average temperatures than control sites. This is likely due to the fact that tower areas have denser vegetation and more surface cover which allow for cooler conditions (Brady & Weil, 2002). However, location D has the only significant difference in temperature between tower and control sites. The control sites at location D have a higher average temperature because these areas are characterized by greater amounts of bare soil and less surface cover than locations B and C.

5.1.2 Soil pH

The ideal pH range to promote the availability of plant nutrients is typically between 5.50 and 7.00 (Brady & Weil, 2002). The results found at locations B, C, and D generally indicate a near perfect acidity for the growth of plants, and there is little to no change when comparing the control sites to the tower sites or surface to depth levels. However, at location D there is a statistically significant difference between pH values at the control region and the tower region.

The control region is located on active agricultural land where agricultural practises, including the addition of fertilizers, herbicides, and pesticides, have caused the pH to be more basic. The lack of change in pH between tower and control sites at locations B and C would indicate that it is unlikely that corrosion alters the level of pH. It is also unlikely that pH at these levels would have an impact on the corrosion process. When considering pH levels at surface and depth, there is no significant difference at all three locations. However, surface pH levels are generally higher as pH is influenced by organic residues and other types of mulch and decaying organic matter on the soil surface (Brady & Weil, 2002).

5.1.3 Soil Moisture Content

The difference in percent soil moisture content is statistically significant between surface and depth levels at locations B and C. It is generally higher at the surface for all locations as there is a high percentage of organic matter at the soil surface which retains moisture. The surface cover surrounding the transmission towers not only shades and protects the moisture from escaping, but also adds to the organic soil horizon through

decomposition (Brady & Weil, 2002). Although only statistically significant at location D, there is generally a higher percent moisture content at the tower sites compared to the control. This is expected as the steel lattice on the transmission towers acts as a rain gutter, collecting water and distributing it on the vegetation below (Jones et al., 1987) (Figure 45).

Figure 45 – Moisture accumulation during rain storm on transmission tower at location D

At location B, the soil matrix is composed of a sandy loam and a medium to coarse sand at the subsurface. These soil textures create a rapidly pervious, low water retention environment. Location B has the lowest average soil moisture content, and the highest average temperature. Location B also has the highest resistivity values. Since resistivity typically increases with a rise in temperature, and decreases with increasing water

content, these results coincide with previously conducted research by Escalante (1989) and Iverson (1971).

According to Brady & Weil (2002), there is a general increase in available moisture storage from sands to loams and silt loams to clays. The larger pore spaces in sandy soils more readily facilitate the movement of air and water as opposed to the smaller pore spaces present in silt and clay textures. This accounts for the increase in percent moisture content at locations C and D when compared to location B. Location C consists of silt loam with some variation of silt clay loam, and a silty clay loam subsurface. Location D consists of a silt loam and a compact, dense, silty clay loam or silty clay subsurface. At location D, the mean percent moisture content at the control sites is lower at the surface than at depth. This is due to the lack of vegetation in these areas.

5.1.4 Resistivity

Locations B and C have very high resistivity values, placing them in the "very mild" corrosion category established by Waters (1952). Although still in the "very mild" corrosion category, there is a noticeable difference between the summer and fall values at location B. This is likely a result of the change in temperature and percent soil moisture content between the fall and summer months.

Resistivity values are extremely low (850.20 Ohm-cm) at location D, and may have been compromised by the addition of agricultural electrolytes to the soil. The addition of electrolytes is often required in agricultural practises to reduce the dispersion of aggregates and aid in the prevention of surface crusting (Brady & Weil, 2002). As electrolytes have a high degree of electrical conductivity, they may account for the

extremely low resistivity values. In addition, location D has the highest percent moisture content which would also contribute to the low resistivity values at this location.

5.2 ZINC CONCENTRATIONS

The Zn results from the Mann-Whitney *U* test and the independent samples t-test were generally identical and resulted in similar conclusions. Also, the hypothesis results of the independent t-test generally coincided with the non-parametric results. This indicates that despite the violation of many statistical assumptions, the difference in Zn levels between the tower and control sites were great enough that both methods resulted in the same conclusions.

At all three locations, the concentration of Zn indentified by the PRS™-probe and ICP-AES samples from beneath the tower legs indicate a higher quantity of Zn when compared to the control samples located 10 m from the base of the towers. The PRS™-probe results also indicate that, at all three locations, the level of Zn is significantly higher at the surface than at depth levels.

The ICP-AES results show that the levels of Zn are significantly higher at the tower sites than at the control sites at locations C and D. However, at location B, the difference is not significant as the p value ($p = 0.066$) falls just shy of determining this. As there were fewer control samples than tower samples, the unequal sample size may have caused the statistical analyses to yield incorrect or misleading results, thereby causing the lack of a significant relationship.

The units of the PRS™-probe and ICP-AES tests are different, and make direct comparison invalid. There is also no correlation between Zn PRS™-probe results and Zn

ICP-AES results. However, as a relative comparison, the PRS™-probe and the ICP-AES results are similar in distribution, and show parallel trends between tower and control sites. In addition, they both generally exhibit statistically significant differences between tower and control sites with respect to Zn levels.

The combined average ICP-AES tower surface value for all three locations was 84.000 µg/g, and the average control surface value was 33.555 µg/g. While the concentrations of Zn below the transmission towers are high when compared to the control sites, they are still well below the maximum acceptable Zn content for agricultural soils as the Contaminated Sites Regulation set by the British Columbia Ministry of Environment (1996) cites levels of 200 – 300 µg/g as acceptable.

The PRS™-probe results indicate higher than normal levels of Zn accumulation around the tower legs in the upper 10 cm of the soil profile. The lower values of the samples taken at approximately 1 m depth show that there is a sharp decline in Zn concentration through the soil column. However, the Zn levels at depth in the tower samples are higher than the Zn levels at depth in the control samples. The high levels of Zn at the soil surface would suggest that the majority of Zn is accumulating from an above ground source. Since most of the observed tower corrosion is occurring underground at an average depth of 1.5 m, it is expected that Zn levels would have a higher value at depth. However, there is a higher surface area of galvanized steel above ground as opposed to below. This explains why there are lower levels of Zn at a depth rather than at the surface.

A more uniform distribution of Zn is evident in the soil profile 10 m from the tower as the surface Zn levels correspond more closely to those at depth. The low Zn levels at

depth at both the tower and control areas suggest that Zn has very little mobility in the soils at locations B, C, and D. The higher Zn levels at depth at the tower sites as opposed to the control may be as a result of Zn from above ground tower corrosion moving down the soil column, and from subsurface corrosion. Given the high values of Zn at the surface, the latter is more likely.

5.3 PLANT ROOT SIMULATOR™ ELEMENTS

It was hypothesized that other by-products of corroding steel transmission towers, besides Zn, could be leaching into the surrounding soil as well. Thus, all the measurements of elements recorded by the PRS™-probes were analyzed. For example, iron oxide (Fe_2O_3) is the chemical composition of rust which is formed by the open air oxidation of iron. Iron oxide is created after the corrosion process has taken place. At locations B and D, the amount of Fe was significantly higher at depth levels than at surface levels. This difference could indicate that iron oxide is leaching from the tower legs into the soil. However, a closer inspection of the data revealed that the control sites had a higher level of Fe at depth than on the surface. There was also no significant difference between tower and control sites at all three locations. Thus, while iron oxide was observed in the soil directly beside the excavated corroding tower legs, the mobility was not observed in the PRS™-probe data.

Many of the elements measured by the PRS™-probes were unrelated to corrosion, and displayed no trends that would suggest an involvement in the corrosion process. However, there was generally a higher concentration of soil nutrient elements in the upper 10 cm of a soil profile due to soil organic matter. As organic matter decays,

nutrients are released as soluble ions that can be taken up by plant roots (Brady & Weil, 2002). In addition, organic matter is the primary source of nitrogen for most plants (Brady & Weil, 2002) which would account for the significant difference in total nitrogen found between surface and depth levels at all three locations. Generally, there was a significant difference in plant nutrients between surface and depth levels at the study locations.

5.4 OBSERVED TOWER CORROSION

Locations B and D were excavated on October 5th, 2009, and July 13th, 2009, respectively. Visual observations revealed evidence of localized underground corrosion occurring on the steel transmission tower legs at both locations. Figure 46 and 47 show two severely corroded legs. The highly localized corrosion on the tower legs caused shallow pits (pitting) on the steel which reduces the structural integrity of the metal (Uhlig & Revie, 1985). The majority of corrosion on the tower legs begins approximately 22.5 cm from the soil surface at location D, and 39.4 cm from the surface at location B. The extent of corrosion was also visually observed to be greater at location D. Differing types of soil and drainage at locations B and D likely accounts for the depth at which corrosion was first observed at each tower, as well as the extent of the corrosion. Location C was not scheduled for excavation during the study period, and therefore no underground visual observations were recorded for this location. However, British Columbia Hydro confirmed that the tower at location C is corroding underground, and is scheduled for corrosion maintenance in the summer of 2010 (Stan Peardon, BC Hydro, personal communication, July 13th, 2009).

Figure 46 – Corroded tower leg at location B

Figure 47 – Corroded tower leg at location D. Notice the contrast between above ground and subsurface steel corrosion.

5.5 SPECTROSCOPY ANALYSIS

Several researchers have identified that heavy metal induced plant stress causes an increased reflectance in the visible, and a decreased reflectance in the infrared (Clevers et

al., 2004; Goetz et al., 1983; Horler et al., 1980; Kooistra et al., 2003; Kooistra et al., 2004; Schuerger et al., 2003; Schwaller et al. 1983; Sridhar et al., 2007). In most cases, changes in the visible and the red-edge region of the reflectance spectra tends to be a generic response to stress induced changes in chlorophyll concentration. Sridhar et al. (2007) found that for Zn treated plants, the leaf spectra showed a decrease in the 800 – 1300 nm, 1470 – 1850 nm and 2000 – 2400 nm regions. They (Sridhar et al., 2007) also found that leaves with high concentrations of Zn showed a decrease in chlorophyll absorption around 680 nm. At location B, as shown in Figure 19, there was no decrease in absorption around 680 nm, but there was a small decrease in reflectance in the 800 – 1300 nm, 1470 – 1850 nm, and 2000 – 2400 nm regions. These values correlate to the general heavy metal induced plant reflectance values concluded by Horler et al. (1980) and Schwaller et al. (1983). The reflectance values from location B would suggest that the vegetation may be responding to the higher levels of Zn in the soil from the corroding transmission tower. However, since the difference in Zn levels between tower and control were not statistically significant, these findings may be coincidental. Reflectance spectra for locations C and D do not parallel the results found at location B. Spectra at location C show an increase in reflectance in the 800 – 1300 nm and 1470 – 1850 nm regions, and location D has very little differentiation in reflectance at all (Figures 27 and 35 respectively). Sridhar et al. (2007) also concluded that Zn treated plants do not show a noticeable decrease in chlorophyll absorption until Zn levels reach 4955.00 μg/g. The highest level of Zn recorded at the study locations was 165.00 μg/g.

5.5.1 NDVI

At all three locations, NDVI values give no indication that the concentration of Zn has had an influence on the NDVI. Higher concentrations of Zn in vegetation should decrease the NDVI value as the vegetation becomes stressed. However, given that Zn is a natural micronutrient, low concentrations may not be distinct enough from control samples to negatively affect the tower vegetation (Sridhar et al., 2007). According to the independent samples t-test and the Mann-Whitney *U* test, there is no statistical difference between tower and control sites when considering NDVI at all three locations (see Appendix E for summary statistics). There is also no statistical correlation between Zn levels (PRS™-probe or ICP-AES) and NDVI.

5.5.2 Structural Band Ratio R_{1110}/R_{810}

Since high levels of Zn affect internal leaf structure, the ratio index R_{1110}/R_{810} was used to indicate foliar structural changes in the vegetation that have accumulated heavy metals. According to Sridhar et al. (2007), higher concentrations of Zn should give higher R_{1110}/R_{810} values. However, there was no statistical correlation found between Zn levels (PRS™-probe or ICP-AES) and the structural band ratio R_{1110}/R_{810}. This is likely due to the fact that there were no distinct differences between control and Zn contaminated sites at locations B and C. Therefore, this index may only be useful when studying vegetation with higher concentrations of Zn accumulation.

According to the independent samples t-test and the Mann-Whitney *U* test, there was also no statistical difference between tower and control sites when considering the ratio index R_{1110}/R_{810} at locations B and C (see Tables 30 and 31, Appendix E for summary

statistics). However, there was a statistical difference between tower and control sites at location D (see Table 32, Appendix E for summary statistics). In this case, the control samples with the lowest levels of Zn concentration appear to have the highest R_{1110}/R_{810} values. This spurious association contradicts previous research conducted by Sridhar et al. (2007). At location D, much of the control vegetation was water deprived as it was situated in very bare and dry soil conditions with little to no surface cover. There was also a strong negative correlation between the structural band ratio R_{1110}/R_{810} and the water band ratio R_{900}/R_{970}. These conditions may have reduced the leaf water content, and in turn negatively affected leaf structure. This would account for the significant difference between tower and control sites.

5.5.3 Water Band Ratio R_{900}/R_{970}

The ratio of R_{900}/R_{970} was used to distinguish differences in vegetation water content as suggested by Sims and Gamon (2003). Vegetation with higher concentrations of Zn should show a decrease in this ratio (Sridhar et al., 2007). At locations B, C and D, there is a high degree of variation, and the ratio R_{900}/R_{970} is not statistically correlated to the tested Zn concentration from both the PRS™-probes and the ICP-AES at the sample sites.

According to the independent samples t-test and the Mann-Whitney *U* test, there is no statistical difference between tower and control sites when considering the ratio index R_{900}/R_{970} at locations B and C (see Tables 30 and 31, Appendix E for summary statistics). On the other hand, location D exhibits similar results to the structural band ratio R_{1110}/R_{810}. There is a statistical difference between tower and control sites at location D

(see Table 32, Appendix E for summary statistics). The control samples with the lowest levels of Zn concentration appear to have the lowest R_{900}/R_{970} values. It was also found that there was a strong positive correlation between water content R_{900}/R_{970} and soil moisture content ($R^2 = 0.527$, r = 0.726(9), p (0.011) < 0.05). This relationship would account for the corresponding results at location D. The low soil moisture content in the control areas resulted in a decrease in vegetation water content, and therefore a decrease in the water band ratio. This is consistent with research conducted by Sims and Gamon (2003) and Sridhar et al. (2007).

5.5.4 First Order Derivative Analysis

Derivative analysis was primarily used to locate the position and height of the inflection point of the red-edge and other peaks that may indicate plant stress. Locations B, C, and D all showed the same REIP located at 717 nm, and the same secondary peak at 723 nm. They also all had a small peak or shoulder around 700 nm.

The shape of the red-edge for the tower and control samples had little variation at all three locations. There was a small decrease in magnitude in the tower site maximum at location B; however, there was no shift in REIP maximum which, according to Horler et al. (1983), Murphy et. al. (2005), Smith et al. (2004), and Tsai & Philpot (1998) indicates that there is no variation in chlorophyll concentration between the tower and control sites. Although, according to Lamb et al. (2002), a decrease in magnitude is linked to a decrease in the magnitude of the NIR plateau in the individual reflectance profile (Figure 18). This is attributed to lower multiple scattering of radiation in NIR wavelengths caused by lower leaf reflectance and transmittance, and a lower chlorophyll concentration

(Lamb et al., 2002). When testing soil-oxygen depletion on grass, wheat, and beans, Smith et al. (2004) noted that as stress increased there was a decrease in the magnitude at the REIP. This is consistent with work conducted by Zarco-Tejada et al. (2003) who also found a stress induced decrease in derivative magnitude. However, both of these researchers noted that in very high stress conditions there was an increase in the shoulder position around 700 nm, and eventually a shift of the derivative maxima.

Unlike location B, locations C and D have little changes in magnitude at the maxima. A small peak or shoulder can be seen around 700 nm where there is a change in magnitude between the control and tower derivatives at both locations. Smith et al., (2004) suggests that an increase in magnitude at the shoulder position is often a response to stress. However, in the case of location C, the control derivative is the lower of the two, and the differences are not consistent with the level of Zn concentration at the tower legs. At location D, the increase at the shoulder position is minimal, and in previous studies there was also a change in magnitude of the REIP (Lamb et al., 2002; Smith et al., 2004; Zarco-Tejada et al., 2003). Since the decrease in magnitude is very minimal, this may also be a product of noise as derivatives are extremely sensitive to noise (Tsai & Philpot, 1998).

Had there been a higher concentration of Zn at the tower locations, stressed Himalayan Blackberry plants may have shown a larger decrease in the magnitude of the peaks at 717 – 725 nm, and an increase of the shoulder position at 700. Since the control site derivative average is presumably based on healthy green vegetation, and there is no shift in the REIP in the Zn contaminated tower derivative spectra, the vegetation in the tower

areas either are not stressed, or the derivative spectra does not show the Zn induced stress in this case.

5.5.5 Continuum Removal Analysis

The results of the continuum removal indicate that there is no major shift of the red-edge at any of the three study locations. A shift of the red-edge position toward shorter wavelengths is usually a leaf reflectance response to plant stress (Lamb et al., 2002; Murphy et al., 2005). The normalized band depth tower reflectance at location D has a shift toward shorter wavelengths, but only in the green-red absorption region (between 560 and 660 nm). Location D also shows a small shift to longer wavelengths between 690 and 745 nm. These shifts would account for the significant statistical difference between tower and control sites when considering total area, left area, and right area at 550 to 750 nm. Noomen et al. (2006) related a shift toward shorter wavelengths in the green-red slope reflectance to a broadening of the red absorption feature due to an increase in chlorophyll content and xanthophyll pigments. Lamb et al. (2002) and Murphy et al. (2005) also noted that there is a broadening and deepening of chlorophyll absorption at approximately 680 nm as the amount of chlorophyll increases. This typically causes a shift to longer wavelengths in the red-edge region (690 – 750 nm).

The normalized band depth tower reflectance at location D also shows a large shift between 405 and 450 nm toward longer wavelengths. This is statistically confirmed as there is a significant difference in band symmetry, total area of absorption, and left area at 400 to 550 nm. A shift to shorter wavelengths in this region can be attributed to a response to plant stress as chlorophyll and carotenoids are highly absorptive between 400

and 540 nm (Smith et al., 2004; Murphy et al., 2005). However, in this case, the control is shifting to shorter wavelengths and the differences are not consistent with the level of Zn concentration at the tower legs. This may be a response to the lower moisture content in the control areas of location D and a degradation of the foliar pigments due to lack of water. However, if this was the case, there would most likely be a more pronounced shift of the red-edge.

The PCA was an efficient statistical procedure to investigate the sources of spectral variance and to visualize the separation and similarity among the samples. However, the results of the regression analysis revealed that ICP-AES Zn levels do not explain a significant portion of the variation in the factor scores produced by the PCA, and there is also no correlation between the variables.

Therefore, the continuum removal did not display any trends that would indicate that the higher concentrations of Zn were negatively affecting the vegetation beneath the corroding transmission towers at the three study locations.

Chapter 6 Conclusion

6.1 THESIS CONCLUSIONS

The objective of this thesis was to investigate the potential advantages of using remote sensing techniques to assess underground transmission tower corrosion. More specifically, to examine the relationship, if any, between underground steel tower corrosion, soil corrosion characteristics, and reflectance spectra of overlying vegetation.

Many researchers have investigated underground soil corrosion (Bushman and Mehalick, 1989; Camitz and Vinka, 1989; Corbett and Jenkins, 1989; Escalante, 1989; Romanoff, 1962; Fitzgerald, 1989; Jones et al., 1988; Palmer, 1989; Uhlig & Revie, 1985) and remote sensing of heavy metal contaminated vegetation (Clevers et al., 2004; Goetz et al., 1983; Horler et al., 1980; Kooistra et al., 2003; Kooistra et al., 2004; Schuerger et al., 2003; Schwaller et al., 1983; Sridhar et al., 2007). However, the importance of this research is that it is the first of its kind to use remote sensing to assess underground corrosion.

Given that there are over 20,000 steel transmission towers in British Columbia, all of which are older than 25 years, it is highly probable that every tower in British Columbia is corroding to some degree. When a galvanized steel transmission tower corrodes, it leaches its protective sacrificial layer of Zn into the surrounding soil. However, results indicate that Zn has little mobility in the soil, and therefore remains isolated to the area directly beneath the corroding towers.

At all three study locations, the quantity of Zn in the soil and vegetation located beneath the galvanized steel transmission towers was considerably higher when

compared to control samples located 10 m from the tower bases. There was generally a statistically significant difference between study samples taken from beneath the corroding transmission towers and control samples. Since Zn is a natural micronutrient and necessary for plant growth, it is taken up by the overlying vegetation. The concentrations of Zn in Himalayan Blackberry plants growing beneath the towers were generally three times higher than concentrations in the same plants growing 10 m away. The PRS™-probe results indicated Zn soil surface levels of generally 30 times higher.

Once the Zn layer has corroded, the exposed steel is defenceless against the corrosion process, and therefore begins to disintegrate. Iron oxide (rust) is created as the steel breaks down. This by-product of the corrosion process has no recorded mobility in the soil, and is not negatively affecting the surrounding environment.

Among the three study locations, the soil at location D was the most prone to corrosion. Location D had the highest percent moisture content of the study areas, and the lowest resistivity values. The combination of available moisture from nearby agricultural watering, local temperate climate, abundant surface cover, silty clay soil type, and the possible addition of agricultural electrolytes provided an optimal environment for the corrosion process to thrive at this location. These results were validated through direct observation as location D had the highest extent of corrosion among the two excavated study locations.

The soils at location B were generally comprised of a sandy loam with a medium to coarse sand subsurface. These soil types have a high degree of drainage which results in a low percent moisture content. The low moisture content causes a reduction in soil

conductivity, and therefore a higher resistivity. Thus, corrosion at this location was less severe than at location D.

The soils at location C were comprised of a silt loam and silty clay subsurface which promote a high degree of water retention. The recorded percent moisture content at the site was lower than at location D, but higher than at location B. These factors, combined with a high sloped surface which promotes drainage, allows one to predict that, upon excavation, the severity of corrosion at location C will be in between that observed at locations B and D.

The spectral analyses did not reveal any indicators or differences between tower and control sites of Zn contamination in the vegetation. The high Zn concentrations recorded from the PRS™-probe and ICP-AES results could not be correlated to the reflectance spectra measured by the field spectrometer. Although NDVI, R_{110}/R_{810}, and R_{900}/R_{970} ratios have been successful at indicating stress levels in vegetation due to heavy metal content, these ratios were not able to isolate distinct trends that would indicate that the vegetation beneath the transmission towers were influenced by the high levels of Zn.

Both derivative reflectance and continuum removal have been used to detect a shift in the red-edge due to plant stress. However, while there was a small change in magnitude in the derivative reflectance at locations B and D, the results were not consistent with previously conducted studies on plant stress. Changes in reflectance in the far-red and infrared were inconsistent when compared to the control samples where low concentrations of Zn were measured. The results of the first order derivative and the continuum removal indicated that vegetation stress levels were not high enough to cause a significant shift of the red-edge in the reflectance spectra. Thus, the vegetation in the

tower areas either are not stressed by the higher than normal levels of Zn, or the derivative spectra and the continuum removed reflectance does not show the Zn induced stress in this case. Since Zn is not negatively affecting the growth of plants, there is no identifier in the reflectance spectra that would indicate that the transmission towers are corroding.

6.2 SUGGESTIONS FOR FUTURE RESEARCH

In order for remote sensing technologies to provide consistent and conclusive results regarding the detection of underground corrosion, additional research and technological innovation must be explored. As plant species vary in their spectral response, analysing the response of a different plant species exposed to Zn contamination may result in a significant trend. This may require that measurements be taken in a controlled test environment.

A more direct approach could be explored as well. An indicator substance, consisting of environmentally friendly soil elements or micronutrients, could be painted on the surface of the steel before the galvanized prevention layer is applied. Once the galvanized layer has disintegrated, the indicator substance would be slowly released as it itself was corroded. This indicator substance would leach into the soil, and be taken up by surrounding vegetation. The indicator substance could then be identified by its spectral response, thereby signifying that corrosion was about to affect the metallic structure.

The integration of remote sensing techniques and underground corrosion explored in this thesis presents unique opportunities for further research in this area of study.

Although using Zn as a spectral corrosion identifier was not successful in this thesis, the presence of a chemical process in which by-products were produced and leached into the soil was evident. Further research of these by-products and their mobility may significantly impact the world of corrosion prevention and structural maintenance.

References

Analytical Spectral Devices, Inc. (ASD Inc.). (2008). *FieldSpec*. Retrieved March 3rd, 2008, from http://www.asdi.com/products-fs3.asp

Ailor, W.H. (1971). *Handbook on Corrosion Testing and Evaluation*. New York, NY: John Wiley & Sons, Inc.

British Columbia Transmission Corporation (BCTC). (2007). *Building Connections - 2007 Annual Report*. Vancouver, BC: Author.

Blackburn, G. A. (1999). Relationships between spectral reflectance and pigment concentrations in stacks of deciduous broadleaves. *Remote Sensing of Environment, 70*, 224-237.

Brady, N.C., & Weil, R.R. (2002). *The Nature and Properties of Soils* (13th ed.). Upper Saddle River, NJ: Prentice-Hall.

British Columbia Ministry of Environment. (1996). *Environmental Management Act: Contaminated Sites Regulation*. Victoria, BC: Queen's Printer.

Bushman, J.B. & Mehalick, T.E. (1989). Statistical Analysis of Soil Characteristics to Predict Mean Time to Corrosion Failure of Underground Metallic Structures. In V. Chaker & J. D. Palmer (Eds.), *Effects of Soil Characteristics on Corrosion* (pp. 107-118). Philadelphia, PA: American Society for Testing and Materials.

Camitz, G. & Vinka, T. G. (1989). Corrosion of Steel and Metal-Coated Steel in Swedish Soils-Effects of Soil Parameters. In V. Chaker & J. D. Palmer (Eds.), *Effects of Soil Characteristics on Corrosion* (pp. 37-53). Philadelphia, PA: American Society for Testing and Materials.

Carter, G. A. (1993). Responses of leaf spectral reflectance to plant stress. *American Journal of Botany, 80*(3), 239-243.

Clark, R. N. (1999). Spectroscopy of Rocks and Minerals, and Principles of Spectroscopy. In A. N. Rencz (Ed.), *Manual of Remote Sensing, Volume 3: Remote Sensing for the Earth Sciences* (3rd ed.)(pp. 3-52). New York, NY: Wiley & Sons.

Clark, R. N., & Roush, T. L. (1984). Reflectance Spectroscopy: Quantitative Analysis Techniques for Remote Sensing Applications. *Journal of Geophysical Research*, *89*(7), 6329-6340.

Clevers, J. G. P. W., Kooistra, L., & Salas, E. A. L. (2004). Study of heavy metal contamination in river flood plains using the red-edge position in spectroscopic data. *International Journal of Remote Sensing, 25*(19), 3883-3895.

Corbett, R.A. & Jenkins, C.F. (1989). Soil Characteristics as Criteria for Cathodic Protection of a Nuclear Fuel Production Facility. In V. Chaker & J. D. Palmer (Eds.), *Effects of Soil Characteristics on Corrosion* (pp. 95-106). Philadelphia, PA: American Society for Testing and Materials.

Curran, P., Dungan, J. L., & Peterson, D. L. (2001). Estimating the foliar biochemical concentration of leaves with reflectance spectrometry: Testing the Kokaly and Clark methodologies. *Remote Sensing of Environment*, *76*(3), 349-359.

Dawson, T. P., & Curran, P. J. (1998). Technical note A new technique for interpolating the reflectance red edge position. *International Journal of Remote Sensing, 19*(11), 2133-2139.

Demetriades-Shah, T. H., Steven, M. D., & Clark, J. A. (1990). High Resolution Derivative Spectra in Remote Sensing. *Remote Sensing of Environment, 33*, 55-64.

Doyle, G., Seica, M. V., & Grabinsky, M. W. (2003). The role of soil in the external corrosion of cast iron water mains in Toronto, Canada. *Canadian Geotechnical Journal, 40*, 225-236.

Duffus, J. H. (2002). "Heavy Metals" – A Meaningless Term? *Pure Applied Chemistry, 74*(5), 793-807.

Dunteman, G. H. (1989). *Principal Components Analysis*. Sage University Paper series on Quantitative Applications in the Social Sciences, series no. 07-069. Newbury Park, CA: Sage.

Ecological Stratification Working Group. (1995). *A National Ecological Framework for Canada*. Ottawa/Hull, Canada: Agriculture and Agri-Food Canada, Research Branch, Centre for Land and Biological Resources Research and Environment Canada, State of the Environment Directorate, Ecozone Analysis Branch.

Eklundh, L. & Singh, A. (1993). A comparative analysis of standardised and unstandardised Principal Components Analysis in remote sensing. *International Journal of Remote Sensing, 14*, 1359-1370.

Elvidge, C. D., & Chen, Z. (1995). Comparison of broad-band and narrow-band red and near-infrared vegetation indices. *Remote Sensing of Environment, 54*, 38-48.

Escalante, E. (1989). Concepts of Underground Corrosion. In V. Chaker & J. D. Palmer (Eds.), *Effects of Soil Characteristics on Corrosion* (pp. 81-94). Philadelphia, PA: American Society for Testing and Materials.

Fitzgerald, J. H., III (1989). The Future as a Reflection of the Past. In V. Chaker & J. D. Palmer (Eds.), *Effects of Soil Characteristics on Corrosion* (pp. 1-4). Philadelphia, PA: American Society for Testing and Materials.

Foy, C. D., Chaney, R. L., & White, M. C. (1978). The physiology of metal toxicity in plants. *Annual Review of Plant Physiology, 29*, 511-566.

Galvão, L. S., & Vitorello, I. (1995). Quantitative approach in the spectral reflectance–lithostratigraphy of the Wind River and Big Horn Basins, Wyoming. *International Journal of Remote Sensing, 16*, 1617-1631.

Galvão, L. S., Filho, W. P., Abdon, M. M., Novo, E. M. M. L., Silva, J. S. V. and Ponzoni, F. J.(2003). Spectral reflectance characterization of shallow lakes from the Brazilian Pantanal wetlands with field and airborne hyperspectral data. *International Journal of Remote Sensing, 21*, 4093-4112.

Gao, B. & Goetz, A. F. H. (1994). Extraction of dry leaf spectral features from reflectance spectra of green vegetation. *Remote Sensing of Environment, 47*, 369-374.

Goetz, A. F. H., Rock, B. N., and Rowan, L. C. (1983). Remote sensing for exploration: an overview. *Economy Geology, 78*, 570-590.

Green, R. O., Eastwood, M. L., Sarture, C. M., Chrien, T. G., Aronsson, M., Chippendale, B. J., Faust, J. A., Pavri, B. E., Chovit, C. J., Solis, M., Olah, M. R., & Williams, O. (1998). Imaging spectroscopy and the Airborne Visible/Infrared Imaging Spectrometer (AVIRIS). *Remote Sensing of Environment, 65*, 227-248.

Hatchell, D. C. (Ed.). (1999). *Analytical Spectral Devices, Inc. (ASD) Technical Guide* (4th ed.). Boulder, CO: Analytical Spectral Devices, Inc.

Hesse, P. R. (1971). *A Textbook of Soil Chemical Analysis*. London, UK: John Murray, Ltd.

Horler, D. N. H., Barber, J., & Barringer, A. R. (1980). Effects of heavy metals on the absorbance and reflectance spectra of plants. *International Journal of Remote Sensing, 1*, 121-136.

Horler, D. N. H., Dockray, M., & Barber, J. (1983). The red edge of plant leaf reflectance. *International Journal of Remote Sensing, 4*, 273-288.

Huang, W. Z., & Schoenau, J.J. (1996). Microsite assessment of forest soil nitrogen, phosphorus, and potassium supply rate in-field using ion exchange membranes. *Communications in Soil Science and Plant Analysis, 27*, 2895-2908.

Hunt, G. R. (1980). Electromagnetic Radiation: The Communication Link in Remote Sensing. In D. S. Siegal & A. R. Gillespie (Eds.), *Remote Sensing in Geology* (pp. 5-45). New York, NY: John Wiley & Sons, Inc.

Iverson, W. P. (1971). Tests in Soils. In W. H. Ailor (Ed.), *Handbook on Corrosion Testing and Evaluation* (pp. 575-597). New York, NY: John Wiley & Sons, Inc.

Jensen, J.R. (2000). *Remote Sensing of the Environment: An Earth Resource Perspective*. Upper Saddle River, NJ: Prentice-Hall.

Jones, R., Prohaska, K.A., & Burgess, M.S.E. (1987). Zinc and Cadmium in corn plants growing near electrical transimission towers. *Water, Air, and Soil Pollution, 37*, 355-363.

Kalra, Y. P., Maynard, D. G., & Radford, F.G. (1989). Microwave digestion of tree foliage for multielement analysis. *Canadian Journal of Forestry Research, 19*, 981-985.

Kelley, C. C., & Spilsbury, R. H. (1939). *Soil Survey of the Lower Fraser Valley. Publication 650, Technical Bulletin 20, Department of Agriculture, Dominion of Canada.* Ottawa, ON: Department of Agriculture.

Kochubey, S. M. & Kazantsev T.A. (2006). Changes in the first derivatives of leaf reflectance spectra of various plants induced by variations of chlorophyll content. *Journal of plant physiology*, *164*(12), 1648-55.

Kokaly, R.F., & Clark, R.N. (1999). Spectroscopic Determination of Leaf Biochemistry Using Band-Depth Analysis of Absorption Features and Stepwise Multiple Linear Regression. *Remote Sensing of Environment, 67*, 267-287.

Kooistra, L., Leuven, R. S. E. W., Wehrens, R., Nienhuis, P. H., & Buydens, L. M. C. (2003). A comparison of methods to relate grass reflectance to soil metal contamination. *International Journal of Remote Sensing, 24*, 4995-5010.

Kooistra, L., Salas, E. A. L., Clevers, J. G. P. W., Wehrens, R., Leuven, R. S. E. W., Nienhuis, P. H., & Buydens, L. M. C. (2004). Exploring field vegetation reflectance as an indicator of soil contamination in river floodplains. *Environmental Pollution, 127*, 281-290.

Krzyzanowski, J., McKendry, I. G., & Innes, J. L. (2005). Evidence of elecated ozone concentrations on forested slopes of the Lower Fraser Valley, British Columbia, Canada. *Water, Air, and Soil Pollution, 173*, 273-287.

Lagacherie, P., Baret, F., Feret, J. B., Netto, J. M., & Robbez-Masson, J. M. (2007). Estimation of soil clay and calcium carbonate using laboratory, field and airborne hyperspectral measurements. *Remote Sensing of Environment*, doi: 10.1016/j.rse.2007.06.014

Lamb, D. W., Steyn-Ross, M., Schaares, P., Hanna, M. M., Silvester,W., & Steyn-Ross, A. (2002). Estimating leaf nitrogen concentration in rye- grass (Lolium spp) pasture using the chlorophyll red-edge: Modelling and experimental observations. *International Journal of Remote Sensing, 23*(18), 3619-3648.

Levesque, J. & King, D. J. (1999). Airborne digital camera image semivariance for evaluation of forest structural damage at an acid mine site. *Remote Sensing of Environment, 68*, 112-124.

Liang, S. (2004). *Quantitative Remote Sensing of Land Surfaces*. Hoboken, NJ: Wiley & Sons.

Luttmerding, H. A. (1980). *Soils of the Langley-Vancouver Map area. Vol. 1. Soil map mosaics and legend, Lower Fraser Valley (scale 1:25,000).* Kelowna, BC: British Columbia Ministry of the Environment.

Mann, H. B. & Whitney, D. R. (1947). On a test of whether one of two random variables is stochastically larger than the other. *Annals of Mathematical Statistics, 18*, 50-60.

McGrew, J. C., Jr & Monroe, C. B. (2000). *An Introduction to Statistical Problem Solving in Geography* (2nd ed.). Boston, MA: McGraw-Hill.

Microsoft Corporation. (2006). *Microsoft® Office Excel® 2007*. Redmond, WA: Microsoft Corporation.

Milton, E. J., Schaepman, M. E., Anderson, K., Kneubuhler, M., & Fox, N. (2007). Progress in field spectroscopy. *Remote Sensing of Environment*, doi: 10.1016/j.rse.2007.08.001

Munyati, C. (1994). Use of Principal Component Analysis (PCA) of remote sensing images in wetland change detection on the Kafue Flats, Zambia. *Geocarto International, 19*(3), 11-22.

Murphy, R. J., Tolhurst, T. J., Chapman, M. G., & Underwood, A.J. (2005). Estimation of surface chlorophyll-a on an emersed mudflat using field spectrometry: accuracy of ratios and derivative-based approaches. *International Journal of Remote Sensing*, *26*(9), 1835-1859.

Newman, A. (1996). Elements of ICPMS. *Analytical Chemistry, 68*, 46-51.

Noomen, M.F., Skidmore, A.K., van der Meer, F.D., & Prins, H.H.T. (2006). Continuum removed band depth analysis for detecting the effects of natural gas, methane and ethane on maize reflectance. *Remote Sensing of Environment, 105*, 262-270.

Palmer, J.D. (1989). Environmental Characteristics Controlling the Soil Corrosion of Ferrous Piping. In V. Chaker & J. D. Palmer (Eds.), *Effects of Soil Characteristics on Corrosion* (pp. 5-17). Philadelphia, PA: American Society for Testing and Materials.

Penuelas, J., Gamon, J. A., Fredeen, A. L., Merino, J., & Field, C. B. (1994). Reflectance indices associated with physiological changes in nitrogen- and water-limited sunflower leaves. *Remote Sensing of Environment, 48*, 135-146.

Perko, H.A. (2004). *Introduction to Corrosion and Galvanizing of Helix Foundation*. Presented at "Helical Foundations and Tiebacks" (November 2004) Specialty Seminar, Helical Foundations and Tiebacks Committee, Deep Foundation Institute. Tampa, FL. Retrieved from http://www.helicalpierworld.com/shared/content/enfineers/Perko_corrosion_of_helix_piers.pdf

Ritchey, F. J. (2008). *The Statistical Imagination: Elementary Statistics for the Social Sciences* (2nd ed.). New York: NY: McGraw-Hill.

Romanoff, M. (1962). Corrosion of Steel Pilings in Soils. In National Bureau of Standards Monography 127, *NBS Papers on Underground Corrosion of Steel Piling* 1962-1971 (pp. 1-23). Washington, DC: U.S. Government Printing Office.

Rout, G. R. & Das, P. (2003). Effect of metal toxicity on plant growth and metabolism: I. Zinc. *Agronomie, 23*, 3-11.

Schuerger, A.C., Capelle, G.A., Di Benedetto, J.A., Mao, C., Thai, C.N., Evans, M.D., Richards, J.T., Blank, T.A., & Stryjewski, E.C. (2003). Comparison of two hyperspectral imaging and two laser-induced fluorescence instruments for the detection of zinc stress and chlorophyll concentration in bahia grass (*Paspalum notatum Flugge*). *Remote Sensing of Environment, 84*, 572-588.

Schwaller, M. R., Schnetzler, C. C., & Marshall, P. E. (1983). The changes in leaf reflectance of sugar maple seedlings in response to heavy metal stress. *International Journal of Remote Sensing, 4*(1), 93-100.

Silva, T. S. F., Costa, M. P. F., Melack, J. M., & Novo, E. M. L. M., (2007). Remote sensing of aquatic vegetation: theory and applications. *Environ Monit Assess*, *140*, 131-145.

Sims, J. E., & Gamon, J. A. (2003). Estimation of vegetation water content and photosynthetic tissue area from spectral reflectance: a comparison of indices based on liquid water and chlorophyll adsorption features. *Remote Sensing of Environment, 84*, 526-537.

Smith, M. O., Johnson, P. E., and Adams, J. B. (1985). Quantitative determination of mineral types and abundances from reflectance spectra using principal components analysis. *Journal of Geophysical Research, 90*, 797-804.

Smith, K., Steven, M. D., & Colls, J. J. (2004). Use of hyperspectral derivative ratios in the red-edge region to identify plant stress responses to gas leaks. *Remote Sensing of Environment*, *92*(2), 207-217.

SPSS Inc. (2004). *SPSS for Windows, Version 13.0*. Chicago, Il: SPSS Inc.

Sridhar, B. B. M., Han, F. X., Diehl, S. V., Monts, D. L., & Su, Y. (2007). Spectral reflectance and leaf internal structure changes of barley plants due to phytoextraction of zinc and cadmium. *International Journal of Remote Sensing, 28*(5), 1041-1054.

Starkey, R. L. & Wight, K. M. (1945). *Anaerobic Corrosion of Iron in Soil*. New York, NY: American Gas Association.

Tan, K.H. (2005). *Soil Sampling Preparation, and Analysis* (2nd ed.). Boca Raton, FL: Taylor & Francis Group.

Tsai, F. & Philpot, W. (1998). Derivative Analysis of Hyperspectral Data. *Remote Sensing of Environment*, *66*(1), 41-51.

Uhlig, H.H. & Revie, R.W. (1985). *Corrosion and Corrosion Control: An Introduction to Corrosion Science and Engineering* (3rd ed.). New York, NY: John Wiley & Sons, Inc.

Ustin, S. L., Smith, M. O., Jacquemond, S., Verstraete, M., & Govaerts, Y. (1999). Geobotany: Vegetation Mapping in Earth Sciences. In A. N. Rencz (Ed.), *Manual of Remote Sensing, Volume 3: Remote Sensing for the Earth Sciences* (3rd ed.)(pp. 189-248). New York, NY: Wiley & Sons.

Waters, F. O. (1952). Soil Resistivity Measurements for Corrosion Control. *Corrosion, 8*(12), 407-416.

Western Ag Innovations, Inc. (2006). *Applying research solutions to agriculture and the environment – Plant Root Simulator (PRS^{TM}) Operations Manual* (3rd print) (pp. 7-25). Saskatoon, SK: Western Ag Innovations, Inc.

White, R., Jr. & Douthit, G. E. (1985). Use of microwave oven and nitric acid – hydrogen peroxide digestion to prepare botanical materials for elemental analysis by inductively coupled argon plasma emission spectroscopy. *Journal of Association of Official Analytical Chemists, 68*, 766-769.

Woolley, J. T. (1971). Reflectance and transmittance of light by leaves. *Plant Physiology, 148*, 515-522.

Yesilnacar, E. & Süzen, M. L. (2006). A land-cover classification for landslide susceptibility mapping by using feature components. *International Journal of Remote Sensing, 27(2)*, 253-275

Zarco-Tejada, P. J., Pushnik, J. C., Dobrowski, S., & Ustin, S. L. (2003). Steady-state chlorophyll a fluorescence detection from canopy derivative reflectance and double-peak red-edge effects. *Remote Sensing of Environment, 84,* 283-294.

Zumdahl, S.S. & Zumdahl, S.A. (2003). *Chemistry* (6th ed.). Boston, MA: Houghton-Mifflin Company.

Appendix A – Temperature and pH Measurements

Table 9 – Location B Temperature (°C). Data collected August 18th, 2008.

	Surface				1m Depth			
	Test 1	**Test 2**	**Test 3**	**Average**	**Test 1**	**Test 2**	**Test 3**	**Average**
SS1	19.9	19.1	20.3	19.77	17.4	17.0	17.4	17.27
SS2	18.9	18.0	19.2	18.70	16.3	16.2	16.1	16.20
SS3	20.6	20.5	20.8	20.63	17.5	17.5	17.6	17.53
SS4	19.9	20.4	19.5	19.93	16.1	17.2	16.2	16.50
SS5	20.5	20.6	19.5	20.20	16.9	16.6	16.9	16.80
SS6	18.5	18.6	19.2	18.77	16.9	16.3	16.5	16.57
SS7	21.1	20.9	21.0	21.00	17.2	17.4	17.2	17.27
SS8	20.9	20.3	20.6	20.60	17.0	17.0	17.1	17.03
SS9	25.0	24.8	25.0	24.93	19.3	19.2	19.2	19.23
SS10	19.5	19.8	18.9	19.40	15.3	15.6	14.9	15.27
SS11	19.4	19.6	19.1	19.37	15.5	15.3	15.3	15.37
Total Average				20.30				16.82

Table 10 – Location B pH. Data collected August 18th, 2008.

	Surface				1m Depth			
	Test 1	**Test 2**	**Test 3**	**Average**	**Test 1**	**Test 2**	**Test 3**	**Average**
SS1	5.87	5.92	5.75	5.85	5.51	5.59	5.83	5.64
SS2	6.24	5.06	4.91	5.40	5.48	5.21	5.35	5.35
SS3	5.76	5.44	5.48	5.56	5.49	5.56	5.78	5.61
SS4	5.85	5.55	5.61	5.67	5.39	5.60	5.63	5.54
SS5	5.32	5.39	5.34	5.35	5.60	5.27	5.53	5.47
SS6	5.48	5.50	5.62	5.53	5.89	5.74	5.71	5.78
SS7	5.68	5.56	5.27	5.50	5.16	5.84	5.61	5.54
SS8	5.69	5.64	5.40	5.58	5.53	5.51	5.30	5.45
SS9	6.00	5.83	5.54	5.79	5.50	5.42	5.52	5.48
SS10	5.98	5.62	5.65	5.75	5.62	5.87	5.52	5.67
SS11	6.25	5.85	5.46	5.85	5.47	5.47	5.32	5.42
Total Average				5.62				5.54

Table 11 – Location C Temperature (°C). Data collected August 25th, 2008.

	Surface				1m Depth			
	Test 1	**Test 2**	**Test 3**	**Average**	**Test 1**	**Test 2**	**Test 3**	**Average**
SS1	15.7	16.4	15.7	15.93	16.5	16.5	16.4	16.47
SS2	15.7	16.0	15.3	15.67	15.5	15.8	15.4	15.57
SS3	17.1	19.6	16.4	17.70	17.0	17.2	17.1	17.10
SS4	15.1	15.4	15.0	15.17	14.5	14.4	14.5	14.47
SS5	15.5	16.0	15.7	15.73	14.9	14.8	14.8	14.83
SS6	14.9	15.2	15.1	15.07	14.5	14.3	14.4	14.40
SS7	15.5	15.3	15.4	15.40	14.4	14.2	14.5	14.37
SS8	15.1	15.0	15.1	15.07	13.8	13.8	14.0	13.87
SS9	16.1	15.3	15.5	15.63	15.2	15.4	14.9	15.17
SS10	17.5	17.4	16.6	17.17	15.4	15.1	15.2	15.23
SS11	18.2	17.9	17.2	17.77	16.0	16.4	16.1	16.17
Total Average				16.03				15.24

Table 12 – Location C pH. Data collected August 25th, 2008.

	Surface				1m Depth			
	Test 1	**Test 2**	**Test 3**	**Average**	**Test 1**	**Test 2**	**Test 3**	**Average**
SS1	5.68	5.63	5.50	5.60	5.64	5.54	6.13	5.77
SS2	6.03	5.82	5.66	5.84	5.71	5.64	5.47	5.61
SS3	6.03	6.03	5.76	5.94	6.28	6.32	6.46	6.35
SS4	6.45	5.89	5.94	6.09	5.73	5.45	5.75	5.64
SS5	5.95	5.47	5.42	5.61	5.22	5.27	5.43	5.31
SS6	5.14	5.41	4.82	5.12	5.05	4.77	5.21	5.01
SS7	5.08	4.92	5.05	5.02	5.06	5.47	5.03	5.19
SS8	5.09	5.10	5.26	5.15	5.14	5.02	4.96	5.04
SS9	6.19	5.60	5.19	5.66	4.76	5.46	5.34	5.19
SS10	5.41	5.31	5.92	5.55	5.50	5.42	5.59	5.50
SS11	5.44	5.31	5.25	5.33	5.42	5.32	5.55	5.43
Total Average				5.54				5.46

Table 13 – Location D Temperature (°C). Data collected September 2nd, 2008.

	Surface				1m Depth			
	Test 1	**Test 2**	**Test 3**	**Average**	**Test 1**	**Test 2**	**Test 3**	**Average**
SS1	13.6	13.1	12.9	13.20	14.2	14.4	14.1	14.23
SS2	13.8	14.6	13.9	14.10	15.1	14.8	14.9	14.93
SS3	14.7	14.4	14.4	14.50	15.2	15.3	15.3	15.27
SS4	13.6	13.7	13.6	13.63	14.1	14.1	14.2	14.13
SS5	14.3	14.3	14.0	14.20	14.6	14.7	14.8	14.70
SS6	14.3	14.6	14.0	14.30	15.2	15.1	15.0	15.10
SS7	14.4	14.9	14.7	14.67	15.9	15.7	15.1	15.57
SS8	14.7	14.1	14.0	14.27	14.8	14.5	14.7	14.67
SS9	17.4	16.6	17.5	17.17	n/a*	n/a*	n/a*	n/a*
SS10	15.6	16.0	16.8	16.13	16.2	16.4	16.0	16.20
SS11	15.6	15.9	15.3	15.60	n/a*	n/a*	n/a*	n/a*
Total Average				14.71				14.98

*Compact soil prohibited 1m depth measurement.

Table 14 – Location D pH. Data collected September 2nd, 2008.

	Surface				1m Depth			
	Test 1	**Test 2**	**Test 3**	**Average**	**Test 1**	**Test 2**	**Test 3**	**Average**
SS1	5.41	5.50	5.05	5.32	4.89	4.77	5.22	4.96
SS2	5.33	5.40	5.48	5.40	5.03	5.48	5.15	5.22
SS3	5.32	5.29	5.57	5.39	5.35	5.64	5.34	5.44
SS4	4.51	5.03	4.45	4.66	4.39	4.45	4.78	4.54
SS5	4.98	5.01	5.18	5.06	5.28	5.12	5.32	5.24
SS6	5.16	5.32	5.36	5.28	5.09	4.75	5.11	4.98
SS7	5.17	5.00	5.42	5.20	5.32	5.09	5.29	5.23
SS8	5.27	5.52	5.40	5.40	5.54	4.90	5.12	5.19
SS9	5.65	5.74	5.45	5.61	n/a*	n/a*	n/a*	n/a*
SS10	6.02	6.08	5.98	6.03	5.59	6.00	5.43	5.67
SS11	5.77	5.77	5.53	5.69	n/a*	n/a*	n/a*	n/a*
Total Average				5.37				5.16

*Compact soil prohibited 1m depth measurement.

Appendix B – Soil Moisture Measurements

Table 15 – Location B Soil Moisture Content. Samples collected July 7th, 2008. Sample analysis conducted October 30th, 2008.

	Bag Weight (g)	Weight of Sample and Bag (g)	Wet Sample Weight (g)	Tin Weight (g)	Dried Sample Weight and Tin (g)	Dry Sample Weight (g)	Moisture Content (g)	Percent Moisture Content (%)
SS1 – Surface	6.88	182.30	175.42	8.21	156.92	148.71	26.71	17.96
SS1 – Depth	6.94	167.00	160.06	15.53	163.59	148.06	12	8.10
SS2 – Surface	6.95	166.73	159.78	15.82	152.29	136.47	23.31	17.08
SS2 – Depth	7.01	178.74	171.73	8.30	166.53	158.23	13.5	8.53
SS3 – Surface	6.98	171.00	164.02	15.60	160.95	145.35	18.67	12.84
SS3 – Depth	7.02	141.69	134.67	15.73	134.23	118.5	16.17	13.65
SS4 – Surface	6.97	174.53	167.56	15.70	154.38	138.68	28.88	20.82
SS4 – Depth	6.86	168.76	161.9	8.20	155.67	147.47	14.43	9.79
SS5 – Surface	6.90	217.11	210.21	15.73	188.69	172.96	37.25	21.54
SS5 – Depth	6.78	257.27	250.49	15.57	243.02	227.45	23.04	10.13
SS6 – Surface	6.81	172.02	165.21	15.77	149.40	133.63	31.58	23.63
SS6 – Depth	6.85	178.98	172.13	15.54	172.83	157.29	14.84	9.43
SS7 – Surface	6.93	195.18	188.25	8.21	169.96	161.75	26.5	16.38
SS7 – Depth	7.09	208.76	201.67	15.88	201.69	185.81	15.86	8.54
SS8 – Surface	6.87	189.27	182.4	15.65	180.85	165.2	17.2	10.41
SS8 – Depth	6.99	210.53	203.54	15.70	199.51	183.81	19.73	10.73
SS9 – Surface	6.75	186.56	179.81	15.83	185.38	169.55	10.26	6.05
SS9 – Depth	6.90	184.00	177.1	15.69	182.03	166.34	10.76	6.47
SS10 – Surface	6.95	160.43	153.48	15.76	142.75	126.99	26.49	20.86
SS10 – Depth	6.92	171.71	164.79	15.60	168.51	152.91	11.88	7.77
SS11 – Surface	6.82	205.20	198.38	15.97	187.14	171.17	27.21	15.90
SS11 – Depth	6.99	177.65	170.66	15.66	171.97	156.31	14.35	9.18

Table 16 – Location C Soil Moisture Content. Samples collected July 14th, 2008. Sample analysis conducted November 17th, 2008.

	Bag Weight (g)	Weight of Sample and Bag (g)	Wet Sample Weight (g)	Tin Weight (g)	Dried Sample Weight and Tin (g)	Dry Sample Weight (g)	Moisture Content (g)	Percent Moisture Content (%)
SS1 – Surface	6.50	155.65	149.15	15.99	147.85	131.86	17.29	13.11
SS1 – Depth	6.58	165.52	158.94	15.52	157.05	141.53	17.41	12.30
SS2 – Surface	6.55	126.19	119.64	15.55	110.63	95.08	24.56	25.83
SS2 – Depth	6.51	136.06	129.55	15.84	129.93	114.09	15.46	13.55
SS3 – Surface	6.46	136.17	129.71	15.68	132.44	116.76	12.95	11.09
SS3 – Depth	6.42	163.63	157.21	15.87	155.93	140.06	17.15	12.24
SS4 – Surface	6.42	150.60	144.18	15.62	122.69	107.07	37.11	34.66
SS4 – Depth	6.42	157.90	151.48	15.73	144.59	128.86	22.62	17.55
SS5 – Surface	6.46	154.97	148.51	15.85	136.44	120.59	27.92	23.15
SS5 – Depth	6.55	162.06	155.51	15.66	159.47	143.81	11.7	8.14
SS6 – Surface	6.53	154.29	147.76	15.84	134.71	118.87	28.89	24.30
SS6 – Depth	6.53	257.69	251.16	15.50	219.27	203.77	47.39	23.26
SS7 – Surface	6.52	182.12	175.6	15.59	150.79	135.2	40.4	29.88
SS7 – Depth	6.45	230.55	224.1	15.74	215.64	199.9	24.2	12.11
SS8 – Surface	6.44	174.62	168.18	15.74	146.39	130.65	37.53	28.73
SS8 – Depth	6.43	192.60	186.17	15.80	166.41	150.61	35.56	23.61
SS9 – Surface	6.41	179.96	173.55	15.79	157.01	141.22	32.33	22.89
SS9 – Depth	6.42	216.94	210.52	15.68	184.80	169.12	41.4	24.48
SS10 – Surface	6.39	147.70	141.31	15.69	137.77	122.08	19.23	15.75
SS10 – Depth	6.40	179.25	172.85	15.80	177.24	161.44	11.41	7.07
SS11 – Surface	6.46	193.56	187.1	15.70	181.46	165.76	21.34	12.87
SS11 – Depth	6.48	206.59	200.11	15.55	197.09	181.54	18.57	10.23

Table 17 – Location D Soil Moisture Content. Samples collected July 21st, 2008. Sample analysis conducted November 26th, 2008.

	Bag Weight (g)	Weight of Sample and Bag (g)	Wet Sample Weight (g)	Tin Weight (g)	Dried Sample Weight and Tin (g)	Dry Sample Weight (g)	Moisture Content (g)	Percent Moisture Content (%)
SS1 – Surface	7.16	155.00	147.84	15.73	125.24	109.51	38.33	35.00
SS1 – Depth	7.13	186.88	179.75	15.55	161.19	145.64	34.11	23.42
SS2 – Surface	7.22	167.06	159.84	15.73	137.19	121.46	38.38	31.60
SS2 – Depth	7.19	145.62	138.43	15.67	130.95	115.28	23.15	20.08
SS3 – Surface	6.44	195.02	188.58	15.65	162.68	147.03	41.55	28.26
SS3 – Depth	6.46	269.42	262.96	15.77	224.64	208.87	54.09	25.90
SS4 – Surface	6.44	165.12	158.68	15.68	133.69	118.01	40.67	34.46
SS4 – Depth	6.49	179.23	172.74	15.85	156.05	140.2	32.54	23.21
SS5 – Surface	6.44	170.85	164.41	15.68	137.28	121.6	42.81	35.21
SS5 – Depth	6.50	193.93	187.43	15.55	166.60	151.05	36.38	24.08
SS6 – Surface	6.46	242.20	235.74	15.84	200.36	184.52	51.22	27.76
SS6 – Depth	6.50	247.40	240.9	15.73	210.65	194.92	45.98	23.59
SS7 – Surface	6.51	187.28	180.77	15.69	153.38	137.69	43.08	31.29
SS7 – Depth	6.49	208.57	202.08	15.83	182.36	166.53	35.55	21.35
SS8 – Surface	6.42	262.86	256.44	15.62	218.07	202.45	53.99	26.67
SS8 – Depth	6.43	196.28	189.85	15.81	168.71	152.9	36.95	24.17
SS9 – Surface	6.44	161.10	154.66	15.99	154.95	138.96	15.7	11.30
SS9 – Depth	6.54	224.57	218.03	15.66	201.25	185.59	32.44	17.48
SS10 – Surface	6.39	191.91	185.52	15.59	173.70	158.11	27.41	17.34
SS10 – Depth	6.41	221.46	215.05	15.50	193.54	178.04	37.01	20.79
SS11 – Surface	6.40	176.01	169.61	15.86	168.31	152.45	17.16	11.26
SS11 – Depth	6.46	202.23	195.77	15.52	161.61	146.09	49.68	34.01

Appendix C – Soil Statistics

Table 18 – Location B PRS™-probe and soil measurement one sample KS tests, and means and standard deviations for tower, control, surface, and depth segments

	Mean and Standard Deviation				KS Test	Normally Distributed
Variable	**Tower**	**Control**	**Surface**	**Depth**		
Zinc levels	M = 132.500 SD = 146.959	M = 3.000 SD = 1.514	M = 176.236 SD = 160.207	M = 18.127 SD = 17.461	KS(22) = 1.394, p = 0.041	No
Moisture Content	M = 13.723 SD = 5.157	M = 11.038 SD = 6.000	M = 16.679 SD = 5.254	M = 9.302 SD = 1.868	KS(22) = 0.975, p = 0.297	Yes
pH levels	M = 5.551 SD = 0.140	M = 5.660 SD = 0.174	M = 5.621 SD = 0.174	M = 5.541 SD = 0.125	KS(22) = 0.493, p = 0.968	Yes
Tot_N	M = 100.325 SD = 154.336	M = 39.433 SD = 63.418	M = 148.036 SD = 173.070	M = 19.400 SD = 17.438	KS(22) = 1.568, p = 0.015	No
NO3	M = 100.325 SD = 154.336	M = 39.433 SD = 63.418	M = 148.036 SD = 173.070	M = 19.400 SD = 17.438	KS(22) = 1.568, p = 0.015	No
Ca	M = 370.600 SD = 323.431	M = 307.633 SD = 223.669	M = 574.546 SD = 272.514	M = 132.309 SD = 42.734	KS(22) = 0.998, p = 0.272	Yes
Mg	M = 77.538 SD = 88.709	M = 66.333 SD = 77.354	M = 134.200 SD = 83.131	M = 14.764 SD = 9.700	KS(22) = 1.328, p = 0.059	Yes
K	M = 216.988 SD = 228.565	M = 189.133 SD = 233.001	M = 341.273 SD = 252.390	M = 77.509 SD = 62.299	KS(22) = 1.179, p = 0.124	Yes
P	M = 3.125 SD = 1.588	M = 1.933 SD = 0.484	M = 3.400 SD = 1.840	M = 2.200 SD = 0.587	KS(22) = 1.025, p = 0.244	Yes
Fe	M = 6.962 SD = 2.147	M = 6.833 SD = 1.732	M = 6.255 SD = 2.272	M = 7.600 SD = 1.505	KS(22) = 0.787, p = 0.565	Yes
Mn	M = 1.325 SD = 1.294	M = 1.267 SD = 0.836	M = 2.000 SD = 1.339	M = .618 SD = 0.140	KS(22) = 1.430, p = 0.033	No
B	M = 1.138 SD = 0.424	M = 1.267 SD = 0.776	M = 1.291 SD = 0.373	M = 1.055 SD = 0.639	KS(22) = 0.799, p = 0.546	Yes
S	M = 20.288 SD = 28.180	M = 19.167 SD = 15.056	M = 30.146 SD = 32.532	M = 9.818 SD = 4.409	KS(22) = 1.387, p = 0.043	No
Al	M = 59.400 SD = 10.058	M = 61.100 SD = 10.820	M = 55.527 SD = 8.732	M = 64.200 SD = 9.691	KS(22) = 0.873, p = 0.432	Yes
Temp_Avg	M = 18.423 SD= 1.709	M = 18.9283 SD = 3.53762	M = 20.300 SD = 1.707	M = 16.822 SD = 1.087	KS(22) = 0.611, p = 0.850	Yes

Table 19 – Location B PRS™-probe and soil measurement, Levene's tests, independent samples t-tests, and Mann-Whitney *U* tests

Variable	Levene's Test/Independent Samples t-test						Mann-Whitney U Test			
	Site	Equal Variances Assumed	Significant Difference	Depth	Equal Variances Assumed	Significant Difference	Site	Significant Difference	Depth	Significant Difference
Zinc levels	p = 0.003	No	Yes	p = 0.008	No	Yes	p = 0.001	Yes	p = 0.015	Yes
Moisture Content	p = 0.310	Yes	No	p = 0.001	No	Yes	p = 0.122	No	p = 0.002	Yes
pH levels	p = 0.143	Yes	No	p = 0.230	Yes	No	p = 0.184	No	p = 0.250	No
Tot_N	p = 0.366	Yes	No	p = 0.034	No	Yes	p = 0.122	No	p = 0.006	Yes
NO3	p = 0.366	Yes	No	p = 0.034	No	Yes	p = 0.122	No	p = 0.006	Yes
Ca	p = 0.667	Yes	No	p = 0.000	No	Yes	p = 0.768	No	p = 0.000	Yes
Mg	p = 0.788	Yes	No	p = 0.001	No	Yes	p = 0.768	No	p = 0.000	Yes
K	p = 0.803	Yes	No	p = 0.006	No	Yes	p = 0.606	No	p = 0.001	Yes
P	p = 0.090	Yes	No	p = 0.062	No	No	p = 0.054	No	p = 0.157	No
Fe	p = 0.897	Yes	No	p = 0.117	Yes	No	p = 0.970	No	p = 0.030	Yes
Mn	p = 0.920	Yes	No	p = 0.007	No	Yes	p = 0.763	No	p = 0.001	Yes
B	p = 0.619	Yes	No	p = 0.302	Yes	No	p = 0.792	No	p = 0.056	No
S	p = 0.928	Yes	No	p = 0.066	No	No	p = 0.712	No	p = 0.001	Yes
Al	p = 0.733	Yes	No	p = 0.039	Yes	Yes	p = 1.000	No	p = 0.028	Yes
Temp Avg	p = 0.652	Yes	No	p = 0.000	Yes	Yes	p = 0.883	No	p = 0.000	Yes

Table 20 – Location C PRS™-probe and soil measurement one sample KS tests, and means and standard deviations for tower, control, surface, and depth segments

	Mean and Standard Deviation				KS Test	Normally Distributed
Variable	**Tower**	**Control**	**Surface**	**Depth**		
Zinc levels	M = 133.488 SD = 178.048	M = 3.667 SD = 3.410	M = 190.018 SD = 190.501	M = 6.146 SD = 5.114	KS(22) = 1.552, p = 0.016	No
Moisture Content	M = 19.594 SD = 8.038	M = 15.548 SD = 6.943	M = 22.024 SD = 7.812	M = 14.958 SD = 6.299	KS(22) = 0.896, p = 0.398	Yes
pH levels	M = 5.518 SD = 0.415	M = 5.443 SD = 0.167	M = 5.537 SD = 0.349	M = 5.458 SD = 0.386	KS(22) = 0.567, p = 0.905	Yes
Tot_N	M = 311.388 SD = 317.168	M = 149.200 SD = 180.827	M = 450.527 SD = 317.100	M = 83.782 SD = 64.744	KS(22) = 0.959, p = 0.317	Yes
NO3	M = 308.400 SD = 317.499	M = 143.133 SD = 182.171	M = 446.836 SD = 318.365	M = 79.818 SD = 65.405	KS(22) = 0.942, p = 0.338	Yes
Ca	M = 826.075 SD = 571.655	M = 776.333 SD = 539.745	M = 1234.655 SD = 434.764	M = 390.364 SD = 236.330	KS(22) = 0.671, p = 0.759	Yes
Mg	M = 173.175 SD = 141.103	M = 160.767 SD = 117.326	M = 278.236 SD = 92.172	M = 61.346 SD = 49.461	KS(22) = 0.771, p = 0.592	Yes
K	M = 343.763 SD = 380.033	M = 331.578 SD = 308.624	M = 573.236 SD = 316.719	M = 134.073 SD = 82.026	KS(22) = 1.276, p = 0.077	Yes
P	M = 3.300 SD = 1.133	M = 2.875 SD = 0.327	M = 3.946 SD = 3.278	M = 1.473 SD = 0.628	KS(22) = 1.213, p = 0.105	Yes
Fe	M = 7.850 SD = 4.580	M = 5.867 SD = 0.561	M = 5.727 SD = 0.855	M = 8.891 SD = 5.205	KS(22) = 1.397, p = 0.040	No
Mn	M = 2.100 SD = 2.674	M = 1.200 SD = 0.947	M = 2.946 SD = 2.900	M = 0.763 SD = 0.709	KS(22) = 1.184, p = 0.121	Yes
B	M = 0.650 SD = 0.297	M = 0.900 SD = 0.374	M = 0.746 SD = .221	M = 0.691 SD = 0.423	KS(22) = 1.295, p = 0.070	Yes
S	M = 47.663 SD =77.789	M = 16.533 SD = 10.926	M = 69.073 SD = 87.086	M = 9.273 SD = 2.922	KS(22) = 1.436, p = 0.032	No
Al	M = 60.438 SD = 8.086	M = 56.833 SD = 8.496	M = 62.000 SD = 56.909	M = 8.329 SD = 7.496	KS(22) = 0.606, p = 0.856	Yes
Temp_Avg	M = 15.426 SD= 1.022	M = 16.190 SD = 1.071	M = 16.028 SD = 1.024	M = 15.241 SD = 1.003	KS(22) = 0.686, p = 0.735	Yes

Table 21 – Location C PRS™-probe and soil measurement Levene's tests, independent samples t-tests, and Mann-Whitney *U* tests

Variable	Levene's Test/Independent Samples t-test						Mann-Whitney U Test			
	Site	Equal Variances Assumed	Significant Difference	Depth	Equal Variances Assumed	Significant Difference	Site	Significant Difference	Depth	Significant Difference
Zinc levels	p = 0.011	No	Yes	p = 0.009	No	Yes	p = 0.006	Yes	p = 0.005	Yes
Moisture Content	p = 0.290	Yes	No	p = 0.030	Yes	Yes	p = 0.269	No	p = 0.039	Yes
pH levels	p = 0.553	No	No	p = 0.620	Yes	No	p = 0.796	No	p = 0.511	No
Tot_N	p = 0.255	Yes	No	p = 0.003	No	Yes	p = 0.140	No	p = 0.002	Yes
NO3	p = 0.247	Yes	No	p = 0.003	No	Yes	p = 0.122	No	p = 0.002	Yes
Ca	p = 0.856	Yes	No	p = 0.000	No	Yes	p = 0.825	No	p = 0.000	Yes
Mg	p = 0.850	Yes	No	p = 0.000	Yes	Yes	p = 0.941	No	p = 0.000	Yes
K	p = 0.819	Yes	No	p = 0.001	No	Yes	p = 0.417	No	p = 0.001	Yes
P	p = 0.009	No	Yes	p = 0.032	No	Yes	p = 0.012	Yes	p = 0.032	Yes
Fe	p = 0.109	No	No	p = 0.073	No	No	p = 0.883	No	p = 0.392	No
Mn	p = 0.436	Yes	No	p = 0.025	Yes	Yes	p = 0.459	No	p = 0.001	Yes
B	p = 0.116	Yes	No	p = 0.709	Yes	No	p = 0.072	No	p = 0.195	No
S	p = 0.347	Yes	No	p = 0.046	No	Yes	p = 0.357	No	p = 0.000	Yes
Al	p = 0.369	Yes	No	p = 0.148	Yes	No	p = 0.238	No	p = 0.140	No
Temp Avg	p = 0.139	Yes	No	p = 0.083	Yes	No	p = 0.113	No	p = 0.076	No

Table 22 – Location D PRS™-probe and soil measurement one sample KS tests, and means and standard deviations for tower, control, surface, and depth segments

	Mean and Standard Deviation				KS Test	Normally Distributed
Variable	**Tower**	**Control**	**Surface**	**Depth**		
Zinc levels	M = 226.275 SD = 171.020	M = 9.200 SD = 11.314	M = 294.489 SD = 168.079	M = 109.822 SD = 133.771	KS(22) = 0.729, p = 0.662	Yes
Moisture Content	M = 27.253 SD = 4.928	M = 18.697 SD = 8.393	M = 26.377 SD = 9.012	M = 23.462 SD = 4.207	KS(22) = 0.425, p = 0.994	Yes
pH levels	M = 5.157 SD = 0.261	M = 5.750 SD = 0.1897	M = 5.367 SD = 0.352	M = 5.163 SD = 0.318	KS(22) = 0.680. p = 0.745	Yes
Tot_N	M = 614.188 SD = 370.450	M = 540.900 SD = 659.731	M = 798.644 SD = 359.437	M = 413.444 SD = 316.629	KS(22) = 0.563, p = 0.909	Yes
NO3	M = 612.500 SD = 370.955	M = 540.900 SD = 659.731	M = 798.044 SD = 359.743	M = 411.044 SD = 316.069	KS(22) = 0.560, p = 0.912	Yes
Ca	M = 1627.725 SD = 1636.900	M = 404.694 SD = 1254.549	M = 1826.533 SD = 466.821	M = 1430.956 SD = 444.853	KS(22) = 0.779, p = 0.578	Yes
Mg	M = 374.663 SD = 182.679	M = 141.900 SD = 90.934	M = 255.711 SD = 72.001	M = 441.889 SD = 225.750	KS(22) = 1.111, p = 0.169	Yes
K	M = 125.500 SD = 94.624	M = 186.600 SD = 22.910	M = 174.467 SD = 98.474	M = 90.111 SD = 63.117	KS(22) = 0.985, p = 0.286	Yes
P	M = 9.738 SD = 7.552	M = 23.200 SD = 19.799	M = 13.044 SD = 10.828	M = 9.422 SD = 8.461	KS(22) = 0.904, p = 0.388	Yes
Fe	M = 22.113 SD = 19.085	M = 23.800 SD = 20.082	M = 13.778 SD = 10.337	M = 30.822 SD = 21.535	KS(22) = 0.837, p = 0.486	Yes
Mn	M = 15.713 SD = 16.642	M = 6.400 SD = 7.354	M = 16.311 SD = 17.677	M = 13.044 SD = 15.062	KS(22) = 1.039, p = 0.230	Yes
B	M = 1.238 SD = 0.770	M = 0.600 SD = 0.283	M = 1.156 SD = 0.555	M = 1.178 SD = 0.951	KS(22) = 1.026, p = 0.243	Yes
S	M = 87.125 SD =76.273	M = 35.600 SD = 28.850	M = 108.422 SD = 75.561	M = 54.378 SD = 65.189	KS(22) = 0.790, p = 0.560	Yes
Al	M = 80.350 SD = 17.227	M = 96.000 SD = 61.377	M = 86.556 SD = 26.845	M = 77.622 SD = 17.782	KS(22) = 1.009, p = 0.261	Yes
Temp_Avg	M = 14.467 SD= 0.5979	M = 16.275 SD = 0.654	M = 14.706 SD = 1.155	M = 14.978 SD = 0.652	KS(22) = 0.688, p = 0.745	Yes

Table 23 – Location D PRS™-probe and soil measurement Levene's tests, independent samples t-tests, and Mann-Whitney *U* tests

Variable	Levene's Test/Independent Samples t-test						Mann-Whitney U Test			
	Site	Equal Variances Assumed	Significant Difference	Depth	Equal Variances Assumed	Significant Difference	Site	Significant Difference	Depth	Significant Difference
Zinc levels	p = 0.000	No	Yes	p = 0.020	Yes	Yes	p = 0.049	Yes	p = 0.047	Yes
Moisture Content	p = 0.007	Yes	Yes	p = 0.347	No	No	p = 0.012	Yes	p = 0.140	No
pH levels	p = 0.000	Yes	Yes	p = 0.195	Yes	No	p = 0.002	Yes	p = 0.138	No
Tot_N	p = 0.808	Yes	No	p = 0.028	Yes	Yes	p = 1.000	No	p = 0.024	Yes
NO3	p = 0.812	Yes	No	p = 0.028	Yes	Yes	p = 1.000	No	p = 0.024	Yes
Ca	p = 0.993	No	No	p = 0.084	Yes	No	p = 1.000	No	p = 0.058	No
Mg	p = 0.101	Yes	No	p = 0.041	No	Yes	p = 0.068	No	p = 0.122	No
K	p = 0.388	Yes	No	p = 0.046	Yes	Yes	p = 0.160	No	p = 0.058	No
P	p = 0.511	No	No	p = 0.441	Yes	No	p = 0.159	No	p = 0.269	No
Fe	p = 0.908	Yes	No	p = 0.048	Yes	Yes	p = 0.573	No	p = 0.024	Yes
Mn	p = 0.455	Yes	No	p = 0.679	Yes	No	p = 0.482	No	p = 0.354	No
B	p = 0.273	Yes	No	p = 0.953	No	No	p = 0.287	No	p = 0.789	No
S	p = 0.368	Yes	No	p = 0.124	Yes	No	p = 0.482	No	p = 0.047	Yes
Al	p = 0.371	No	No	p = 0.417	Yes	No	p = 1.000	No	p = 0.536	No
Temp Avg	p = 0.000	Yes	Yes	p = 0.539	Yes	No	p = 0.002	Yes	p = 0.254	No

Appendix D – ICP-AES Statistics

Table 24 – Location B ICP-AES one sample KS tests, and means and standard deviations for tower and control segments

Variable	Mean and Standard Deviation		KS Test	Normally Distributed
	Tower	Control		
C	M = 46.601 SD = 0.540	M = 46.540 SD = 0.148	KS(11) = 0.644, p = 0.801	Yes
N	M = 2.028 SD = 0.351	M = 2.040 SD = 0.207	KS(11) = 0.452, p = 0.987	Yes
S	M = 0.213 SD = 0.046	M = 0.203 SD = 0.012	KS(11) = 0.599, p = 0.865	Yes
Al	M = 32.250 SD = 10.011	M = 29.667 SD = 11.015	KS(11) = 0.476, p = 0.976	Yes
B	M = 10.000 SD = 7.616	M = 6.000 SD = 2.646	KS(9) = 0.797, p = 0.549	Yes
Ca	M = 8464.250 SD = 1563.589	M = 9442.000 SD = 492.155	KS(11) = 0.389, p = 0.998	Yes
Fe	M = 71.625 SD = 12.603	M = 56.333 SD = 9.452	KS(11) = 0.438, p = 0.991	Yes
K	M = 9888.000 SD = 2452.136	M = 9478.667 SD = 902.965	KS(11) = 0.454, p = 0.986	Yes
Mg	M = 2501.125 SD = 535.560	M = 3054.000 SD = 504.028	KS(11) = 0.410, p = 0.996	Yes
Mn	M = 102.750 SD = 46.946	M = 152.000 SD = 62.698	KS(11) = 0.456, p = 0.985	Yes
Na	M = 29.000 SD = 22.226	M = 14.333 SD = 1.528	KS(11) = 1.189, p = 0.119	Yes
P	M = 1472.375 SD = 304.964	M = 1405.000 SD = 128.265	KS(11) = 0.770, p = 0.594	Yes
Zn	M = 79.500 SD = 37.121	M = 41.333 SD = 30.039	KS(11) = 0.686, p = 0.734	Yes

Table 25 – Location B ICP-AES Levene's tests, independent samples t-tests, and Mann-Whitney *U* tests

Variable	Levene's Test	Independent Samples t-test		Mann-Whitney U Test	
	Equal Variances Assumed	Site	Significant Difference	Site (Sig. 2-tailed)	Significant Difference
C	Yes	p = 0.855	No	p = 0.414	No
N	Yes	p = 0.956	No	p = 0.838	No
S	Yes	p = 0.706	No	p = 0.683	No
Al	Yes	p = 0.718	No	p = 0.838	No
B	No	p = 0.330	No	p = 0.653	No
Ca	Yes	p = 0.329	No	p = 0.153	No
Fe	Yes	p = 0.092	No	p = 0.082	No
K	Yes	p = 0.790	No	p = 0.414	No
Mg	Yes	p = 0.157	No	p = 0.153	No
Mn	Yes	p = 0.186	No	p = 0.306	No
Na	Yes	p = 0.298	No	p = 0.051	No
P	Yes	p = 0.726	No	p = 0.838	No
Zn	Yes	p = 0.148	No	p = 0.066	No

Table 26 – Location C ICP-AES one sample KS tests, and means and standard deviations for tower and control segments

Variable	Mean and Standard Deviation		KS Test	Normally Distributed
	Tower	Control		
C	M = 46.975 SD = 0.328	M = 46.447 SD = 0.197	KS(11) = 0.664, p = 0.770	Yes
N	M = 2.747 SD = 0.350	M = 2.662 SD = 0.605	KS(11) = 0.530, p = 0.786	Yes
S	M = 0.254 SD = 0.031	M = 0.245 SD = 0.032	KS(11) = 0.654, p = 0.786	Yes
Al	M = 44.125 SD = 17.033	M = 36.333 SD = 8.505	KS(11) = 0.590, p = 0.878	Yes
B	M = 3.667 SD = 1.966	M = 8.000 SD = 4.583	KS(9) = 0.564, p = 0.908	Yes
Ca	M = 8088.875 SD = 732.399	M = 10444.000 SD = 1829.160	KS(11) = 0.785, p = 0.568	Yes
Fe	M = 73.875 SD = 16.754	M = 92.000 SD = 22.716	KS(11) = 0.947, p = 0.332	Yes
K	M = 12588.000 SD = 1208.852	M = 13374.000 SD = 491.674	KS(11) = 0.607, p = 0.855	Yes
Mg	M = 3110.500 SD = 593.874	M = 3779.667 SD = 635.201	KS(11) = 0.867, p = 0.440	Yes
Mn	M = 132.875 SD = 72.831	M = 229.333 SD = 48.003	KS(11) = 0.804, p = 0.538	Yes
Na	M = 16.625 SD = 2.615	M = 21.000 SD = 3.606	KS(11) = 0.683, p = 0.739	Yes
P	M = 1751.125 SD = 229.805	M = 1872.000 SD = 433.771	KS(11) = 0.508, p = 0.959	Yes
Zn	M = 91.375 SD =43.563	M = 31.000 SD = 8.000	KS(11) = 0.637, p = 0.812	Yes

Table 27 – Location C ICP-AES Levene's tests, independent samples t-tests, and Mann-Whitney *U* tests

Variable	Levene's Test	Independent Samples t-test		Mann-Whitney U Test	
	Equal Variances Assumed	Site	Significant Difference	Site (Sig. 2-tailed)	Significant Difference
C	Yes	p = 0.030	Yes	p = 0.052	No
N	Yes	p = 0.770	No	p = 0.838	No
S	Yes	p = 0.710	No	p = 0.682	No
Al	Yes	P = 0.478	No	p = 0.838	No
B	Yes	p = 0.077	No	p = 0.089	No
Ca	No	p = 0.149	No	p = 0.041	Yes
Fe	Yes	p = 0.176	No	p = 0.041	Yes
K	No	p = 0.161	No	p = 0.414	No
Mg	Yes	p = 0.136	No	p = 0.102	No
Mn	Yes	p = 0.066	No	p = 0.102	No
Na	Yes	p = 0.051	No	p = 0.050	Yes
P	Yes	p = 0.551	No	p = 0.838	No
Zn	Yes	p = 0.046	Yes	p = 0.014	Yes

Table 28 – Location D ICP-AES one sample KS tests, and means and standard deviations for tower and control segments

Variable	Mean and Standard Deviation		KS Test	Normally Distributed
	Tower	Control		
C	M = 46.345 SD = 0.366	M = 46.457 SD = 0.398	KS(11) = 0.477, p = 0.977	Yes
N	M = 3.122 SD = 0.648	M = 2.256 SD = 0.347	KS(11) = 0.559, p = 0.914	Yes
S	M = 0.304 SD = 0.064	M = 0.232 SD = 0.014	KS(11) = 0.372, p = 0.999	Yes
Al	M = 49.500 SD = 6.392	M = 144.667 SD = 58.620	KS(11) = 1.215, p = 0.105	Yes
B	M = 8.286 SD = 2.928	M = 20.333 SD = 2.517	KS(10) = 0.809, p = 0.496	Yes
Ca	M = 9651.500 SD = 1627.220	M = 10340.000 SD = 1361.572	KS(11) = 0.570, p = 0.901	Yes
Fe	M = 109.375 SD = 16.344	M = 188.333 SD = 58.526	KS(11) = 0.830, p = 0.496	Yes
K	M = 10713.375 SD = 1573.662	M = 10195.667 SD = 2550.465	KS(11) = 0.506, p = 0.960	Yes
Mg	M = 3299.750 SD = 653.215	M = 3901.667 SD = 537.124	KS(11) = 0.477, p = 0.977	Yes
Mn	M = 258.625 SD = 91.216	M = 134.000 SD = 90.835	KS(11) = 0.736, p = 0.650	Yes
Na	M = 16.750 SD = 3.732	M = 33.667 SD = 13.204	KS(11) = 0.994, p = 0.276	Yes
P	M = 2323.125 SD = 518.420	M = 1763.333 SD = 269.871	KS(11) = 0.479, p = 0.976	Yes
Zn	M = 81.125 SD = 42.633	M = 28.333 SD = 8.737	KS(11) = 0.663, p = 0.772	Yes

Table 29 – Location D ICP-AES Levene's tests, independent samples t-tests, and Mann-Whitney *U* tests

Variable	Levene's Test	Independent Samples t-test		Mann-Whitney U Test	
	Equal Variances Assumed	Site	Significant Difference	Site (Sig. 2-tailed)	Significant Difference
C	Yes	p = 0.669	No	p = 0.540	No
N	Yes	p = 0.060	No	p = 0.066	No
S	Yes	p = 0.092	No	p = 0.066	No
Al	No	p = 0.106	No	p = 0.014	Yes
B	Yes	p = 0.000	Yes	p = 0.016	Yes
Ca	Yes	p = 0.534	No	p = 0.414	No
Fe	No	p = 0.141	No	p = 0.014	Yes
K	Yes	p = 0.687	No	p = 0.683	No
Mg	Yes	p = 0.191	No	p = 0.221	No
Mn	Yes	p = 0.074	No	p = 0.152	No
Na	No	p = 0.153	No	p = 0.023	Yes
P	Yes	p = 0.115	No	p = 0.066	No
Zn	Yes	p = 0.069	No	p = 0.041	Yes

Appendix E – Spectroscopy Statistics

Table 30 – Location B band index one sample KS tests, Levene's tests, independent samples t-tests, Mann-Whitney *U* tests, and means and standard deviations for tower and control segments

Variable	KS Test	Normally Distributed	Levene's Test	Independent Samples t-test		Mann-Whitney U Test		Mean and Standard Deviation	
			Equal Variances Assumed	Site	Significant Difference	Site (Sig. 2-tailed)	Significant Difference	Tower	Control
R_{1110}/R_{810}	KS(11) = 0.692, p = 0.725	Yes	Yes	p = 0.975	No	p = 0.838	No	M = 1.02 SD = 0.015	M = 1.021 SD = 0.018
NDVI	KS(11) = 0.665, p = 0.768	Yes	Yes	p = 0.897	No	p = 0.540	No	M = 0.888 SD = 0.011	M = 0.888 SD = 0.004
R_{900}/R_{970}	KS(11) = 0.777, p = 0.582	Yes	No	p = 0.561	No	p = 1.000	No	M = 1.055 SD = 0.005	M = 1.050 SD = 0.012

Table 31 – Location C band index one sample KS tests, Levene's tests, independent samples t-tests, Mann-Whitney *U* tests, and means and standard deviations for tower and control segments

Variable	KS Test	Normally Distributed	Levene's Test	Independent Samples t-test		Mann-Whitney U Test		Mean and Standard Deviation	
			Equal Variances Assumed	Site	Significant Difference	Site (Sig. 2-tailed)	Significant Difference	Tower	Control
R_{1110}/R_{810}	KS(11) = 0.575, p = 0.895	Yes	Yes	p = 0.790	No	p = 1.000	No	M = 1.028 SD = 0.011	M = 1.030 SD = 0.015
NDVI	KS(11) = 0.466, p = 0.982	Yes	Yes	p = 0.384	No	p = 0.307	No	M = 0.867 SD = 0.020	M = 0.879 SD = 0.020
R_{900}/R_{970}	KS(11) = 0.352, p = 1.000	Yes	No	p = 0.949	No	p = 0.683	No	M = 1.054 SD = 0.005	M = 1.055 SD = 0.014

Table 32 – Location D band index one sample KS tests, Levene's tests, independent samples t-tests, Mann-Whitney *U* tests, and means and standard deviations for tower and control segments

Variable	KS Test	Normally Distributed	Levene's Test	Independent Samples t-test		Mann-Whitney U Test		Mean and Standard Deviation	
			Equal Variances Assumed	Site	Significant Difference	Site (Sig. 2-tailed)	Significant Difference	Tower	Control
R_{1110}/R_{810}	KS(11) = 0.515, p = 0.954	Yes	Yes	p = 0.007	Yes	p = 0.025	Yes	M = 1.015 SD = 0.008	M = 1.035 SD = 0.010
NDVI	KS(11) = 0.455, p = 0.986	Yes	Yes	p = 0.476	No	p = 0.414	No	M = 0.884 SD = 0.021	M = 0.874 SD = 0.019
R_{900}/R_{970}	KS(11) = 0.678, p = 0.748	Yes	Yes	p = 0.007	Yes	p = 0.025	Yes	M = 1.067 SD = 0.005	M = 1.054 SD = 0.007

Appendix F – Sample Site PRS™-probe and ICP-AES Zinc Concentrations

(SS1)

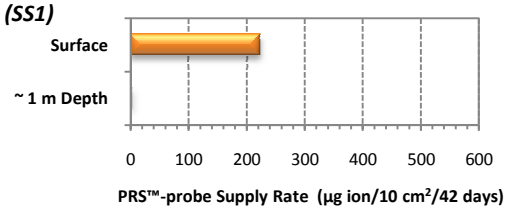

(SS2)

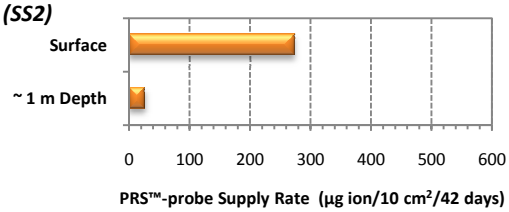

(SS3)

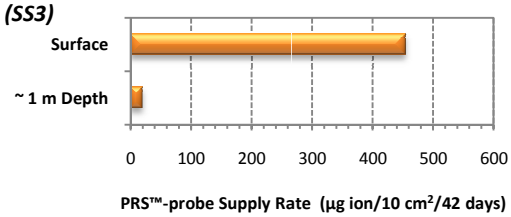

(SS4)

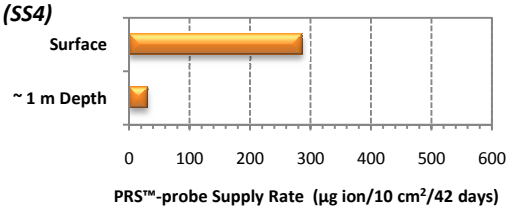

(SS5)

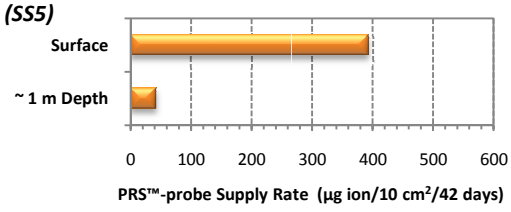

(SS6)

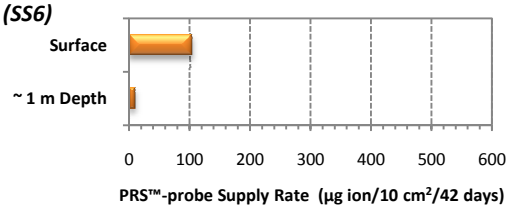

(SS7)

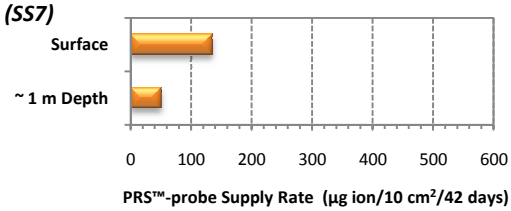

(SS8)

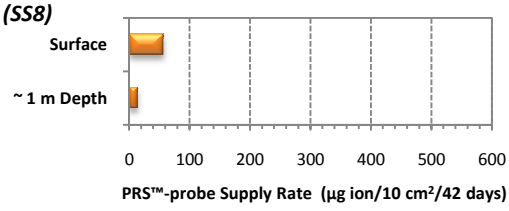

(SS9)

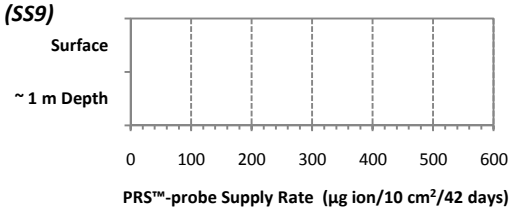

(SS10)

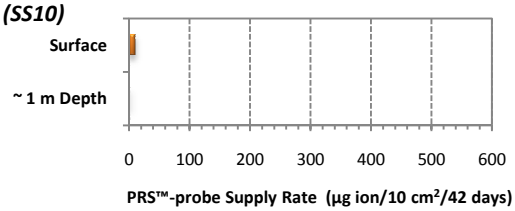

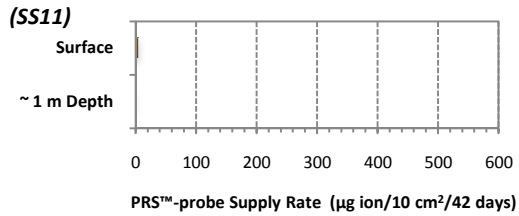

Figure 48 – PRS™-probe Zn concentrations at location B transmission tower sampling sites, Langley, British Columbia. SS1 through SS8 indicate samples sites directly beneath transmission tower. SS9 through SS10 indicate control samples taken 10 m away from tower.

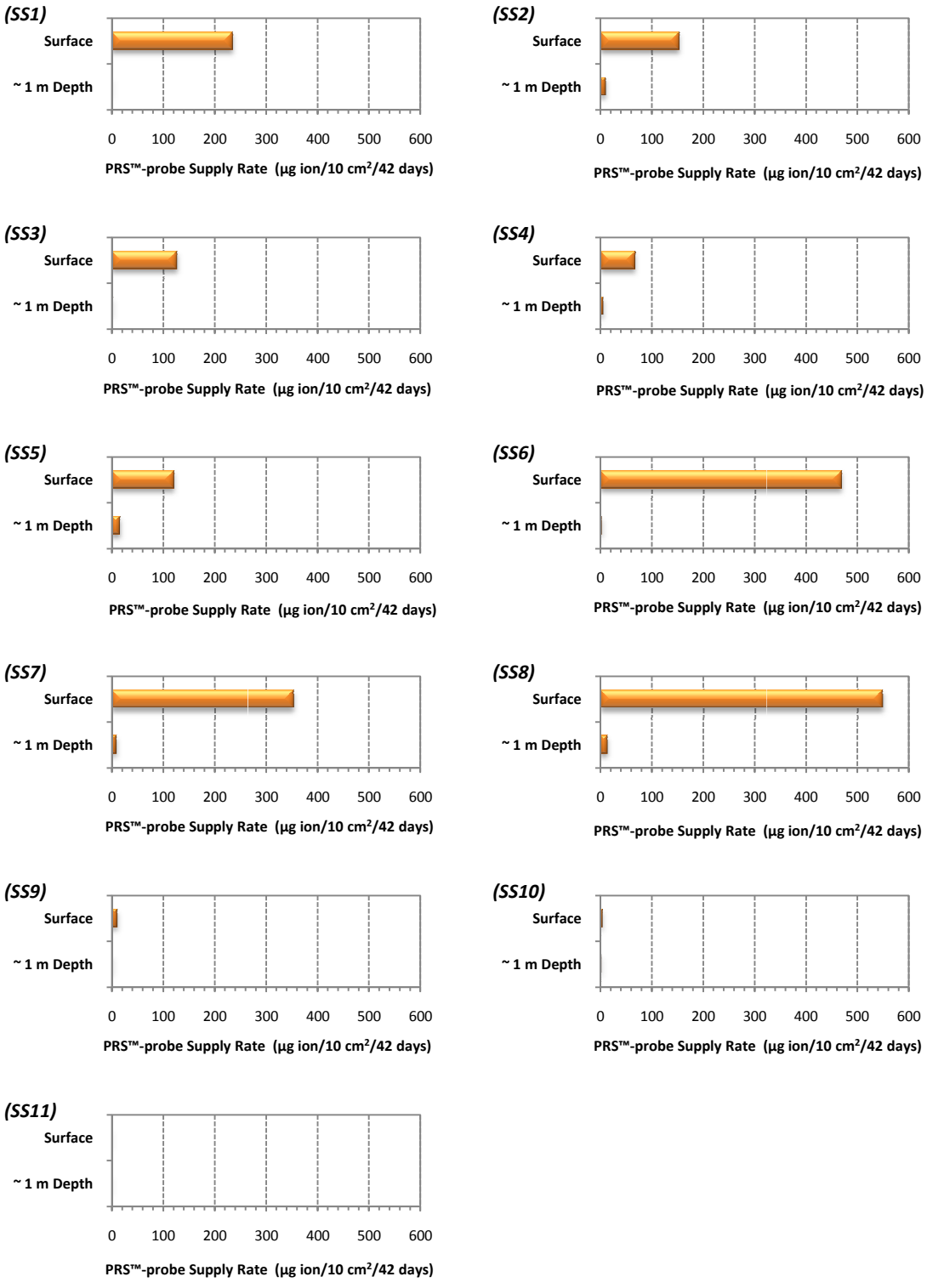

Figure 49 – PRS™-probe Zn concentrations at location C transmission tower sampling sites, Langley, British Columbia. SS1 through SS8 indicate samples sites directly beneath transmission tower. SS9 through SS10 indicate control samples taken 10 m away from tower.

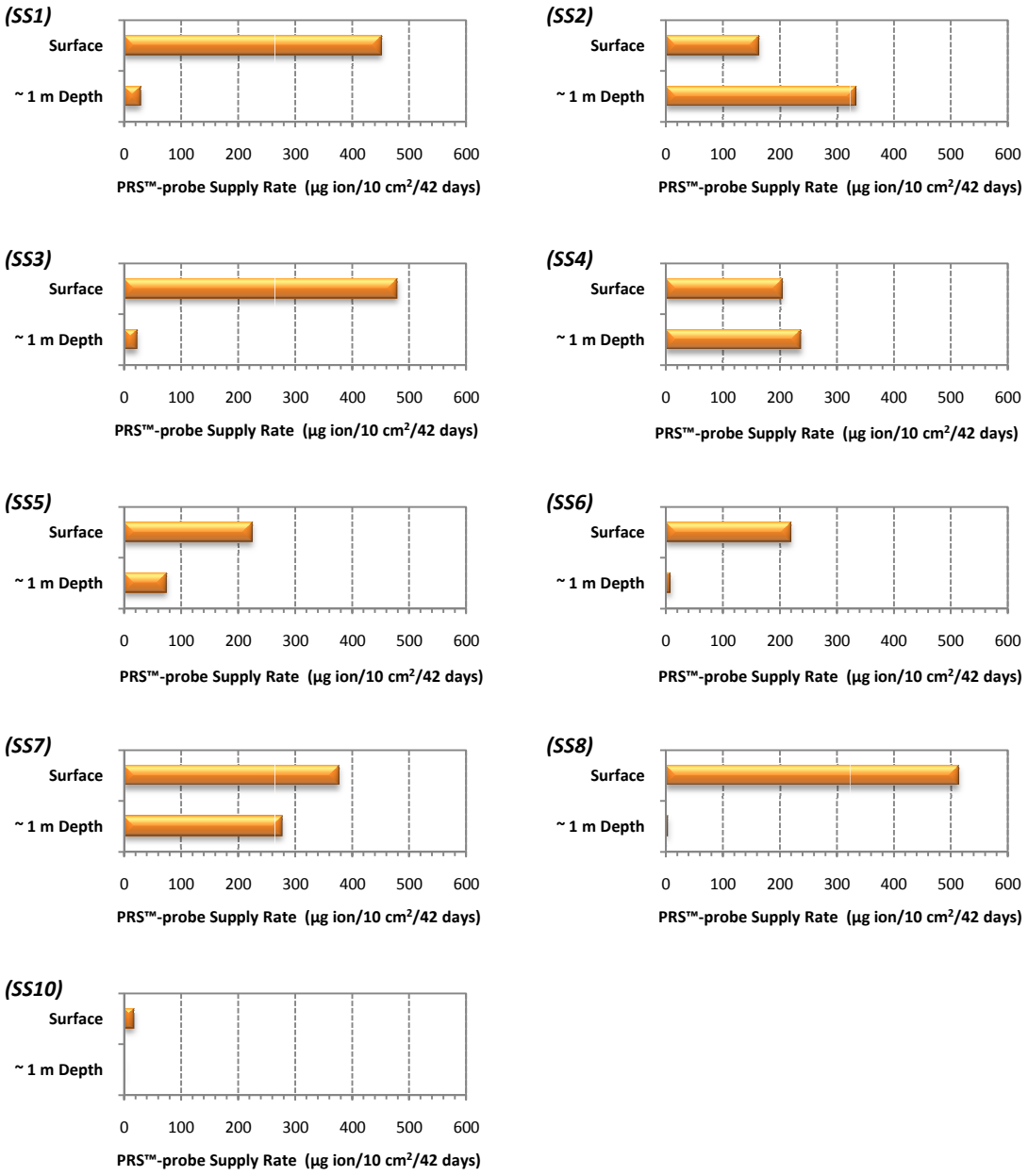

Figure 50 – PRS™-probe Zn concentrations at location D transmission tower sampling sites, Aldergrove, British Columbia. SS1 through SS8 indicate samples sites directly beneath transmission tower. SS10 indicates control samples taken 10 m away from tower. Note that SS9 and SS11 were not available.

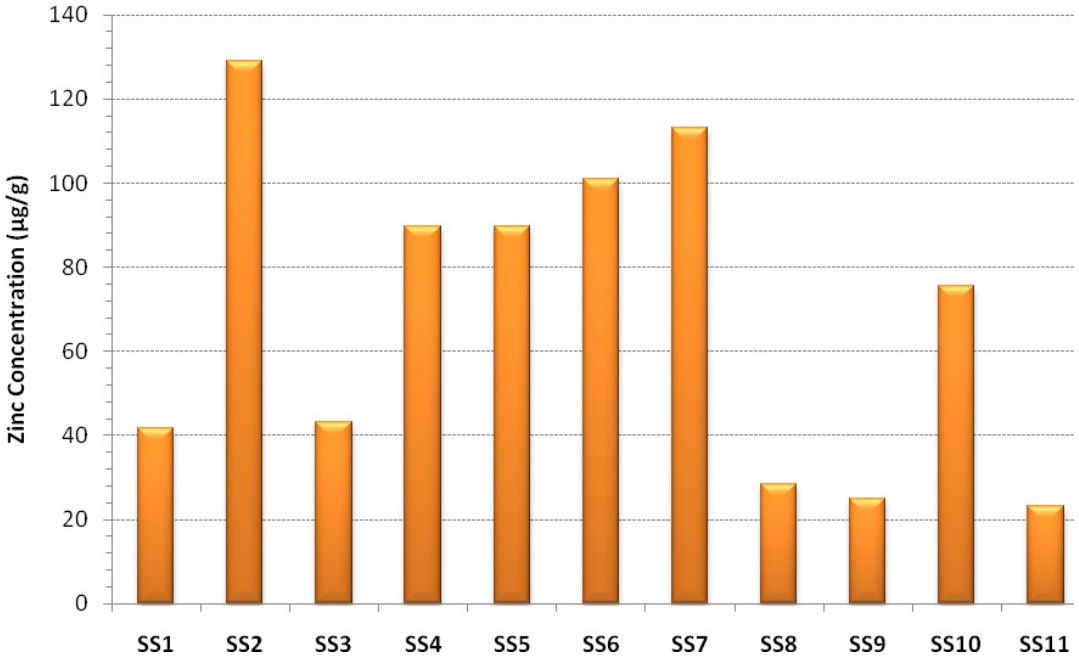

Figure 51 – ICP-AES Zn concentrations at location B transmission tower sampling sites, Langley, British Columbia. SS1 through SS8 indicate samples sites directly beneath transmission tower. SS9 through SS10 indicate control samples taken 10 m away from tower.

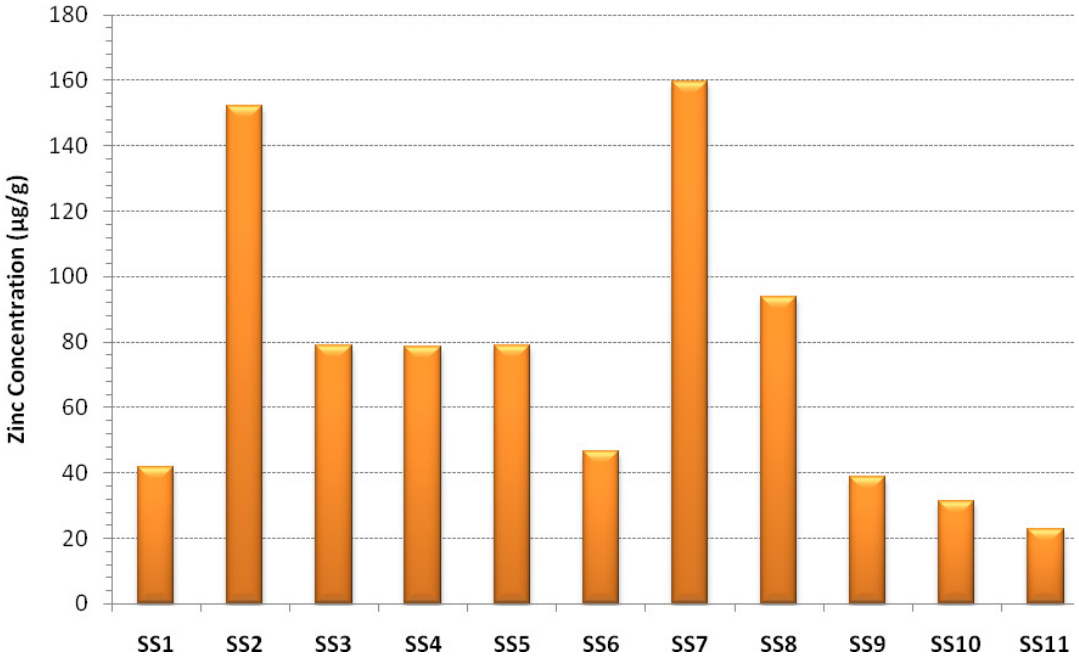

Figure 52 – ICP-AES Zn concentrations at location C transmission tower sampling sites, Langley, British Columbia. SS1 through SS8 indicate samples sites directly beneath transmission tower. SS9 through SS10 indicate control samples taken 10 m away from tower.

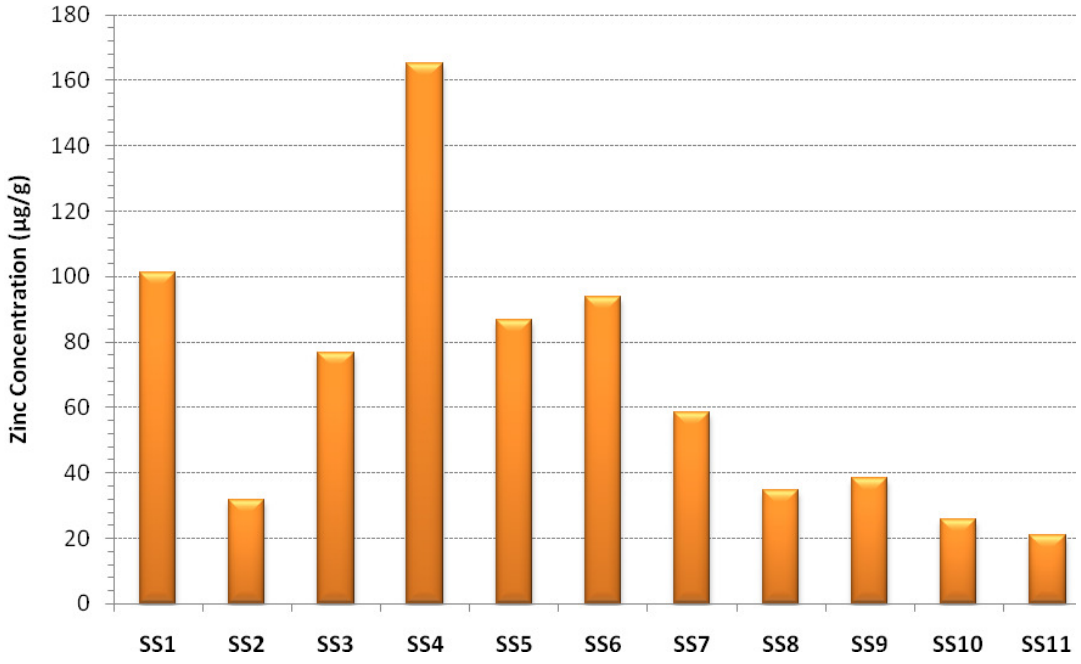

Figure 53 – ICP-AES Zn concentrations at location D transmission tower sampling sites, Aldergrove, British Columbia. SS1 through SS8 indicate samples sites directly beneath transmission tower. SS9 through SS10 indicate control samples taken 10 m away from tower.

Appendix G – Principal Component Analysis Results

Principal Component Analysis – 400 to 550 nm

All of the variables fit well with the factor solution and no variables have to be omitted from the analysis. Communalities indicate the amount of variance in each variable that is accounted for (SPSS, 2004). The communality output suggests that PCA explains all of the variables quite well. Band depth center has the lowest variation at 0.912 (Table 33).

Table 33 – PCA communalities table, 400 to 550 nm

Variable	Extraction Communalities
Band Depth Center	0.912
Symmetry	0.989
Total Area	0.994
Area Right	0.996
Area Left	0.990

The results of the PCA indicate that at all three locations, principal component one and two account for a cumulative 97.638% of the variance. Since only eigenvalues of one or more are retained, the total eigenvalues for variables 3 to 5 are discarded (Figure 55). Therefore, only the first two components are retained.

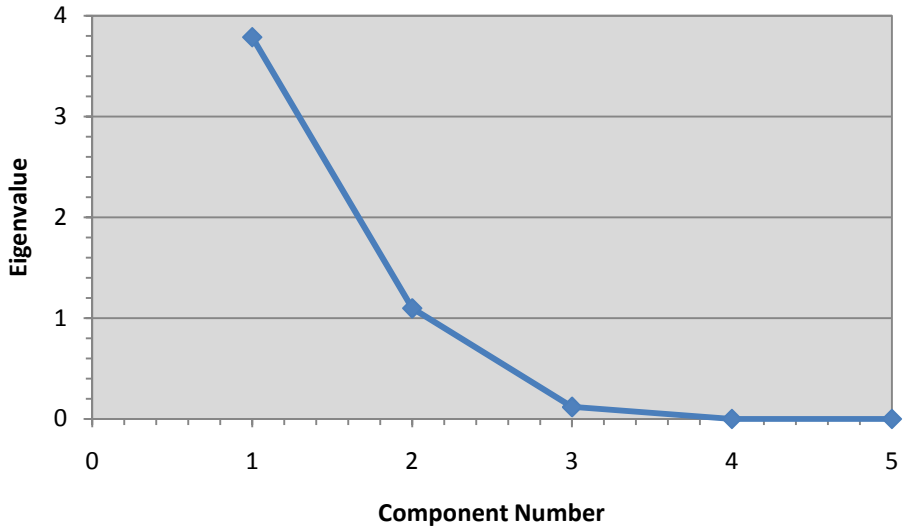

Figure 54 – Eigenvalue scree plot of principal components, 400 to 550 nm

The component matrix shows the factor loadings for each variable. Each component loading represents the correlation between the variable and the unrotated factor. Figure 55 shows the plotted component matrix.

Table 34 – Component matrix, 400 to 550 nm

Variable	Component	
	1	2
Area Left	0.995	0.001
Symmetry	0.993	- 0.055
Total Area	0.958	0.275
Band Depth Center	0.942	- 0.160
Area Right	- 0.059	0.996

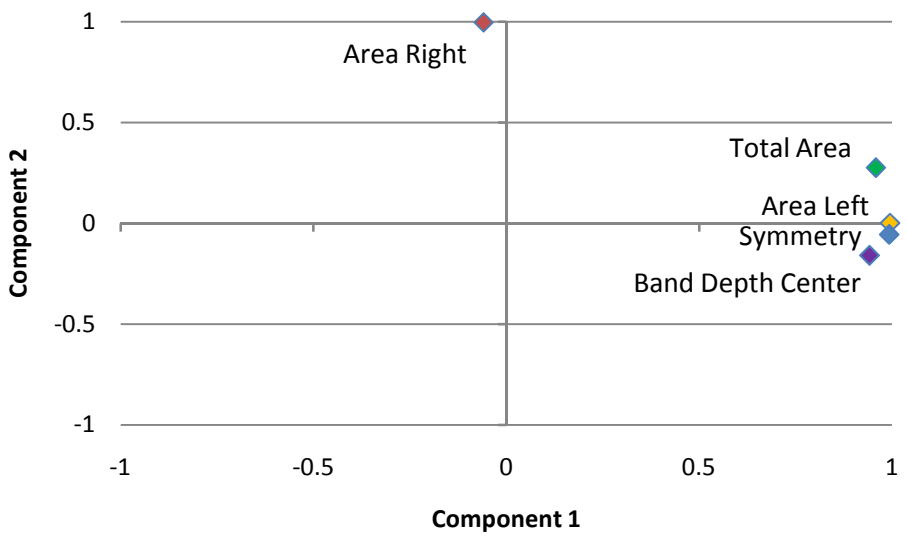

Figure 55 – Component plot, 400 to 550 nm

Given these results, the variables can be generalized into two components. The first, accounting for 75.704% of the variance, includes total area, area left, symmetry, and band depth center. The second, accounting for 21.934% of the variance, includes area right.

Principal Component Analysis – 550 to 750 nm

All of the variables fit well with the factor solution and no variables have to be omitted from the analysis. Communalities indicate the amount of variance in each variable that is accounted for (SPSS, 2004). The communality output suggests that PCA explains all of the variables quite well. Band depth center has the lowest variation at 0.758 (Table 35).

Table 35 – PCA communalities table, 550 to 750 nm

Variable	Extraction Communalities
Band Depth Center	0.758
Symmetry	0.914
Total Area	0.956
Area Right	0.815
Area Left	0.992

The results of the PCA indicate that at all three locations, principal component one and two account for a cumulative 88.715% of the variance. Since only eigenvalues of one or more are retained, the total eigenvalues for variables 3 to 5 are discarded (Figure 56). Therefore, only the first two components are retained.

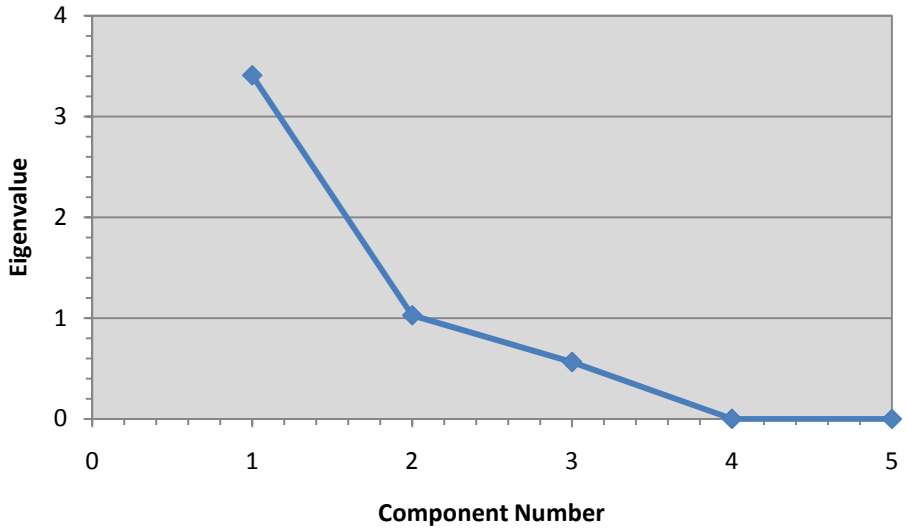

Figure 56 – Eigenvalue scree plot of principal components, 550 to 750 nm

The component matrix shows the factor loadings for each variable. Each component loading represents the correlation between the variable and the unrotated factor. Figure 57 shows the plotted component matrix.

Table 36 – Component matrix, 550 to 750 nm

Variable	Component	
	1	2
Area Left	0.947	-0.308
Symmetry	0.795	-0.531
Total Area	0.976	0.060
Band Depth Center	0.494	0.717
Area Right	0.826	0.365

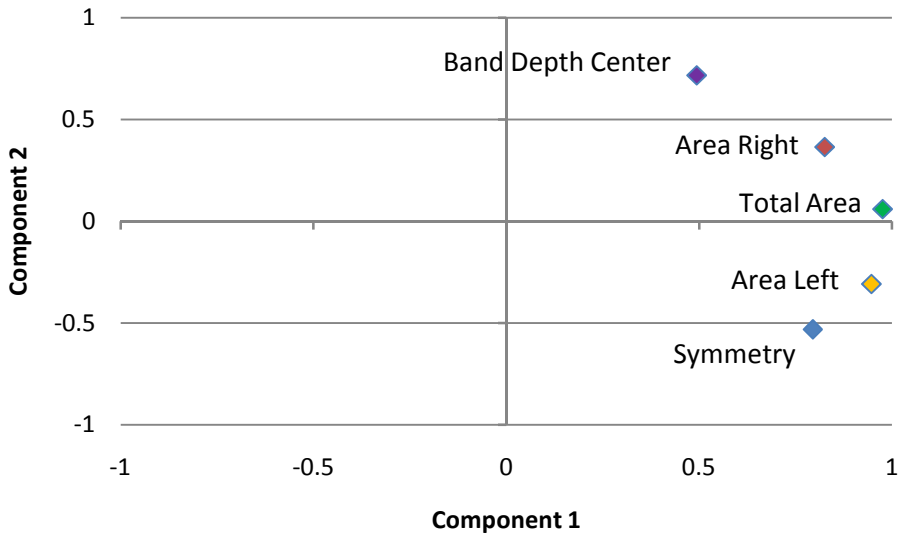

Figure 57 – Component plot, 550 to 750 nm

Given these results, the variables can be generalized into two components. The first, accounting for 68.154% of the variance, includes total area, area left, symmetry, and area right. The second, accounting for 20.561% of the variance, includes band depth center.

Principal Component Regression Analysis

A regression analysis was conducted on the principal component factor scores from 400 to 550 nm and 550 to 750 nm against ICP-AES Zn levels. Results from the regression analysis infer with 95% accuracy that the Zn (ICP-AES) ($R^2 = 0.027$, r = 0.164(4), p (0.940) > 0.05) levels do not explain a significant portion of the variation in the continuum removal principal components.